Universidade de Aveiro
2020

Ana Sofia Rodrigues Neto

Estruturas porosas de fosfatos de cálcio para terapias avançadas na regeneração óssea

Porous calcium phosphate bone graft scaffolds for advanced therapies

Universidade de Aveiro
2020

Ana Sofia Rodrigues Neto

Estruturas porosas de fosfatos de cálcio para terapias avançadas na regeneração óssea

Porous calcium phosphate bone graft scaffolds for advanced therapies

Tese apresentada à Universidade de Aveiro para cumprimento dos requisitos necessários à obtenção do grau de Doutor em Materiais e Processamento Avançados, realizada sob a orientação científica do Professor Doutor José Maria da Fonte Ferreira, Professor Associado com Agregação do Departamento de Engenharia de Materiais e Cerâmica da Universidade de Aveiro e do Professor Doutor Jorge Fernando Jordão Coelho, Professor Catedrático do Departamento de Engenharia Química da Universidade de Coimbra.

Apoio financeiro da FCT (PD/BD/114132/2015)

Aos meus pais

o júri

presidente

Prof. Doutor José Carlos Esteves Duarte Pedro
professor Catedrático, Universidade de Aveiro

Prof. Doutor Joaquim Manuel Vieira
professor Catedrático, Universidade de Aveiro

Prof. Doutor João Paulo Miranda Ribeiro Borges
Professor Associado com Agregação, Universidade Nova de Lisboa

Prof. Doutora Anabela Baptista Pereira Paula
professora Auxiliar, Universidade de Coimbra

Prof. Doutora Aureliana Filipa de Castro e Sousa
investigadora, I3s – Instituto de Investigação e Inovação em Saúde

Prof. Doutor José Maria da Fonte Ferreira
professor Associado com Agregação, Universidade de Aveiro

acknowledgements

Este trabalho não é o resultado de um esforço individual, mas sim de um conjunto de esforços que o tornaram possível. Sem todo o apoio que tive seria difícil terminar este trabalho. Assim queria expressar o meu agradecimento àqueles que contribuíram com o todo o seu apoio.

Queria agradecer ao Programa Doutoral de Processamento Avançado de Materiais e à Fundação para a Ciência e Tecnologia pelo apoio financeiro, PD/BD/114132/2015.

Ao meu orientador Professor José Maria Ferreira por ter acreditado em mim e me ter dado a oportunidade de desenvolver este trabalho do seu laboratório e sob a sua supervisão. Queria expressar o meu agradecimento por todos os valiosos conselhos e incentivo para superar os diferentes obstáculos.

Ao meu co-orientador Professor Jorge Coelho, o meu sincero agradecimento por todo o seu apoio científico e valiosos concelhos que que enriqueceram o meu trabalho e me ajudaram a melhora o meu conhecimento científico.

À UA, CICECO e DEMaC por todo o apoio durante estes anos. Queria agradecer todo o apoio técnico dado pela Célia e Ana. Ao Artur e à Celeste por toda a ajuda com o XRD e FTIR-ATR, respetivamente. À equipa técnica do Laboratório Central de Análises pela ajuda com a análise ICP. Por fim, queria também agradecer ao Tiago e à Marta pela ajuda na realização das sessões de SEM.

À UC e ao departamento de engenharia química pelo apoio dado durante estes anos e pela disponibilidade de colocar vários meios à minha disposição. Ao Rafael Rebelo pela ajuda e paciência no corte das minha amostras.

À Dr. Ana Fonseca por todo o trabalho na preparação dos diferentes polímeros. Mais ainda, queria agradecer pela orientação e transmissão de conhecimento na área de polímeros. Todos os seus valiosos comentários foram úteis para melhorar a qualidade do trabalho.

Ao Dr. João Abrantes pela sua disponibilidade para realizar o refinamento de Rietveld de diferentes amostras.

Ao Professor João Ramalho, Dr. Ana Sofia Rodrigues, Professor Luís Almeida, Dr. Catarina Miranda e Inês Barros o meu sincero agradecimento por toda a ajuda e apoio nos ensaios in vitro de cultura celular. O meu obrigada por todo o conhecimento que me transmitiram e que foi muito útil para a realização do meu trabalho.

A todos os meus colegas de laboratório e em especial ao Bo, Anuraag e Daniela com quem eu partilhei a maioria do meu tempo no laboratório. Obrigada pela vossa amizade, todo o apoio e partilha de momentos que certamente me enriqueceram tanto a nível pessoal como profissional.

Aos meus amigos que na maioria me acompanham desde os tempos da licenciatura Carla, Francisco, Joana, Diogo, Hugo, Diana, Francisco, Daniela, Tiago, Maria, João e Bárbara. Obrigada pela vossa amizade e por me transmitirem palavras de apoio e coragem para ultrapassar os momentos mais difíceis.

Aos suspeitos do costume, Margarida, Nuno, Sara, Ricardo e Manuel que estiveram sempre presentes e me apoiaram neste trajeto. Obrigada pelas vossas palavras de carinho e encorajamento.

A minha profunda gratidão aos meus pais e à minha irmã Mariana pelo apoio incondicional, paciência e por sempre acreditarem em mim.

Ao Antony por todo o amor e carinho. Obrigada por todo o apoio e pela transmissão de energia positiva que me ajuda a superar as minhas inseguranças.

palavras-chave

Osso de choco, fosfátos de cálcio, substituição ionica, revestimento polimérico, vidro bioactivo, sistema de libertação controlada, regeneração óssea

resumo

Esta tese teve como principal objetivo o desenvolvimento de *scaffolds* multifuncionais à base de fosfatos de cálcio (CaP) para substitutos ósseos.

As *scaffolds* bifásicas de fosfatos de cálcio (BCP) não dopadas e dopadas (Sr^{2+}, Mg^{2+} e/ou Zn^{2+}) foram obtidas através do tratamento hidrotermal (HT) do osso de choco (CB). A microestrutura única do CB foi preservada após a HT e a sua completa transformação foi confirmada por difração de raios-X (XRD). A presença dos elementos dopantes nas *scaffolds* de BCP foi observada através da deslocação dos padrões de XRD para diferentes ângulos e as diferenças na quantificação de fases for obtida por refinamento de Rietveld. No entanto, a espectrometria de emissão atómica com fonte de plasma mostrou que a quantidade de iões dopantes era significativamente inferior à planeada. A coloração live/dead das células mesenquimais humanas que estiveram na presença das diferentes *scaffolds* indicaram que as células mantiveram a sua viabilidade durante as 72 h. Através do ensaio com MTT observou-se que a presença dos iões dopantes (Sr^{2+}, Mg^{2+} e Zn^{2+}) melhorou a proliferação celular.

Numa abordagem alternativa à substituição parcial do cálcio na estrutura cristalina do BCP, os iões dopantes foram introduzidos através de um revestimento de superfície com vidro bioativo obtido por sol-gel. Este revestimento melhorou as propriedades mecânicas das *scaffolds* e também a atividade de bio mineralização in vitro quando imerso em fluido corporal simulado (SBF). Apesar das vantagens deste revestimento, os ensaios preliminares de MTT demonstraram alguma toxicidade induzida pelo pH elevado associado à lixiviação iónica do revestimento.

De forma a ultrapassar a principal desvantagem das *scaffolds* BCP obtidas através de CB (fragilidade e baixa tenacidade à fratura) foram feitos revestimentos poliméricos nas superfícies das *scaffolds*. Com esse objetivo, dois polímeros comerciais, poli(ε-caprolactona) (PCL) e poli(DL-láctico) (PDLA), e dois outros polímeros sintetizados em laboratório, poli(éster amida) (PEA) e poli(éster ureia) (PEU). Os revestimentos poliméricos melhoraram as propriedades mecânicas sem comprometer a estrutura porosa interconecta, tal como observado por microscopia eletrónica de varrimento. As *scaffolds* revestidas com PEU registaram os valores mais altos de resistência à compressão. A presença dos polímeros foi ainda confirmada por FTIR. Os resultados preliminares dos ensaios de cultura celular in vitro realizados com *scaffolds* dopadas por substituição parcial de cálcio por Sr^{2+}, Mg^{2+} e Zn^{2+} mostraram uma maior proliferação celular para aquelas revestidas com PEU.

O efeito sinergético entre CaP e polímeros foi explorado para permitir a libertação de rifampicina (RFP) como um antibiótico modelo, conferindo às *scaffolds* a capacidade de libertação controlada de fármaco. A presença do fármaco foi confirmada pela alteração de cor de branco para cor-de-laranja e pelos estudos de libertação do fármaco. Os polímeros influenciam diferentemente os perfis de libertação do fármaco. A cinética de libertação foi mais rápida nas *scaffolds* revestidas com PCL em comparação com as amostras revestidas com PEA ou PEU. As amostras com RFP demonstraram ter uma forte atividade antibacteriana contra Gram-negativa *Escherichia coli* e Gram-positiva *Staphylococcus aureus*.

Em conclusão, obtivemos com sucesso *scaffolds* BCP não dopadas e dopadas derivadas de CB. A combinação destas *scaffolds* com PCL, PDLA, PEA e PEU melhorou as propriedades mecânicas e permitiu uma libertação controlada do fármaco. Estas scaffolds podem ser potencialmente utilizadas como substitutos ósseos para melhorar a regeneração óssea e impedir a formação de um biofilme bacteriano.

.

keywords

Cuttlefish bone, calcium phosphates, ionic substitution, polymeric coating, bioactive glass, drug delivery system, bone regeneration.

abstract

The main aim of this thesis was to develop multifunctional porous calcium phosphate (CaP) based scaffolds as bone grafts for advanced therapies.

Undoped and doped (Sr^{2+}, Mg^{2+} and/or Zn^{2+}) biphasic calcium phosphate (BCP) scaffolds were obtained through a hydrothermal treatment (HT) of cuttlefish bone (CB). The unique microstructure of CB was preserved after HT and its complete transformation was confirmed by X-ray diffraction (XRD). The presence of the doping elements on BCP scaffolds was observed through the shifts of XRD patterns to different angles and the differences of phase quantification were obtained by Rietveld refinement. Nevertheless, inductively couple plasma spectroscopy revealed that the incorporated amounts of the doping elements were significantly lower than the planned ones. The live/dead staining results of human mesenchymal stem cells cultured in vitro in the presence of different scaffolds indicated that cells maintain their viability for 72 h. The presence of doping elements (Sr^{2+}, Mg^{2+} and Zn^{2+}) improved cell proliferation as observed by MTT assay.

As an alternative approach to calcium partial replacement in the crystalline lattices of BCP, the doping elements were incorporated as sol-gel derived bioactive glass (BG) surface coating. This coating improved the mechanical properties of the scaffolds and their in vitro biomineralization activity when immersed in simulated body fluid (SBF). Despite the apparent advantages of this coating, preliminary MTT assay results indicated some pH-induced toxicity associated with ionic leaching from the coating.

To overcome the major drawbacks of BCP scaffolds obtained from CB (brittleness and low fracture toughness), polymeric coatings were applied onto their surfaces. With this purpose, two commercial polymers, poly(ε-caprolactone) (PCL) and poly(DL-lactide) (PDLA), and two other polymers synthesized in the laboratory, poly(ester amide) (PEA) and poly(ester urea) (PEU) were used. The polymeric coatings enhanced the overall mechanical properties, without compromising the interconnected porous structure, as observed by scanning electron microscopy. Higher values of compressive strength were registered for scaffolds coated with PEU. The presence of the polymers was further confirmed by FTIR. The preliminary in vitro cell culture results performed with polymer coated BCP scaffolds doped by calcium partial substitution with Sr^{2+}, Mg^{2+} and Zn^{2+} showed a greater cell proliferation for those coated with PEU.

The synergetic effect between CaP and polymers were explored to release rifampicin (RFP) as a model antibiotic, conferring to the scaffolds sustained drug delivery capabilities. The presence of the drug was confirmed by the colour change from white to orange and by the drug release studies. The polymers influence differently the drug release profiles. The release kinetics were faster for the scaffolds coated with PCL in comparison to the samples coated with PEA or PEU. The RFP loaded samples demonstrated to have a strong antibacterial activity against both Gram-negative Escherichia coli and Gram-positive Staphylococcus aureus.

In conclusion, we successfully obtain undoped and doped BCP scaffolds derived from CB. The combination of these scaffolds with PCL, PDLA, PEA or PEU improved the mechanical properties and enabled a sustained drug release. These scaffolds can potentially be used as bone graft substitutes to improve bone regeneration and prevent bacterial biofilm formation.

Index

Chapter 3

Chapter 4

List of Abbreviations

ACC	Amorphous calcium carbonate
ALP	Alkaline phosphatase
AM	Additive manufacturing
ANOVA	One-way analysis of variance
ASCs	Autologous adipose tissue-derived stem cells
BCG	Bovine cancellous graft
BCP	Biphasic calcium phosphate
bFGF	Basic fibroblast growth factors
BG	Bioactive glass
BMSCs	Bone marrow stromal cells
BMPs	Bone morphogenetic proteins
CAD	Computer-aided design
CaP	Calcium phosphate
CB	Cuttlefish bone
CB-HA-COL	Raw CB with hydroxyapatite and collagen
CBA	Allograft
CBHA	Hydroxyapatite scaffolds derived from CB
CDHA	Carbonated calcium deficient HA
CFUs	Colony-forming units
CMC	Carboxymethyl cellulose
ColI	Collagen type I
ColIα1	Collagen type I α1
CPO	Calcium peroxide
CS	Compressive strength
DBM	Demineralized bone matrix

DFDD	Demineralized freeze-dried dentin
DMSO	Dimethyl sulfoxide
DSC	Differential scanning calorimetry
DTA/TG	Differential and gravimetric thermal analyses
ECM	Extracellular matrix
EDS	Energy dispersive spectroscopy
FTIR	Fourier transform infrared
GTR	Guided tissue regeneration
HA	Hydroxyapatite
hBMSCs	human BMSCs
HT	Hydrothermal transformation/treatment
ICP	Inductively couple plasma
IGF	Insulin-like growth factors
LB	Luria-Bertani medium
MC3T3-E1	Mouse embryonic pre-osteoblasts cells
Micro(μ)-CT	Micro-computed tomography
MSCs	Mesenchymal stem cells
MTT	Formazan assay
OC	Osteocalcin
ON	Osteonectin
OPN	Osteopontin
PBS	Phosphate buffered saline
PCL	Poly(ε-caprolactone)
PCL-co-PEG	Polycaprolactone-co-polyethyleneglycol
PDGF	Platelet-derived growth factors
PDL	Periodontal ligament

PDLA	Poly(DL-lactide)
PEA	Poly(ester amide)
PEU	Poly(ester urea)
PGA	Poly(glycolic acid)
PHBV	Poly(3-hydroxybutyrate-*co*-3-hydroxyvalerate)
PLA	Poly(lactic acid)
PLGA	Poly(lactic-co-glycolide
PPF	Poly(propylene fumarate)
PRP	Platelet Rich Plasma
PTFE	Poly(tetrafluorethylene)
rBMSCs	rat bone marrow stromal cells
RFP	Rifampicin
RGD	Arginine-glycine-aspartic
rGO	graphene oxide
$rhVEGF_{165}$	Recombinant human vascular endothelial growth $factor_{165}$
rMSCs	rat MSCs
RT	Room temperature
Runx2	Runt-related transcription factor 2
SBF	Simulated body fluid
SD	Standard deviation
SEM	Scanning electron microscopy
SSA	Specific surface area
SVA	Simvastatin acid
TCP	Tricalcium phosphate
TEOS	Tetra-ethyl-ortho-silicate
TEP	Triethyl phosphate

TGF-β	Transforming growth factor-beta
VEGF	Vascular endothelial growth factor
XRD	X-ray diffraction
YM	Young's modulus
ZTA	Zirconia-toughened alumina
3D	Three-dimensional
β-TCP	β-tricalcium phosphate

Preface

The life expectancy has been increasing over the past decades. Nevertheless, the birth rates have been decreasing and, therefore, Europe has been facing a demographic ageing trend [1]. The ageing of population is intrinsically associated with the increasing incidence of health problems in the musculoskeletal system namely osteoporosis, bone tumours and fractures, requiring suitable solutions to support the quality of life. To meet these demands, significant research efforts have been undertaken to develop novel bone grafts.

The mineral component of bone consists of non-stoichiometric and poly-substituted calcium phosphate (CaP), thus CaPs are widely used in bone remodelling applications [2]. Among the different CaP compositions, biphasic calcium phosphate (BCP), mixture of hydroxyapatite (HA) and β-tricalcium phosphate (β-TCP), have gain special interest and currently can be considered the gold standard of CaP due to the possibility of adjusting the proportions between HA and β-TCP and, therefore, control the dissolution and degradation rates [3]. Since bone mineral is a poly-substituted CaP, the incorporation of trace elements like strontium (Sr^{2+}), magnesium (Mg^{2+}) or zinc (Zn^{2+}) into the structure of CaP biomaterials has been gaining significant importance in the field [4]. It is important to highlight that bone is a composite, where besides the mineral phase, it has 35% organic phase. Thus, combination of these two types of materials has been explored to create composite scaffolds. The use of synthetic biodegradable polymers offers several advantages over the natural ones, including their ability for tailoring relevant properties, such as mechanical performance and degradation rates, and batch to batch uniformity.

Marine skeletons like cuttlefish bone (CB), are mainly composed of calcium carbonate that can be hydrothermally converted into CaP. The CB architecture, its interconnected porous structure and the high degree of porosity (93%) makes this material unique and suitable for bone repair and regeneration. Scaffolds with such unique porous structures like CB are difficult to obtain by conventional techniques (*e.g.* chemical/gas foaming) or even by using additive manufacturing techniques (*e.g.* robocasting). The previous literature reports about the hydrothermal transformation of CB into CaP targeted the formation of HA as the end product [5]. Nevertheless, the advantages of BCP over the HA in terms of the *in vivo* performance are recognized [3]. Moreover, the

incorporation of trace elements existing in bone composition like silicon (Si^{4+}) [6] and fluorine (F^-) [7] has been reported to improve the bioactivity, and the new bone formation ability. Strontium (Sr^{2+}), magnesium (Mg^{2+}) and zinc (Zn^{2+}), also present in bone composition, are also known to play important roles in bone development.

One of the main drawbacks associated with these highly porous scaffolds concerns their brittleness and low strength. This shortcoming could be mitigated by applying a polymeric coating with poly(ε-caprolactone) (PCL) [8,9]. Although, polyesters (*e.g.* PCL) are the most used synthetic polymers in bone tissue engineering, α-amino acid based poly(ester amide) (PEA) and poly(ester urea) (PEU) demonstrated to have promising properties in the biomedical field. These polymers allow combining the biodegradability of polyesters and the mechanical and thermal behaviour of polyamides [10,11].

Nevertheless, the efforts done to transform CB into CaP and improve their properties still suffer from some shortcomings and justify the continuous research to obtain a material with a good potential to be used in bone tissue engineering.

The main aim of this thesis was to develop a multifunctional bone graft material based on doped scaffolds combined with different polymers that allow a sustained drug release. In this regard, the objectives of the current thesis are: (i) to transform CB into BCP scaffolds through hydrothermal transformation (HT); (ii) to introduce Sr^{2+}, Mg^{2+} and/or Zn^{2+} in different concentrations during HT; (iii) to coat the BCP scaffolds derived from CB with a Sr-, Mg- and Zn- doped sol-gel derived bioactive glass (BG) aiming an improvement of the scaffolds properties; (iv) functionalization of undoped and doped BCP scaffolds derived from CB with different polymers, commercial polymers, PCL and poly(DL-lactide) (PDLA); and synthesized with pre-determined structures, poly(ester amide) (PEA) and poly(ester urea) (PEU) to improve the mechanical properties of the scaffolds; (v) to use the polymeric coatings as a drug delivery systems; (vi) to assess the relevant physical, chemical and structural properties of the scaffold systems and their bioactivity and biocompatibility.

Considering the above perspective, this thesis is divided into **six chapters. Chapter 1** presents a broad literature overview addressing the bone morphology, composition and its repair and regeneration capacity. Moreover, this chapter describes the materials (polymers, ceramic and composite) and techniques (additive manufacturing techniques and derived from marine skeletons) most commonly used to obtain scaffolds

for bone tissue engineering applications. It is important to highlight that this chapter was published as a review on *Materials* and consequently covers more topics than those investigated in the frame of this thesis. Indeed, besides addressing the use of CB as a biomaterial for bone tissue engineering applications, it also reports on the research efforts made with corals, another kind of marine skeleton and a prospering additive manufacturing technique, robocasting. **Chapter 2** describes the transformation of CB into BCP scaffolds and the subsequent application of polymeric coatings with commercial (PCL and PDLA) and synthesized (PEA and PEU) polymers. It is demonstrated the ability to achieve a complete transformation of CB into BCP scaffolds and introduce different doping ions, Sr^{2+}, Mg^{2+} and/or Zn^{2+}, into the crystalline structure. Importantly, it is shown that the polymeric coatings successfully improve the mechanical properties. This chapter was published on *Materials Science and Engineering C*. **Chapter 3** reports on the production of Sr- Mg- and Zn- doped sol-gel derived BG, and its use to coat the BCP scaffolds derived from CB as a way of improving their bioactivity and mechanical properties. This chapter represents a published article on *Materials*. **Chapter 4** is mainly devoted to the study of *in vitro* behaviour of the cells in contact with the scaffolds developed and characterized in **Chapter 2** and **Chapter 3**. **Chapter 5** addresses the capacity of using the polymeric (PCL, PEA or PEU) coated BCP scaffolds as drug delivery systems. It was observed that the type of polymer used as coating has a direct influence in drug release profile. The RFP loaded scaffolds showed strong antibacterial activity against Gram-positive *Staphylococcus aureus* and Gram-negative *Escherichia coli*. **Chapter 6** provides the concluding remarks and some suggestions for future research aiming at an improvement of the properties and functionalities of bone grafts obtained from CB.

References

[1] EuroStat Statistics Explained, Population structure and ageing, (2019). http://ec.europa.eu/eurostat/statistics-explained.

[2] S. V. Dorozhkin, Calcium-orthophosphate-based bioactive ceramics, Elsevier Ltd., 2018. doi:10.1016/B978-0-08-102203-0.00013-5.

[3] J.M. Bouler, P. Pilet, O. Gauthier, E. Verron, Biphasic calcium phosphate ceramics for bone reconstruction: A review of biological response, Acta

Biomater. 53 (2017) 1–12. doi:10.1016/j.actbio.2017.01.076.

[4] E. Boanini, M. Gazzano, A. Bigi, Ionic substitutions in calcium phosphates synthesized at low temperature, Acta Biomater. 6 (2010) 1882–1894. doi:10.1016/j.actbio.2009.12.041.

[5] J.H.G. Rocha, A.F. Lemos, S. Agathopoulos, P. Valério, S. Kannan, F.N. Oktar, J.M.F. Ferreira, Scaffolds for bone restoration from cuttlefish, Bone. 37 (2005) 850–857. doi:10.1016/j.bone.2005.06.018.

[6] B.S. Kim, S.S. Yang, J.H. Yoon, J. Lee, Enhanced bone regeneration by silicon-substituted hydroxyapatite derived from cuttlefish bone, Clin. Oral Implants Res. 00 (2015) 1–8. doi:10.1111/clr.12613.

[7] S. Kannan, J.H.G. Rocha, S. Agathopoulos, J.M.F. Ferreira, Fluorine-substituted hydroxyapatite scaffolds hydrothermally grown from aragonitic cuttlefish bones, Acta Biomater. 3 (2007) 243–249. doi:10.1016/j.actbio.2006.09.006.

[8] D. Milovac, G. Gallego Ferrer, M. Ivankovic, H. Ivankovic, PCL-coated hydroxyapatite scaffold derived from cuttlefish bone: Morphology, mechanical properties and bioactivity, Mater. Sci. Eng. C. 34 (2014) 437–445. doi:10.1016/j.msec.2014.05.034.

[9] B.S. Kim, H.J. Kang, J. Lee, Improvement of the compressive strength of a cuttlefish bone-derived porous hydroxyapatite scaffold via polycaprolactone coating, J. Biomed. Mater. Res. - Part B. 101 (2013) 1302–1309. doi:10.1002/jbm.b.32943.

[10] A. Rodriguez-Galan, L. Franco, J. Puiggali, Degradable poly(ester amide)s for biomedical applications, Polymers (Basel). 3 (2011) 65–99. doi:10.3390/polym3010065.

[11] A.C. Fonseca, J.F.J. Coelho, M.H. Gil, P.N. Simões, Poly(ester amide)s based on l-lactic acid oligomers and glycine: the role of the central unit of the l-lactic acid oligomers and their molecular weight in the poly(ester amide)s properties, Polym. Bull. 71 (2014) 3085–3109. doi:10.1007/s00289-014-1239-6.

Chapter 1

Synthetic and Marine-Derived Porous Scaffolds for Bone Tissue Engineering

Synthetic and Marine-Derived Porous Scaffolds for Bone Tissue Engineering

Ana S. Neto and José M.F. Ferreira

Department of Materials and Ceramic Engineering, CICECO, University of Aveiro, 3810-193 Aveiro, Portugal

Materials 11 (2018) 1702

doi:10.3390/ma11091702

Abstract

Bone is a vascularized and connective tissue. The cortical bone is the main part responsible for the support and protection of the remaining systems and organs of the body. The trabecular spongy bone serves as the storage of ions and bone marrow. As a dynamic tissue, bone is in a constant remodelling process to adapt to the mechanical demands and to repair small lesions that may occur. Nevertheless, due to the increased incidence of bone disorders, the need for bone grafts has been growing over the past decades and the development of an ideal bone graft with optimal properties remains a clinical challenge. This review addresses the bone properties (morphology, composition, and their repair and regeneration capacity) and puts the focus on the potential strategies for developing bone repair and regeneration materials. It describes the requirements for designing a suitable scaffold material, types of materials (polymers, ceramics, and composites), and techniques to obtain the porous structures (additive manufacturing techniques like robocasting or derived from marine skeletons) for bone tissue engineering applications. Overall, the main objective of this review is to gather the knowledge on the materials and methods used for the production of scaffolds for bone tissue engineering and to highlight the potential of natural porous structures such as marine skeletons as promising alternative bone graft substitute materials without any further mineralogical changes, or after partial or total transformation into calcium phosphate.

Keywords: Bone tissue engineering; biomaterials; bone scaffolds; additive manufacturing techniques/robocasting; marine-derived biomaterials

1. Introduction

Bone is a vascularized connective tissue responsible for the support and protection of the remaining systems and organs of the body and serves as the storage of ions and bone marrow [1,2]. As a dynamic tissue, bone is in a constant remodelling process to adapt to the mechanical demands and to repair small lesions that may occur [3]. Nonetheless, the presence of a critical size bone defect results in delayed unions or non-unions, which negatively affect the restoration of bone function [4].

One of the causes of the increase of life expectancy over the last decades is the extensive use of medical implants, among which bone substitutes are one of the most commonly used ones. Indeed, bone is the second most transplanted tissue worldwide, right after blood transfusions. The use of bone grafts for tissue repair and regeneration is not only due to the aging population, but can also be due to bone fractures, tumour resection, and bone diseases [5]. Autologous grafts are the strategy used in the majority of cases since they contain all the elements essential for bone regeneration (osteogenic cells, osteoinductive growth factors, and a matrix that supports bone adhesion and growth), and are collected in the individual, which minimize the risks of infection. However, their availability is limited and there is a risk of donor site morbidity [6,7]. Allografts emerge as an alternative to overcome the drawbacks associated with harvesting the autografts; however, they are associated with risk of infection and a high non-union rate with host tissue [6,8]. Thus, bone tissue engineering has been proposed as a promising alternative to the current bone grafting approaches. Even before Christ, several metals such as bronze and copper were used for the union of fractures. It was this type of thinking that persuaded several heath care professionals to try to introduce foreign materials into the bone tissue to compensate for bone defects and restore function [9].

A biomaterial may be defined “as any substance (other than drugs) or a combination of substances of synthetic or natural origin, which may be used for any period of time, as a whole or as part of a system which treats, tissue, organ or function of the organism”. The performance and success of biomaterials are dependent on the interactions that occur at their interface with the organism, which, in turn, are intrinsically related to the compositional and morphological properties of the material, in addition to the health status and daily activities of the individual in whom the biomaterial is inserted. All these features determine the biocompatibility of the material, which assumes that the implanted

biomaterial does not cause adverse reactions that are either toxic or carcinogenic to the individual in which it is applied [10,11].

The biomaterials employed for bone tissue engineering are mainly divided into two main groups: ceramics or polymeric materials. Each of these materials has specific advantages and disadvantages [12]. The close resemblance between the chemical composition of the inorganic part of the bone and hydroxyapatite (HA-$Ca_{10}(PO_4)_6(OH)_2$, almost bioinert) and tricalcium phosphate (TCP-$Ca_3(PO_4)_2$, resorbable) stimulated intensive research efforts to develop synthetic calcium phosphates (CaP) based bone grafts, including pure and biphasic compositions [10,11]. The discovery of the bone bonding ability of bioactive glasses through the formation of a layer of HA when exposed to physiological fluid [13] was an important milestone in the development of synthetic bone grafts. Nevertheless, these materials are brittle and exhibited unpredictable dissolution rates [14]. On the other hand, synthetic polymers have been developed with tailored characteristics; however, due to their lower bioactivity, they can be associated with a risk of rejection. Natural polymers, despite being biocompatible and enhancing cell adhesion and differentiation, have a limited supply and they exhibit poor mechanical properties and immunogenicity [15]. Bone is a composite material with an inorganic phase, HA, and an organic phase, mainly composed of collagen. Thus, the ceramic-polymer composites strategy has been widely explored by combining two different materials, thus overcoming the drawbacks of the individualised components [14–18].

The bone tissue engineering strategy involves the use of porous three-dimensional (3D) scaffolds that act as temporary supports and provide a suitable environment and architecture for bone regeneration and development [19]. Scaffolds for bone tissue engineering should have an interconnected porous structure and be highly porous with an adequate size for allowing cell adhesion and proliferation and also to ensure the diffusion of oxygen and nutrients to the cells and the removal of waste products. Moreover, the degradation rate should be similar to the formation of new tissue and the mechanical properties should match those of bone [12]. With the conventional techniques used to obtain porous scaffolds, it is difficult to have satisfactory control over the pore size, geometry, spatial distribution, and interconnectivity. These obstacles can be overcome using solid freeform fabrication techniques like robocasting, which enables precise control over the internal scaffold structure to be exerted [20]. Over the past years, significant efforts have been made towards developing scaffolds for bone regeneration,

the development of CaP scaffolds, the preparation of composite scaffolds, and the incorporation of cells and growth factors into the scaffolds.

On the other hand, natural marine materials, like corals or cuttlefish bone (CB), which possess unique and very attractive architectures, have been studied as potential materials to support bone growth [21,22]. Regarding corals, the research has mainly focused on their partial or total transformation and their posterior combination with mesenchymal stem cells (MSCs) and/or growth factors. On the other hand, CB has been explored as a biomaterial in its natural form, but also after being transformed into CaP materials, with or without the incorporation of polymers to obtain composite materials with enhanced mechanical integrity

2. Bone Tissue

Bone is a specialized, mineralized, and vascularized connective tissue that, along with cartilage, forms the skeletal system. Physically, bone acts as a support and site of muscle attachment for locomotion. The bone rigidity and hardness originating from the deposition of minerals such as CaP and carbonate inside the organic matrix in an organized functional way allows the skeleton to maintain the shape of the body and the protection of vital organs and bone marrow. In addition, the bone physiological functions include hematopoiesis, a process by which blood cells are formed, and mineral homeostasis, a reservoir for calcium, phosphate, sodium, potassium, zinc, and magnesium [1,23].

2.1. Bone Morphology

Bone tissue is composed of two main parts: a compact shell called cortical bone and a porous core known as cancellous bone [2]. Cortical bone forms the outer wall of all bones and, in the adult human skeleton, represents 80% of the skeletal mass. It is composed of repeating osteon units and, the majority of it is calcified (80 to 90% of volume). It is associated with mechanical properties and, thereby, responsible for the supportive and protective function of the skeleton. The remaining 20% of the bone is cancellous bone, made of an interconnecting framework of trabeculae where only 15 to 25% of the volume is calcified and the empty spaces that are usually filled with bone marrow are the source of undifferentiated cells. It is mainly associated with metabolic functions, but also plays a role in biomechanical functions [1,2,23]. The degree of porosity of cancellous bone

contrasts with the denser structure of cortical bone irrigated by a series of fine channels filled with blood vessels. The outer and inner bone surfaces are covered by the periosteum and the endosteum membranes, respectively, which play important roles in the nutrition of the bone tissue and supply of osteoprogenitor cells, which divide by mitosis and differentiate into bone forming cells, osteoblasts, and osteoclasts for bone formation and repair [2]. Additionally, the trabeculae and osteon units are composed of collagen and CaP crystals. The collagen fibrils include a 67 nm periodicity and 40 nm gaps between collagen molecules. The CaP crystals are embedded in these gaps between collagen molecules and increase the rigidity of the bone (Figure 1) [23].

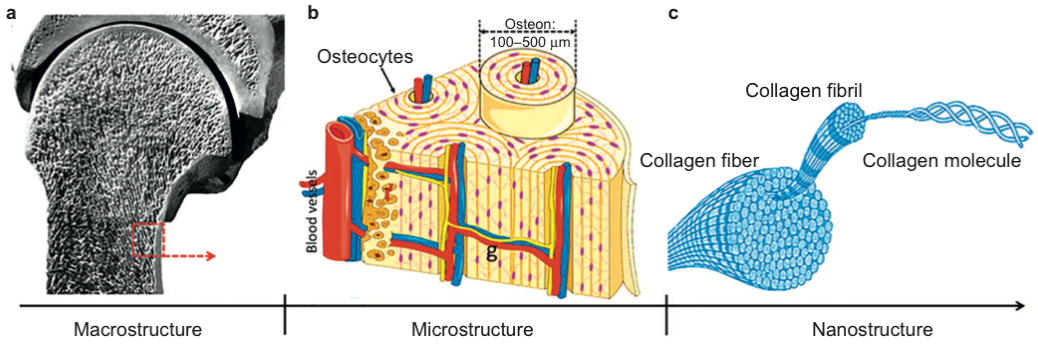

Figure 1. Hierarchical organization of bone tissue: **(a)** Macrostructure of cortical (dense shell) and cancellous bone (porous bone at both ends); **(b)** Microstructures of the osteons (20–30 concentric layers of collagen fibres, called lamellae) and trabeculae; **(c)** Nanostructures of collagen fibrils, which form the collagen fibres. The HA crystals are embedded in these gaps between collagen molecules and increase the rigidity of the bone [23].

2.2. Bone Composition

Bone tissue consists of a bone matrix (~90%) and bone cell populations (~10%), namely osteoblasts, osteoclasts, osteocytes, and bone lining cells [2]. The bone matrix is a composite material consisting of 65% mineral phase, HA, and 35% organic phase (~90% type I collagen (ColI**)**, ~5% noncollagenous proteins, ~2% lipids by weight), in addition to a residual amount of water [24,25].

2.2.1. Mineral Phase of Bone

Bone mineral consists of carbonated HA that is thin (1.5–4 nm) plate- or needle-shaped, incorporated within collagen fibrils, and orientated with the c-axis in the direction of the fibril [26,27]. The inorganic matrix material essentially consists of a carbonated calcium deficient HA (CDHA) [2]. The carbonate ions (CO_3^{2-}) might be incorporated

into the HA lattice, partially substituting the OH^- sites or the PO_4^{3-} groups to form A-type HA or B-type HA, respectively, or AB-type HA when both substitutions occur concomitantly [6]. But several other ionic impurities can be found in the inorganic matrix of biological HA, including small additions of citrate, fluorine, chorine, sodium, potassium, magnesium, strontium, zinc, iron, etc., incorporated in the crystalline lattice or adsorbed by its surface [2].

2.2.2. Organic Phase of Bone

The organic phase of bone is mainly composed of ColI; nonetheless, other proteins, the so-called noncollagenous proteins, account for ~5% of the total bone weight [28].

ColI is essential in the bone since it provides elasticity to the tissue, stabilizes the extracellular matrix (ECM), acts as a template for initial mineral deposition, and binds to other macromolecules [28]. This molecule consists of a unique triple helical molecule, forming spaces within the collagen fibrils [29]. Additionally, these spaces are aligned to form thin and extended grooves where the intrafibrillar crystals form, thereby limiting the possible primary growth of mineral crystals, forcing them to be discrete and discontinuous [26,30]. Although ColI is the most abundant protein in mature bone, other collagen types, including types III, V, and VI, are also present in the bone [26].

Bone is also composed by non-collagenous proteins. Most of these proteins are not exclusive to bone; however, some of them, such as osteocalcin (OC), osteonectin (ON), osteopontin (OPN), and alkaline phosphatase, play fundamental roles in bone [25,26,28]. Generally, some of these proteins play a structural and mechanical role and other non-collagenous proteins modulate the functions of different bone cells by interacting with their cell-surface receptors, proteases, hormones, and other biomolecules, including proteoglycans and collagens. Particularly, OC and OPN are important for fracture resistance, and in older osteonal bone, their concentrations are lower [31]. Additionally, these proteins can also regulate collagen fibril mineralization and modulate cell division, migration, differentiation, and maturation [25].

2.2.3. Bone Cells

Osteoblasts

Osteoblasts, which represent 4–6% of the total bone cells, are cuboidal cells that are accommodated in clusters along the bone surface and, therefore, do not function

individually. These cells are derived from osteoprogenitor mesenchymal stem cells of the bone marrow stroma, which are multipotent adult cells that can differentiate into specialized cells including osteoblasts, chondrocytes, and adipocytes when appropriate stimuli are applied [32–35]. Osteoblasts are responsible for the synthesis of the bone matrix and subsequent mineralization. These cells are also responsible for the synthesis of the organic matrix and regulation of calcium and phosphate fluxes [2]. Under a variety of stimuli, osteoblasts can produce diverse growth factors including insulin-like growth factors (IGF), platelet-derived growth factors (PDGF), basic fibroblast growth factors (bFGF), transforming growth factor-beta (TGF-β), and bone morphogenetic proteins (BMPs) [3,36]. The production of the bone matrix by osteoblasts (Figure 2) occurs in three successive phases: the production and maturation of the osteoid matrix and its subsequent mineralization. Firstly, osteoblasts secrete collagen proteins, mainly ColI, and non-collagenous proteins and proteoglycan which form the organic matrix. Thereafter, mineralization takes place in vesicular and fibrillar phases [3,36,37].

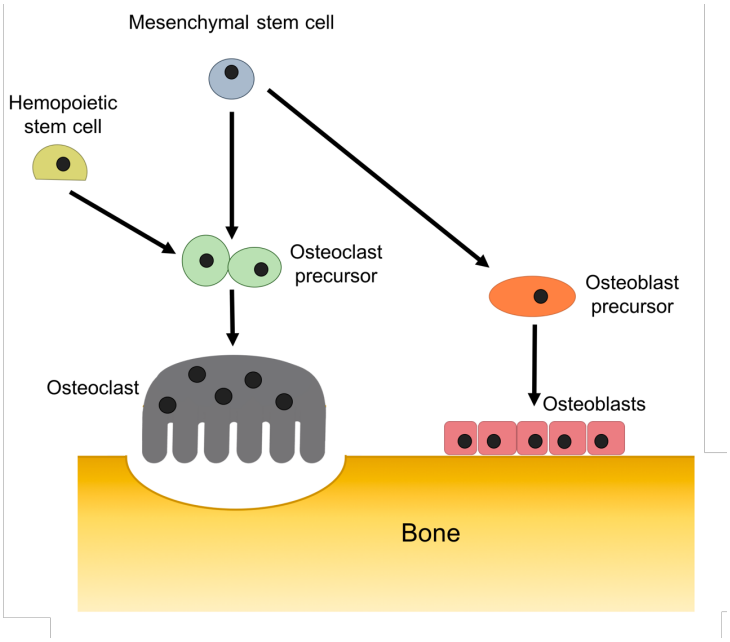

Figure 2. Evolution of osteoblasts and osteoclasts of bone.

Osteoclasts

Osteoclasts, responsible for bone resorption, are giant multinucleated cells containing one to more than 50 nuclei [1–3,36]. These cells are derived from mononuclear cells of the hematopoietic stem cells lineage, under the influence of a variety of factors (Figure 2) [38]. These cells are normally found in contact with a calcified bone surface and within a lacuna (Howship's lacunae) due to its own resorptive activity. Osteoclasts

bind to the bone surface through a process that involves the binding of integrins expressed in the osteoclast with specific amino acid sequences within proteins at the surface of the bone matrix [3]. Osteoclasts resorb bone by acidification and proteolysis of the bone matrix and HA crystals encapsulated within the sealing zone. Firstly, the process involves the mobilization of the HA crystals through the digestion of their link to collagen. Afterwards, the residual collagen fibers are digested and the residues are either internalized or transported across the cells and released at the basolateral domain [3,39].

2.2.3.3. Osteocytes

Osteoblasts have the capacity to secrete bone matrix during the differentiation process and some of them are immobilized and involved in their own bone matrix and give rise to osteocytes [40,41]. These are the most abundant cells in bone, representing 90–95% of the total bone cells [36]. These cells are responsible for the detection of microfractures and, thereby, play a crucial role in bone remodelling through the regulation of osteoclast and osteoblast activity, functioning as an endocrine cell [41]. Nevertheless, the functional activity of the osteocytes is modified with cell age. On one hand, a young osteocyte has most of the structural characteristics of the osteoblast and a low cell volume and capacity of protein synthesis. On the other hand, an older osteocyte, which is located deeper within the calcified bone, presents with a further decrease in cell volume and an accumulation of glycogen in the cytoplasm. Lastly, the osteocytes are phagocytosed and digested during osteoclastic bone resorption [41].

Bone Lining Cells

Bone lining cells are flattened osteoblasts derived from the bone matrix and their function is to control the flow of minerals between the bone tissue and the extracellular fluid and the coordination between bone resorption and formation [42].

2.3. Bone Remodeling

Bone is a dynamic tissue that undergoes constant remodelling through life. It possesses a unique self-regeneration capacity, which, in many cases, enables bone injuries and fractures to heal without scar formation by responding to metabolic needs and adapting to the mechanical stresses applied to the tissue. This process is fundamental to maintaining an adequate bone mass, appropriate mechanical properties, and the integrity of the skeleton [3,42–44].

The remodelling is a consequence of a synchronized action of osteoclasts and osteoblast cells. The cellular activity at the remodelling site is characterized by four consecutives phases that transform a resting surface into a remodelling zone: activation, resorption, reversal, and formation (Figure 3). The activation phase consists of the recognition of the lesion suffered or the mechanical requests of the osteocytes. This activation will cause the retraction of bone lining cells and the recruitment of osteoclast cells through the release of cytokines [32]. Resorption begins upon a signal that leads to the migration of partly differentiated mononuclear preosteoclasts to the bone surface, which consequently form multinucleated osteoclasts. This process is characterized by a demineralization of the bone matrix, from a process of acidification of the zone to being adsorbed, dissolving crystals of HA, and degradation of the organic part of the bone by the action of proteolytic enzymes, leading to the formation of gaps. After the resorption phase, the reversal phase takes place. During this phase, mononuclear cells prepare the bone surface for bone formation and provide signals for the recruitment of osteoblast precursor cells that will proliferate and differentiate. Once the reversal phase is completed, bone formation takes place, where osteoblasts lay down until the resorbed bone is fully replaced by new bone [3,32,42]. The formation of bone tissue occurs in two stages: bone matrix production and its mineralization. Initially, osteoblasts synthesize the osteoid that will function as a support for the deposition of the mineral phase [2]. Mineral deposition occurs between the collagen fibers, due to the conformation of the collagen molecule that acts as a nucleation agent for HA that precipitates as mineral nodules [45]. When bone formation is completed, the osteoblasts can undergo apoptosis or terminal differentiation in osteocytes or bone lining cells, concluding the remodelling process [42]. A prolonged resting period begins and lasts until the beginning of a new remodelling cycle [3].

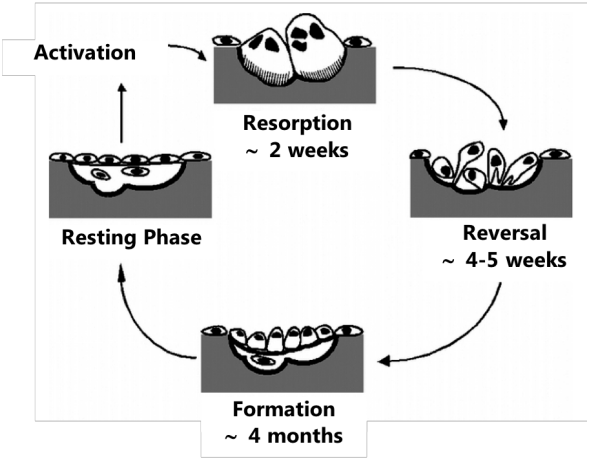

Figure 3. Bone remodelling cycle. Adapted from [1].

Importantly, in homeostatic equilibrium, bone resorption and bone formation take place in a coordinated way and, therefore, old bone is replaced by new tissue adapting to the mechanical load and strain. This homeostatic equilibrium only occurs during the first three decades. Indeed, it is precisely in the third decade when bone mass is at the maximum, and this is maintained with small variations until the age of 50. Posteriorly, resorption predominates and bone mass starts to decrease [3,40,43].

3. Bone Grafts

3.1. Evolution of Life Expectancy and the Need of Bone Grafts

The human life expectancy at birth has remarkably increased, especially since the mid-1800s, and has continued to rise during the following century [46]. There has been an impressive gain of about 30 years in life expectancy in western Europe, the USA, Canada, Australia, and New Zealand and even larger gains in Japan and some western European countries, such as Spain and Italy. This trend is consensually attributed to a complex interplay of advances in medicine and public health, coupled with new organization modes at different societal levels, including economic-, political-, and behavioral-related changes [47]. Indeed, improvements in medicine are often pointed out as the most impacting factor responsible for the gains in human life expectancy [48]. However, it is worth mentioning that the earlier industrial revolution and the innovations in agricultural production and distribution enabled nutritional diversity and consistency for large numbers of people and are also seen as other important driving factors for lowering mortality [45]. In this regard, the former infectious leading causes of death

(infectious and parasitic diseases) were gradually replaced by degenerative diseases such as cancers and diseases of the circulatory system, dramatically decreasing the risk of dying at earlier ages and postponing death to old ages [49].

The fantastic improvements in human life expectancy, behavioural nutrition, and physical activity came together with serious consequences in the function of the entire human musculoskeletal system, including: (i) the loss of bone mass or density due to decreasing contents of calcium and other minerals by osteoporosis, resulting in the increased brittleness and breakage of bone. This problem is commonly observed with a higher incidence in women after the menopause; (ii) increased incidence of degenerative diseases such as osteoarthritis in which the joints become stiffer and less flexible and the cartilage may begin to rub together and wear away concomitantly with a decrease of the synovial fluid in the joints and the eventual deposition of minerals (calcification). This bone joints breakdown may also lead to inflammation, pain, stiffness, and deformity. There is also an increased incidence of bone tumor resections; (iii) the decrease of the cushioning effect exerted by the gel-like invertebral disks in the spine because they gradually lose fluid and become thinner, resulting in shrinkage of the trunk and in a consequent overall height decrease; (iv) increased rate of teeth loss or extraction and the need to maintain a dense and healthy jaw through bone augmentation to prevent its natural deterioration; (v) increased incidence of serious trauma injuries associated with lifestyle changes (participation in sports); and (vi) the refusal of the public to tolerate the slightest limitation in mobility.

The presence of these pathological conditions (critical-size defects) is intrinsically related to an insufficient blood supply which impairs proper revascularization and negatively influences bone differentiation. Together, these events result in delayed unions or non-unions. As a consequence, there is a requirement for the bone grafts substitutes, that when accepted by the body provide a suitable framework for the growth of new living bone [50,51]. As the native bone grows, it gradually replaces the graft material, resulting in a fully integrated region of new bone.

3.2. Ideal Bone Graft

An ideal bone graft should provide osteointegration, osteconduction, osteoinduction, and osteogenesis [52]. Osteointegration is the ability to have a structural and functional connection between the living bone and the surface of the graft, and in this way, the formation of fibrous tissue does not take place at the bone-implant interface [52–54].

Osteoconduction is a characteristic by which bone grows on the surface of the graft [52,53]. Osteoinduction, is the ability of primitive, undifferentiated, and pluripotent cells from the surrounding host tissue to develop osteoprogenitor cells followed by the production of osteoblasts [51–53]. Osteogenesis is the capacity to produce new bone by osteoblasts present within the bone graft [51,52].

The most common sources of bone grafts include autografts, allografts, xenografts, and natural or synthetic bone graft substitutes [55]. These different bone grafts and their respective virtues and disadvantages are described in the following section.

3.3. Autografts

Autografts remain as the gold standard, constituting approximately 58% of bone grafts [5,51,56]. They can be harvested from non-essential bones of the patient, such as the iliac crest (the most common source), fibula, or metaphyses of long bones. Autografts for dental procedures are typically harvested from the jaw, hard palate, or the chin. If there is not enough bone available in these areas, the tissue graft may be taken from the hip or shinbone [7,56,57]. Autografts are known to be an optimal option with osteoinductive, osteogenic, and osteoconductive properties. Fresh autografts contain all the elements essential for bone regeneration, like the preservation of the trabecular architecture, and the presence of viable cells and growth factors (BMP-2 and -7, bFGF, IGF, and PDGF). In this way, autografts are rapidly incorporated into the host site which lacks immunogenicity [7,51,55]. The periosteum and nutrient artery are generally harvested with the piece of autologous bone and blood vessels that can be anastomosed to the blood vessel at the recipient site. Once the transplanted bone is secured into its new location, it generally restores the blood supply to the bone in which it has been attached. Despite the advantages, the use of autografts implies additional surgery, with a donor-site morbidity related to blood loss, wound complications, local sensory loss, and chronic pain [51,52]. Besides the limited availability, autografts require additional surgical time and costs. Therefore, other bone graft options should be considered [51,52,55,56].

3.4. Allografts

The drawbacks associated with the use of autografts can be overcome by the use of allografts, which in turn represent about 34% of bone substitutes [56]. Allografts are derived from humans, like autografts; however, they are harvested from an individual other than the one receiving the graft [51]. Different sources can be used, and they can be

harvested from cadavers of human individual donors who donate their bodies for the benefit of science. A multi-organ donor is another source of bone, which is associated with the long bones acquired under a sterile condition in the operating theatre after organ explantation. They can also be sourced from people who are in need of repairing and regenerating bone defects and in which the most common source is the femoral head of a patient undergoing a hip replacement. Before the use of any allograft, the donor must be thoroughly screened to ensure that no infectious diseases are present. Nevertheless, there is always a risk of the transmission of an undetected viral or bacterial disease [8,58]. Allografts can be applied as structural forms or as bone chips. Additionally, they can be processed as mineralized or demineralized, fresh, fresh-frozen, or fresh-dried forms. Allografts have osteoinductive and osteoconductive properties; however, they also have lower osteogenic potential due to the absence of viable cells [8,51,55]. Complications linked with allografts include infections, a high non-union rate with host tissue, and fracture [51,52].

3.5. Xenografts

Xenografts are another alternative to autografts. This type of bone graft is harvested from non-human species, commonly from pigs, cows, and horses. The first bone graft procedure dating from 1668 was allegedly performed by the Dutch surgeon Job Van Meekeren, who harvested a bone derived from a dog's cranium and implanted it in a soldier's skull to successfully repair a traumatic defect [59]. In this regard, due to the large quantity of donors, xenografts may be more readily available and less expensive. Nevertheless, the potential transmission of bioactive material that causes diseases or rejection in the host remains as a threat. Many studies have attempted to investigate protocols that might be suitable for eliminating bioactive components such as heterologous cells, xeno-antigens, and DNA material, while preserving those that are essential for the proper functioning of ECM such as collagen helical macromolecules and water absorbing proteoglycans [60,61]. The adverse consequences of the decellularization process on the natural organization and physiological functionality of tissues intended as bio-inspired scaffolds have been addressed by several authors [62–66]. In order to avoid unfavourable immune responses, xenografts require a more sterile process, which can result in a loss of osteogenic and partly osteoinductive properties [51,67]. An alternative approach to prepare safe xenografts for bone regeneration involves chemical and thermal treatments in order to remove all the organic substances

from fresh animal bones. Sang-Hoon Rhee, et al. [68] patented a method for preparing safe bovine-derived hone graft substitutes, which do not have the risk of infection with bovine spongiform encephalopathy. The method comprises treating bovine bone with sodium hypochlorite, followed by a heat treatment at temperatures within the range of 600–1000 °C. The organic substances are burned out and the resulting bone graft substitute does not cause an immune response. The patent is associated with a commercial product (Geistlich Bio-Oss®, Switzerland), which has allegedly been documented in more than 900 publications [69,70]. Other similar porcine- and bovine-derived commercial bone graft materials are available. Some examples are the products under the trade names of Symbios®, Switzerland, Endobone®, United States of America, and Straumann® XenoGraft, Switzerland [71].

Despite this, several concerns still persist in relation to the use of bone grafts to face all the health problems derived from aging, trauma, and degenerative diseases, leaving room for an increasing search for alternative synthetic bone substitutes [72].

4. Bone Tissue Engineering

The shortcomings of bone grafts and the need to face all the health problems originating from aging, trauma, and degenerative diseases are the main driving forces for developing new synthetic biomaterials. Other stimulating reasons for the recent boom in the development of new synthetic biomaterials and implantation devices include: (i) increasing awareness among patients and doctors of the numerous co-morbidities associated with autograft harvesting; (ii) the elevated regulatory scrutiny and recalls imposed on allograft tissue banks for distributing human bone and soft tissue products that were improperly screened for infectious diseases; and (iii) the recent developments in surgical procedures and materials that allow new procedures to be available. Accordingly, a wide variety of synthetic bone substitutes have been developed and employed over the past 50 years, contributing to the actual market trend for shifting away from autografts to bone graft substitutes, and from cadaveric allografts to synthetics [71].

Bone tissue engineering is a multidisciplinary field that applies the knowledge of bioengineering, biology, cell transplantation, and material science to create new biomaterials that will interact with biological systems to treat, strengthen, and, thereby, regenerate damage tissues and restore their function, instead of replacing them [12,73]. Normally, it involves the use of porous 3D scaffolds that, along with cells and bioactive

factors, provide structural support for cells to spread, migrate, multiply, and differentiate, and for new tissue to be formed [12,74]. In this way, scaffolds act as a temporary ECM inducing the natural processes of tissue regeneration and development [75].

4.1. Biomaterials for Bone Tissue Engineering

Biomaterials have evolved through three generations. The first generation of biomaterials was developed during the 1960s and 1970s and was intended to provide adequate functional properties without causing harmful effects on the host. This generation of biomaterials was not specifically developed for medical use and consisted of widely available industrial materials like elastomeric polymer and silicon rubbers. Their selection was based on their bioinertness and suitable physical properties. With the emergence of the first generation of biomaterials, tens of millions of individuals had their quality of life improved in 20 years. The goal of the second generation of biomaterials was to shift from a completely bioinert reaction to the production of materials that could induce a controlled reaction with the host tissue in order to have a therapeutic effect and hence have a bioactive behaviour. This generation of materials is associated with the development of resorbable biomaterials in which the degradation rates could be adjusted to the desired applications. In this way, the implanted material could be degraded into a soluble and non-toxic product by the host, consequently eliminating the interface between the implanted site and the host tissue. These materials are in clinical use in fields like orthopaedic and dental surgeries, in localized drug release applications, and in cardiac assist devices. The third generation of biomaterials has the objective to support and stimulate the regeneration of functional tissue, thereby inducing cellular responses at the molecular level by using two routes, tissue engineering and in situ tissue engineering. These approaches involve the use of scaffolds, cells, and growth factors and have already been responsible for the successful replacements of damaged skin, cartilage, bladders, corneal epithelium, and trachea [11,76,77].

The field of biomaterials for bone tissue engineering is constantly evolving. These biomaterials can be subdivided into organic polymers, which can be subdivided according to their synthetic or natural source, and inorganic materials, such as CaP and bioactive glasses. By combining the former materials, it is possible to form composites [12,78,79].

4.1.1. Organic Materials

Polymer materials are extensively used in tissue engineering. They can be divided into natural and synthetic polymers.

Natural Polymers

Natural polymers constitute the native ECM and, thereby, have an excellent biocompatibility and a low immunogenic potential. They are bioactive as they have the capacity to interact with the host's tissue. Their structure is organized and comprises ligands that can be bound to cell receptors [18,80,81]. Although, in some cases (e.g., chitosan and starch), their source is almost unlimited, most of them lack a high enough quantity. These polymers are difficult to process and their degradation behaviours change from patient to patient since degradation involves enzymatic processes [81].

Collagen is the main component of ECM and, therefore, has an inherent biocompatibility, non-cytotoxicity, and non-inflammatory reaction. It has functional groups that improve cell adhesion and proliferation. This natural polymer, despite having a lower mechanical property, has a stable structure related to covalent cross-linking among the collagen fibrils. Moreover, it can be processed into different forms, powders, sponges foams, sheets, fibres, membranes, films, and injectable viscous solutions. However, collagen has a bath-to-bath variation in terms of physicochemical and degradation properties and is associated with a relative risk of infection [80,81]. Gelatin is a denatured protein of collagen and, thereby, has a relatively low antigenicity. It is a biocompatible and bioresorbable polymer with arginine-glycine-aspartic (RGD) sequences in its structure, the recognition sites of integrins, which mediate cell-cell and cell-ECM interactions and, consequently, improve cell adhesion. Moreover, its functional groups are more accessible, enabling chemical modifications. Despite all the advantages, gelatin has a limited mechanical strength and, normally, is combined with other polymers or ceramic materials to improve the mechanical properties [82].

Chitosan, the deacetylated chitin derivative, is a natural polymer with interesting properties for biomedical applications due to its biocompatibility, biodegradability, low toxicity, non-immunogenicity, and intrinsic anti-bacterial nature. This polymer enables cell adhesion and proliferation and, in addition, supports the formation of the bone matrix. As collagen, it can be processed into different forms. The degree of degradation can be adjusted regarding the degree of deacetylation [80,81].

Alginate, a polymer obtained from brown algae, has been widely used in the biomedical field. It has an exceptional biocompatibility, biodegradability, and non-toxicity. It is not an expensive polymer and is available in abundance. Alginate is a polymer that that can be easily modified, and, for instance, alginate gels produced through cross-linking with calcium, can be introduced through a minimal invasive procedure. Some drawbacks are associated with alginate like the slow degradation rate and inappropriate mechanical integrity that precludes long-term biomaterial implants.

Hyaluronic acid, obtained from the ECM of all connective tissue, exhibits good biocompatibility, immunoneutrality, and viscoelasticity [80,81]. It is beneficial for bone regeneration [83].

Synthetic Polymers

Synthetic polymers can be obtained under controlled conditions and, thereby, have a predictable batch-to-batch uniformity with reproducible and adjustable physicochemical properties (e.g., mechanical behaviour and degradation rate). Synthetic polymers enable tailoring the shape, porosity, and pore size, and incorporating chemical functional groups that improve tissue growth [80]. Normally, the degradation of synthetic polymers occurs through a hydrolysis process and, in this way, it does not vary between hosts [84]. In some cases, synthetic polymers are combined with natural polymers to improve cellular adhesion due to the presence of ligands that can bind to cell receptors in natural polymers [85,86].

Polyesters are the most used polymers in the field of bone tissue engineering and include poly(glycolic acid) (PGA), poly(lactic acid) (PLA), poly(lactic-co-glycolide (PLGA) (which is a copolymer of PGA and PLA), and poly(ε-caprolactone) (PCL). Polyesters can be dissolved in organic solvents, with the exception of PGA, which is only soluble in highly fluorinated solvents due to its highly crystalline structure. These polymers are biocompatible and the by-products originating from degradation are glycolic acid and lactic acid, which are natural metabolites and, therefore, not harmful to the human body. Nevertheless, these by-products can reduce the local pH and, consequently, may induce an inflammatory reaction [80,81]. PGA has a short degradation period (from four to 12 months) and high values of tensile strength and modulus of elasticity. On the other hand, due to its hydrophobicity, the degradation rate of PLA is between 12 months and two years. The low values of PLA tensile strength and modulus of elasticity can be improved by the use of copolymers of lactic acid and glycolic acid

like PLGA [81,84]. PCL has a degradation rate slower than the other polyesters, and can reach 24 months. An improvement of this degradation rate can be achieved by a co-polymerization process. Additionally, PCL is biocompatible and exhibits suitable mechanical properties for bone tissue engineering.

In comparison with polyesters, polyamides exhibit better mechanical and thermal behaviour, but they take a long time to degrade in the human body. In this regard, poly(ester amide)s have received particular attention, since they can combine the biodegradability of polyesters and the mechanical and thermal behaviour of polyamides [87,88]. Alternatively, poly(ester urea)s have been explored in the field of tissue engineering since they are non-toxic and the degradation rate and the mechanical properties can be adjusted. Moreover, the versatility in the functionalization of these polymers can be beneficial in designing a scaffold for bone tissue engineering [89,90].

Poly(propylene fumarate) (PPF) is an unsaturated linear polyester that, upon degradation, forms propylene glycol and fumaric acid, products that are biocompatible and easily removed from the body. The mechanical properties can be improved via cross-linking through the fumarate double bond or via thermal or photo cross-linking through the active double carbon chain, and in this case, also the degradation rate can be tailored [80,81]. PPF is in liquid form before cross-linking, which allows it to be injectable and, consequently, to be suitable for orthopaedic implants in minimal invasive procedures.

Polyanhydrides are biocompatible degradable polymers with good properties of drug-controlled release. Nevertheless, they lack appropriate mechanical properties for load-bearing applications. To overcome this drawback, polyanhydrides are copolymerized with polyamides with surface-eroding properties [80,81] or alternatively become photo cross-linkable and injectable [81].

Polyurethanes started to be particularly explored as a biomaterial for bone tissue engineering in the past two decades, since when adequately designed, these polymers enjoy a set of interesting properties, including non-cytotoxicity, biocompatibility, biodegradability, and the capacity to promote in vivo calcification. They can be applied as injectable void fillers, drug delivery systems, scaffolds, and shape memory materials due to their capacity to vary from hydrophobic to hydrophilic, and from rigid to flexible, or to exhibit thermoplastic to thermosetting behaviours [91].

4.1.2. Inorganic Materials

CaP, such as β-TCP and HA, and bioactive glasses have been explored as bone substitute biomaterialsdue to their chemical and structural similarity to the mineral component of bones and teeth.

Calcium Phosphates

CaP materials (Table 1) can be found in various forms from thin coatings in metallic implants, improving their biocompatibility for temporary structures that are replaced by new bone. They can be produced in large quantities, with a relatively low-cost. In addition, CaP are stable and, therefore, are available off-the-shelf [27,92].

Table 1. Main calcium orthophosphate compounds [27,92–95].

Compound	Formula	*Ca/P* Molar Ratio	Mineral	Symbol
Monocalcium phosphate anhydrous	$Ca(H_2PO_4)_2$	0.50	—	MCPA
Monocalcium phosphate monohydrate	$Ca(H_2PO_4)_2 \cdot 2H_2O$	0.50	—	MCPM
Dicalcium phosphate anhydrous	$CaHPO_4$	1.00	Monetite	DCPA
Dicalcium. phosphate dihydrate	$CaHPO_4 \cdot 2H_2O$	1.00	Brushite	DCPD
Octacalcium phosphate	$Ca_8H_2(PO_4)_6 \cdot 5H_2O$	1.33	—	OCP
Amorphous calcium phosphate [1]	$Ca_XH_Y(PO_4)_Z \cdot nH_2O$	0.67–1.50	—	ACP
α-Tricalcium phosphate	$\alpha\text{-}Ca_3(PO_4)_2$	1.50	—	α-TCP
β-Tricalcium phosphate	$\beta\text{-}Ca_3(PO_4)_2$	1.50	—	β-TCP
Calcium-deficient hydroxyapatite [2]	$Ca_{10-x}(HPO_4)_x(PO_4)_{6-x}(OH)_{2-x}$	1.5–1.67	—	CDHA
Sintered hydroxyapatite	$Ca_{10}(PO_4)_6(OH)_2$	1.67	Hydroxyapatite	HA
Tetracalcium phosphate	$Ca_4(PO_4)_2O$	2.00	Hilgenstockite	TTCP

HA and β-TCP are two of the most used CaPs. HA is one of the most stable phases under physiological conditions and has a low solubility and, consequently, a slower resorption rate. Traditionally, HA is prepared in aqueous precipitation by mixing adequate quantities of Ca^{2+} and PO_4^{3-} containing solutions at a pH above 9, followed by filtration, drying, and sintering. The as-synthesized HA is poorly crystalline and often non-stoichiometric. On the other hand, β-TCP is a high-temperature phase, which is only prepared at temperatures above 800 °C. However, it is important to note that, for temperatures approximately above 1125 °C, β-TCP transforms into a high-temperature phase α-TCP. When compared with HA, β-TCP is more soluble and has a lower mechanical stability [85,86]. Therefore, an optimum balance is often achieved by combining the more stable HA phase and a more soluble β-TCP phase to obtain biphasic CaP (BCP). This combination leads to materials with controlled bioactivity and a more

appropriate balance between resorption/solubilisation, which guarantees the stability of the biomaterials while promoting bone ingrowth [87,88].

Since CaPs are similar to the mineral phase of bone, they are recognized as biocompatible, a material not foreign to the body, and also non-toxic. Importantly, CaPs exhibit a bioactive behaviour and are integrated into the body by processes that are equal to those of bone remodelling, leading to an intimate physicochemical bond between the biomaterial and bone. Moreover, CaPs are known to be osteoconductive and support cell adhesion and proliferation [93]. The main drawback associated with CaP biomaterials is their poor mechanical properties. Namely, their brittle nature, with a low fracture strength, represents a main concern in high load-bearing applications [27,79,92,93]. This brittle nature is associated with high-strength ionic bonds and can be manipulated by composition, crystallinity, grain size, and grain boundaries, as well as by porosity [92].

The crystalline structure of CaPs enables the incorporation of trace amounts of certain ions existing in bone composition [96]. It is recognized that the incorporated ions like strontium (Sr) [97–100], magnesium (Mg) [98,100], manganese (Mn) [7,99,100], or zinc (Zn) [101,102] in a single or combined manner, play fundamental roles in bone development. Sr is present in bone in considerable amounts and, in particular, at regions of elevated metabolic turnover [96,100]. Its presence is associated with the increase of osteoclast apoptosis and the enhancement of osteoblastic cell proliferation and collagen synthesis, which subsequently maintain bone formation and inhibit bone resorption [97,98]. Mg is related to the mineralization of calcified tissue, and its amount starts to be higher and then decreases during the calcification process. Further, this ion influences bone metabolism as it plays a role in osteoblast and osteoclast activity [96]. The incorporation of Mn exerts positive effects on bone growth as it promotes cell adhesion due to the fact that in the presence of Mn, there is an increase of the ligand-binding affinity of integrins, which are receptors that mediate the interaction between cells and the ECM and activate cell adhesion [100]. Zn, in a similar way as Mg, promotes bone formation and its deficiency in the body is associated with a decrease of bone density. Furthermore, Zn influences the crystallinity and morphology of biological apatite crystals [101,103].

4.1.3. Composite Materials

Hard tissues, like bone, should be able to support the load and when compared to soft tissues, should be stiffer and stronger. Thus, in most cases, instead of polymers, ceramics and metals have gained more attention. Nevertheless, some important drawbacks are

associated with these two materials. Ceramics are more brittle and, in some cases, stiffer than bone; and metals are considerable stiffer than the bone. On the other hand, despite being more ductile, polymers do not normally exhibit enough stiffness for bone graft applications [104].

With this in mind, composite materials have been widely explored in the bone tissue engineering field since they combine at least two different materials in order to obtain bone graft substitutes with improved functionalities in terms of mechanical and osteoconductive properties.

This section will be focused on composites that combine ceramics and polymers, and despite recognizing that the resulting composite scaffolds can be obtained by mixing ceramic powder with a polymer solution and using different manufacturing techniques [17,105,106], by depositing ceramics onto polymers [17,107,108], or by the deposition of polymers onto ceramics [17,109–113], only the last one will be reviewed here.

Motealled et al. [109] produced 45S5 bioglass scaffolds by robocasting and studied the effect of their coating with natural (gelatin, alginate, and chitosan) or synthetic (PCL or PLA) polymers on the mechanical and in vitro bioactivity and degradation behaviour. The chitosan coating was highlighted for its mechanical and biological properties. The incorporation of this polymer enabled mazimixing the compressive strength and toughness (strain energy density). An improved bioactivity of the 45S5 scaffolds, translated by an accelerated formation of an apatite surface layer, was also registered in the presence of the chitosan coating. In addition, there was a decrease in the degradation rate of the majority of the coatings, and a consequent positive impact on the evolution of their mechanical properties. Shi et al. [113] produced a β-TCP scaffold through the polymeric sponge replication method and aimed to improve the mechanical properties of the scaffolds by coating them with PCL. It was observed that PCL addition significantly improved the compressive and bending strength, with the highest value being registered for the scaffolds containing 40% of β-TCP and 5% of PCL. Furthermore, the presence of PCL did not compromise the osteoblast cells' proliferation and differentiation. The reinforcement of BCP scaffolds with not only PCL, but also with HA particles of different sizes and morphologies, was studied by Roohani-Esfahani et al. [112]. The produced BCP scaffolds were subsequently coated with PCL and nano (needle shape) or micron HA. The PCL coating enhanced the compressive strength of BCP scaffolds from 0.1 ± 0.05 MPa to 0.29 ± 0.07 MPa and 2.1 ± 0.17 MPa when using micro or nano HA particles, respectively. Moreover, among all the scaffolds, those coated with needle-shaped HA and

PCL exhibited the strongest osteoblast differentiation and the highest alkaline phosphatase (ALP) activity, and an upregulation of osteogenic gene expression, namely runt-related transcription factor 2 (Runx2), ColI, OC, and bone sialoprotein. Apart from the former advantages, the polymer coating on ceramic scaffolds has also been widely used for drug delivery systems. For instance, Li et al. [110] coated 45S5 scaffolds with a solution containing poly(3-hydroxybutyrate-*co*-3-hydroxyvalerate) (PHBV) and vancomycin, an antibiotic used for infections that occur during bone disease treatment. The authors observed that the polymer coating improved the compressive strength and mechanical stability, while not negatively affecting the in vitro bioactivity. A sustained and controlled drug release was observed in the coated scaffold (99.9% in six days), contrary to what was observed when the drug was directly adsorbed on the 45S5 scaffold (99.5% in three days). The thickness and structure of the polymer coating can be dependent on the texture of the scaffold material, particularly on the specific surface area (SSA). Canal et al. [111] studied the influence of the previous parameters on the Simvastatin acid (SVA) release, a component that despite being used for the cholesterol treatment, is also known to stimulate osteogenesis by the up-regulation of BMP-2 expression. In this regard, β-TCP and CDHA scaffolds were coated with polycaprolactone-co-polyethyleneglycol (PCL-co-PEG) loaded with SVA. A low pressure plasma process was used, allowing the coating of inner regions of the scaffolds up to a certain depth. The work was divided into two parts: firstly, CaP discs were used to characterize the polymeric layer; in the second part, the release profiles of SVA from the coated CaP scaffolds were studied. The polymer layer on the β-TCP was about two times thicker in comparison to that on the CDHA, with the difference being attributed to a much higher SSA of CDHA (~33 times). Although the plasma coating of the polymer loaded with SVA had been beneficial for controlled drug release in the case of CDHA scaffolds, the thicker polymer coating on β-TCP tended to hinder the SVA release. On CDHA scaffolds, 90 min of continuous wave plasma discharges treatment blocked the drug release in the first 1.5 h and allowed a slow diffusion over 11 days. Reducing the treatment to 20 min enabled the slow release process to start from the beginning of the experiment.

4.2. Scaffolds for Bone Tissue Engineering

A wide variety of biomaterials and manufacturing techniques have been explored to produce a scaffold able to regenerate the bone. When designing an ideal scaffold for bone

tissue engineering, some important characteristics should be considered: (i) firstly, the scaffold must be biocompatible. It should have the ability to support cell adhesion and proliferation on the surface and through the scaffold, without any negative effect on the host tissue, which may lead to reduced healing or cause rejection by the body [114]; (ii) the underlying premise of bone tissue engineering is to allow the replacement of the implanted scaffold by the ECM over time. In this regard, the scaffolds must be biodegradable and preferably able to degrade at a similar rate to bone formation. The by-products originating from the degradation process should be non-toxic and removed from the body without interference with other organs [12]; (iii) the scaffolds must have a highly interconnected porosity for successful bone growth and vascularization. Nowadays, it is recognized that a hierarchical porosity from macro- to nanoporous is beneficial for the development of new bone tissue [56,115]. Scaffolds with a pore size between 200 and 350 μm have been revealed to be optimal for bone growth. This allows cell infiltration and, subsequently, the formation of ECM, as well as the diffusion of nutrients and oxygen and the removal of waste products [114]. The presence of micro and nano porosity plays a fundamental role in cell attachment, biomineralization, and in vivo osteointegration [115]; (iv) an ideal bone scaffold should have mechanical properties that match the host bone properties and should be strong enough to allow surgical handling during implantation. Importantly, bone scaffolds must maintain their integrity from the time of implantation to the end of the remodelling process. The healing rate significantly changes with age, which should be considered when designing the scaffolds. Fractures from young individuals normally heal in approximately six weeks and mechanical integrity returns one year after fracture; however, in elderly people, this bone regeneration slows down. Furthermore, it is known that the enhancement of mechanical properties often occurs with the detriment of highly interconnected porous scaffolds. An implanted scaffold with good in vitro potential is likely to fail in vivo if the vascularization capacity is insufficient. With this in mind, it is essential to maintain a balance between mechanical properties and porous structure upon designing a successful scaffold [12].

5. Scaffold Fabrication Techniques for Bone Tissue Engineering—Robocasting

As previously mentioned, several aspects should be taken into consideration when designing a scaffold for bone tissue engineering, namely the porosity at different dimensions to allow cell adhesion and proliferation, but also vascularization for

subsequent bone growth. Mechanical properties are also fundamental to providing an adequate mechanical support for bone repair and regeneration. Having close control over the pore size, geometry, spatial distribution, and interconnectivity is difficult when using conventional fabrication techniques to produce porous scaffolds (e.g., freeze drying, chemical/gas foaming, melt molding, phase separation, fiber meshing, supercritical-fluid technology, and solvent casting in combination with particulate leaching) [20,77,116]. These obstacles can be overcome using additive manufacturing (AM) techniques, which enable the production of scaffolds with precise control of the internal scaffold architecture, without the need for subsequent machining [20,79,116]. Solid freeform fabrication, rapid prototyping, and 3D printing are some of the AM techniques that have been reviewed in detail elsewhere [19,20]. AM technologies enable the creation of complex 3D layer-by-layer structures directly from a computer-aided design (CAD). Alternatively, AM technologies enable using data from computerized tomography or magnetic resonance image medical scans to create CAD models that are then converted into STL-files. By using these STL-files, it is possible to match the scaffold's external shape to the damage tissue site [20,77,116]. Along with the important advantage previously mentioned, AM techniques do not require many process steps and include little manual interaction [77].

Robocasting is one of the AM techniques that allows researchers to build scaffolds using a concentrated colloidal suspension (ink/paste) with neglible contents of organic additives without the need for a sacrificial supporting material [116,117]. Robotic deposition of a continuous filament capable of fully supporting their own weight takes place through a nozzle during the assembly layer-by-layer. To prevent non-uniform drying during assembly, during the fabrication process, the process of deposition is conducted within a non-wetting oil bath (Figure 4) [116,118,119].

The colloidal inks developed for robocasting require careful characterization and must satisfy two important criteria. Firstly, the ink must exhibit a well-controlled viscoelastic response so that it yields upon extrusion, but sets immediately upon deposition, to facilitate shape retention. Second, the ink must have a high colloidal volume fraction to minimize drying-induced shrinkage after assembly. In other words, the particle network must be able to resist compressive stress arising from capillary tension and, therefore, the extruded filaments can retain their shape across unsupported spans, and the subsequent layers do not cause the layers beneath to significantly yield and deform. These criteria require suitable control over the colloidal forces to first generate a

highly concentrated stable suspension and then induce a dramatic change in the rheology of the system that promotes a fluid-to-gel transition [117,120].

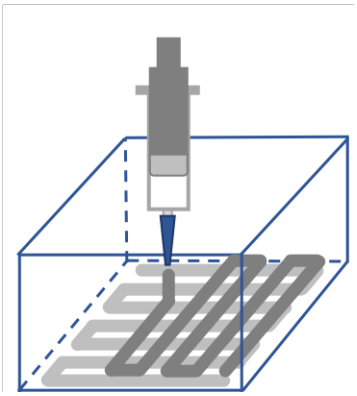

Figure 4. Schematic representation of the robocasting fabrication process. The ceramic scaffold is built layer-by-layer from a CAD model. The three-axis robotic arm moves the injection syringe while expressing the ceramic ink through the conical deposition nozzle to create the desired structure immersed in an oil bath.

Porosity in robocasting can be tailored on macro- (greater than 100 μm), micro- (1–30 μm), and submicron (less than 1 μm) scales. Macroscale porosity is introduced directly by the robocasting process as it draws successive layers. Robocast filaments arranged in latticed patterns create macroporous pathways in three dimensions. By varying the rod spacing and size, these pathways can be precisely constructed to produce highly uniform macropores. By incorporating porogen microspheres into the suspension prior to extrusion, it is possible to create micropores. With a suitable volume fraction of microspheres, the microporosity is interconnected. Lastly, the submicron porosity can be controlled by varying the temperature profile at which the produced scaffolds are sintered [120].

Due to all of the advantages of robocasting, this technique has been widely explored for the production of scaffolds in the field of bone tissue engineering. For instance, Miranda et al. [121] obtained β-TCP and HA scaffolds by robocasting. In order to achieve the ink for printing, the powder was firstly dispersed in distilled water containing a suitable amount of dispersant to obtain a highly concentrated suspension. Hydroxypropyl methylcellulose was subsequently added to increase the viscosity and an ink with the desired viscoelastic properties was obtained upon the addition of a flocculant agent like polyethylenimine. HA scaffolds were demonstrated to have a better compressive strength than the β-TCP scaffolds and this performance was emphasised upon the immersion for three weeks in simulated body fluid (SBF). Recognizing the advantages of a BCP

material, Houmard et al. [119] reported the production of pure HA and two biphasic compositions (60HA/40 β-TCP and 20HA/80β-TCP) by robocasting using water-based Pluronic inks. The mechanical strength varied between 3 and 50 MPa according to the porosities, which varied from 80 to 25 vol.%, respectively, and also according to the rod size, in which thinner rods improved the mechanical properties. Furthermore, mechanical properties were also dependent on the composition, where HA exhibited the highest values and 60HA/40β-TCP the lowest. No evident degradation of the scaffolds in SBF or water was observed, despite a slight increase of Ca and P ions in water being recorded after five months. Using a similar procedure to obtain the ink for printing as Miranda et al. [121], Marques et al. [122] produced undoped and doped strontium and silver BCP scaffolds by robocasting. They studied different pore sizes and demonstrated that the mechanical properties were intrinsically correlated with the porosity fraction. Furthermore, the presence of doping elements improved the mechanical strength and cell proliferation and were effective in terms of the antimicrobial activity against *Staphylococcus aureus* and *Escherichia coli*. On the other hand, the incorporation of MSCs, as well as growth factors, into porous scaffolds enhanced bone formation and with this in mind, Del Rosario et al. [123] studied the effect of the incorporation of BMP-2, PDGF, and rat MSCs (rMSCs) in a β-TCP scaffold obtained by robocasting. BMP-2 was incapsulated in PLGA microspheres to allow a more sustained release and PDGF, in which the goal is to act in the first stages of bone repair, was crosslinked with alginate and formed a thin layer. The scaffolds exhibited a good cell viability and biocompatibility in vivo. A release of approximately 90% of BMP-2 and 80% of PDGF was observed after three weeks and two days, respectively. Nevertheless, there was no beneficial effect upon a dual delivery of BMP-2 and PDGF or upon the combination of BMP-2 and rMSCs. Aiming at producing composites from polymers and CaP, Hong et al. [124] and Maazouz et al. [125] developed PCL/HA and gelatine/HA scaffolds, respectively. Hong et al. [124] produced a composite scaffold with a PCL/HA ratio of 1. A lower cell adhesion on the composite scaffolds was observed when compared to a conventional cell seeding technique; nevertheless, the adhered cells remained viable. Moreover, it was demonstrated that the composite scaffolds stimulate osteogenic differentiation. Indeed, when compared with scaffolds of pure PCL, the PCL-HA scaffolds, there was an increase of ALP activity of rat bone marrow stromal cells (rBMSCs), as well as an up-regulation of the expression of bone-associated genes (ALP, ColI). α-TCP is a widely used material for the production of CaP cements that, when combined with water, leads to the formation

of CDHA. Furthermore, the incorporation of gelatine enhanced the processing ability, and the mechanical and biological properties. With this in mind, and assuming that gelatine could ensure the viscoelastic properties for printing, Maazouz et al. [125] used a reactive ink that combined α-TCP with gelatine for the production of HA/gelatine scaffolds by robocasting. It was observed that gelatine was retained by chemical crosslinking. In order to allow enough time for printing, the setting reaction needed to be delayed. Upon setting, the scaffolds improved their compressive strength and a further increase was registered after the crosslinking reaction. The presence of gelatine improved cell adhesion and proliferation.

Some large bone grafts lack oxygen diffusion throughout the implant. The oxygen release is important in tissue survival during formation and can be achieved by the incorporation of peroxide into hydrophobic polymers, with a slow and sustained release of oxygen, or when incorporated into hydrophilic polymers upon undergoing rapid water absorption, originating from a faster polymer decomposition and oxygen generation. With this in mind, Touri et al. [126] used robocasting to produce BCP scaffolds that were posteriorly coated with a thin film of PCL, a hydrophobic polymer, in which different concentrations of calcium peroxide (CPO) were encapsulated. A sustained CPO release was observed. A coating with 3% CPO exhibited the best properties regarding osteoblast viability and proliferation under hypoxic conditions, which is a good indicator for bone growth.

Apart from CaP materials, bioactive glasses are also widely used in bone tissue engineering and have thereby been explored for the production of scaffolds by robocasting. Eqtesadi et al. [127] obtained 45S5 bioglass scaffolds via robocasting using a single processing additive, carboxymethyl cellulose (CMC). The scaffolds were sintered within the range of 500–1050 °C and for all of the temperatures, exhibited sufficient mechanical integrity and a compressive strength comparable to the one of cancellous bone. However, to mitigate the brittleness of these scaffolds and enhance the mechanical properties, they reinforced these scaffolds with graphene oxide (rGO) contents ranging from 0–3 vol.%, followed by sintering at 550 or 1000 °C. The mechanical properties were optimal for 1 vol.% of rGO reinforcement and a sintering temperature of 550 °C, for which there were enhancements in the fracture toughness and compressive strength of 850% and 290%, respectively [128]. Olhero et al. [129] used an alkali-free bioactive glass, FastOs® BG (Portugal), containing 70% diopside ($CaMgSi_2O_6$), 10% fluorapatite ($Ca_5(PO_4)_3F$), and 20% tricalcium phosphate (3CaO

P_2O_5), to obtain porous scaffolds by robocasting. They obtained scaffolds with three different pore sizes (200, 300, and 500 μm) from pastes containing 47 vol.% solids using hydroxypropyl methylcellulose and Aristoflex® TAC as binder and gelation agents, respectively. The measured compressive strength of the scaffolds was similar to the cancellous bone for all investigated pore sizes.

Zirconia-toughened alumina (ZTA) is a widely used material in hip arthroplasty because of its attractive mechanical properties. With this in mind, Stanciuc et al. [130] produced ZTA scaffolds by robocasting. They started from inks with solid loadings of 70 wt.% (~35.5 vol.%), which are too low for optimal processing. Shape retention during printing was only achieved by using an acidic water bath (deionized water and HCl; pH = 1.5) since it allowed ink coagulation. The authors reported that human primary osteoblasts were able to adhere onto the scaffolds and the microporous structure enhanced the expression of runx2 and ALP when compared to 2D-ZTA.

6. Marine-Derived Bioceramics as Scaffolds for Bone Tissue Engineering

Significant changes in the production of scaffolds have been introduced over the last years with the adoption of AM techniques and the noticeable increase of affordable AM bioprinters. Despite this, the development of technologies to facilitate the implementation of these bioprinters in regenerative medicine and clinical manufacturing is still the major identified roadblock. One of the most vital, but to date limiting, components required for the widespread adoption of bioprinting in regenerative medicine is the availability of effective bioinks.

Oceans are abundant sources of diverse materials with potential applications in healthcare, including, among others, bioceramics, biopolymers, fatty acids, toxins and pigments, nanoparticles, and adhesive materials [131]. In this regard, and in order to overcome the drawbacks associated with AM, marine skeletons, mainly composed of aragonite ($CaCO_3$), have proved to be a promising alternative for bone tissue engineering taking advantage of their porous structure and mechanical strength [21,132].

Once cleaned, marine skeletons can be used as bone graft substitutes, either in aragonite or preferably after being hydrothermally transformed into CaP scaffolds, while keeping exactly the same porous architecture. The transformation can be partial or total, depending on the hydrothermal treatment conditions (temperature, time, chemical environment). The partial conversion of $CaCO_3$ from marine exoskeletons into CaP

means that the obtained products consist of composite materials with an inner calcium carbonate core and an outer layer with a composition close to that of the mineral part of the bone, making them viable bone grafts substitute materials [22,133–136]. The conversion from corals to porous HA was first performed by Roy and Linnehan in 1974 [133]. Since then, marine skeletons of cuttlefish [137], marine sponges skeletons [138], and nacre seashell [139] have been converted to HA, while maintaining their original structures, aimed at obtaining bone graft substitutes. In turn, sea urchin spines that consist of large crystals of Mg-rich calcite [$(Ca,Mg)CO_3$] have been hydrothermally transformed into Mg-substituted TCP [140] that has been used as templates with an optimal range of pore size, channels, and structural network for bone growth.

The following sections of this review will be focused on the use of corals and CB as scaffolding systems in the area of biomedical applications.

6.1. Corals

Corals are marine invertebrates typically living in compact colonies of many identical individual polyps. Each polyp is a small sac-like animal that is only a few millimetres in diameter and a few centimetres in length and has a set of tentacles surrounding a central mouth opening. Near the base, polyps absorb elements present in seawater, namely carbonic acid and calcium ions, and produce a calcium carbonate exoskeleton in an aragonite form, which grows over many generations. Apart from calcium carbonate, which represents 97–99%, corals also have oligoelements (0.5–1%), sodium (0.4–0.5%), magnesium (0.05–0.2%), amino acids (0.07%), and potassium (0.02–0.03%). Individual heads may grow by the asexual reproduction of polyps. But polyps also breed sexually by releasing gametes simultaneously over a period of one to several nights around a full moon [137,141]. Polyps feed on a variety of small organisms, from microscopic zooplankton to small fish. These organisms are immobilized or killed by the poison carried in the nematocysts existing in the polyp's tentacles, which is discharged in response to contact with another organism. The tentacles then manoeuvre the prey to the mouth and into the stomach [142].

6.1.1. Coral-Derived Bone Grafts Substitutes

Coral-derived bone graft substitutes have attracted the interest of many experimental researches aiming at the characterization and selection of the most appropriate coral species for the intended applications, and at evaluating their in vitro and in vivo

performances. The interest in this topic is also highlighted in a few review articles giving accounts of the literature reports published mostly in the last three decades [137,143,144]. The use of only natural or HA-derived corals, but also the combination of these porous structures with cells and/or growth factors, have been explored. The various coral bone graft substitutes currently available for experimental and biomedical applications and ongoing investigations of coral-derived bone replacement materials are summarised elsewhere [146]. *Porites*, *Goniopora*, and *Montipora* digitate, also known as finger coral, are some of the most common coral species exploited in medical applications [144–146]. *Porites* species possess an anatomical structure, and physical and chemical characteristics that more closely simulate the cortical bone, with a porosity <60%, and interconnecting pore sizes of ~190 μm, the average diameter of an osteon in human bone. The structure of *Goniopora* more closely resembles that of cancellous bone, with a porosity >70% and larger pore sizes [144,145].

Natural and Partial Transformed Corals

Sergeeva et al. [147] studied the cytocompatibility and biocompatibility of five coral scaffolds derived from *Acroporidae* and *Pocilloporidae*. Cytocompatibility was in vitro evaluated using human fibroblasts and by the formazan assay (MTT), and their biocompatibility was in vivo studied by implantation of the scaffolds into bone defects in rats. All of the specimens were cytocompatible and biocompatible. A comparison between a coral and autograft was accomplished by Puvanesway et al. [148], with the aim of studying their morphological and chemical composition, as well as the osteogenic differentiation potential in vitro using rabbit MSCs. The SEM analysis of bone and coral grafts revealed interconnected pores, and micro-CT measurements confirmed pore sizes in the range of 107–315 μm and 103–514 μm, respectively, with total porosity fractions >92%, which seems to be exaggerated in comparison to other reported values [146]. Significantly higher levels of osteogenic differentiation markers, namely, ALP and OC, and of ON and Runx2 integrin gene expression, were detected in the coral graft cultures in comparison with those in the bone graft cultures. The authors concluded that coral grafts enhanced the osteogenic differentiation of rabbit MSCs relative to the bone graft culture system.

Mangano et al. [149] used calcium carbonate in sinus elevation procedures and evaluated its clinical performance through histologic and histomorphometric analysis. After a six-month post-implantation period, the mean vertical bone gain was about 7 mm

and the histomorphometric analysis revealed a residual calcium carbonate of ~15%, ~28% of newly formed bone, and ~57% of marrow spaces. The reported implant survival rate after one to five years of follow-up was 98.5%. The osteoconductivity and suitability of coral-derived calcium carbonate was compared with S53P4 bioactive glass and allogeneic fresh frozen bone by Gunn et al. [150] through the implantation of the material into cylindrical bone defects drilled in the femoral condyles of adult rabbits. Histologic and histomorphometric analyses were performed at 3, 6, 12, and 24 weeks. All three materials were found to be biocompatible and osteoconductive. Coral was observed to degrade more quickly, leaving more empty space in the defects, being considered the least suitable bone filler, with no statistically significant difference being observed between the allograft and the bioactive glass.

As previously mentioned, calcium carbonated coral skeletons can be hydrothermally converted into CaP scaffolds. In this regard and in order to understand whether coral-HA can be a promising alternative to intraarticular autologous structural bone grafts, Koëter et al. [151] filled a defect in the femoral trochlea of goats with a coral-HA scaffold. They showed that coral-HA did not cause an inflammatory reaction and there was good bone growth in the defect filled with the scaffolds.

The potential of coral-HA, along with other biomaterials such as cryopreserved bone allograft (CBA), demineralized freeze-dried dentin (DFDD), and cementum, for periodontal regeneration was studied by Devecioğlu et al. [152]. The authors studied in vitro the adhesion, proliferation, and mineralization of periodontal ligament (PDL) cells and mouse embryonic pre-osteoblasts cells (MC3T3-E1). Both the CBA and coral-HA exhibited a better initial PDL cell adhesion and regarding the long-term PDL cell adhesion, there was an increase in the presence of coral-HA. In the tests with MC3T3-E1 cells, the mineral-like nodule formation was significantly higher in DFDD biomaterial. According to the authors, the overall outcome was good biocompatibility with both types of cell for all the analysed biomaterials.

Recognizing that the incorporation of additional elements in the scaffolds could improve their properties, Zhang et al. [153] combined silver with coral-HA, aiming to introduce antibacterial properties to the scaffold. The scaffolds were prepared through an adsorption process at the surface and an ion-exchange reaction between the Ag^{+} from silver nitrate and Ca^{2+} from the coral-HA. It was observed that the scaffolds' morphology is dependent on the Ag^{+} concentration. The scaffold cytocompatibility was analyzed using MC3T3-E1 cells and it was demonstrated that cell morphology and proliferation is

dependent on the Ag^+ concentration; for instance, better results were achieved with lower Ag^+ concentrations [(13.6 µg/mL)/coral-HA and (1.7 µg/mL)/coral-HA]. Importantly, the scaffold that combined silver with coral-HA exhibited an excellent biocidal potential against both Gram-negative (*Escherichia coli*) and Gram-positive bacteria (*Staphylococcus aureus*).

As stated earlier, corals are potential scaffolds for bone tissue engineering; however, their excessive use may damage their natural habitats. In this regard, Mahanani et al. [154] mimicked coral structure and studied their capacity for MSC adhesion and proliferation. The synthetic scaffolds were prepared from bovine gelatine and calcite $CaCO_3$ powder with a 10% w/v solid concentration. They observed that MSC exhibited a good adhesion ability and when Platelet Rich Plasma (PRP) was incorporated into the scaffolds, the cell proliferation improved.

Natural and Partial Transformed Corals Combined with Mesenchymal Stem Cells

Manassero et al. [155] studied the potential of *Acropora* coral scaffolds for MSC delivery in an animal model. Upon in vitro cell adhesion and proliferation, the coral scaffolds were placed into a critical bone defect in sheep. They observed an almost complete scaffold resorption six months after the operation which, consequently, is associated with bone regeneration. The authors concluded that the presence of MSCs is beneficial for osteoinductive behaviour. A comparation between *Acropora* or *Porite* coral granules combined with MSCs for their potential use in bone regeneration was performed by Decambron et al. [156]. The cells were seeded on both types of coral granules, placed in a perfusion bioreactor, and then implanted into bone defects in sheep. They observed that despite an early resorption of coral scaffolds that led to a bone non-union, a superior bone formation was registered for *Acropora* scaffolds. Further, the former scaffolds resorbed slowly when compared to *Porite* scaffolds and, thereby, are closer to the clinical use. Moreover, the osteogenic potential of these two coral species (*Acropora* and *Porites*) was compared with β-TCP scaffolds and banked bone in the presence or absence of MSCs. Bone formation was only registered in the samples containing MSCs and the coral scaffolds demonstrated the best bone formation capability [157].

The osteogenic potential of human BMSCs to induce bone formation even in ectopic sites has been already demonstrated in BMSC-soaked coral or HA implants in intramuscular pockets in rats [158] and in the repair of critical-sized mandibular defects in large mammals [159,160]. Similar conclusions were drawn by the same research group

when coral scaffolds seeded with BMSCs were utilized [161] instead of β-TCP scaffolds used in the previous study [159]. Defects treated with coral alone were used as an experimental control. The engineered bone with coral/BMSCs achieved satisfactory biomechanical properties at 32 weeks post-operation, which was very close to that of the contralateral edentulous mandible. This contrasted with minimal bone formation with an almost solely fibrous connection in the group treated with coral alone [161].

Considering that adipogenic and osteogenic cells share part of the early differentiation cascade of MSCs and when compared to BMSCs are easily isolated, in relative abundance, and rapidly expanded, adipocytes have been used for the repair and regeneration of different tissues. For instance, Ruth et al. [162] investigated whether adipocytes that have initiated differentiation along one lineage could be converted into an osteogenic lineage by merely interacting with marine corals (*Porites lutea*). Through morphological, histological, enzymatic, and quantitative PCR analyses made at different time points (1, 2, 5, 7, 14, 21, and 28 days post-seeding), they demonstrated that preadipocytes could differentiate into bone-forming cells when grown on a biomatrix of marine origin without the addition of other bone morphogenesis inducers. Following the same line, Cui et al. [163] loaded autologous adipose tissue-derived stem cells (ASCs) onto natural coral scaffolds and investigated their potential for a cranial bone defect in a canine model. After 12 weeks of ASC-coral implantation, it was already possible to observe new bone formation and upon 24 weeks, 84.19 ± 6.25% of the defect had been repaired, whilst in the control group, coral alone, only 25.04 ± 18.82% was repaired. In a more recent work, the same authors studied the hypothesis of healing the same defect with allogeneic ASCs seeded onto coral scaffolds without the need of immunosuppressive therapy. They observed that the use of allogenic osteo-differentiated ASCs did not cause any significant systemic immune response or local inflammation and, importantly, micro-computed tomography (micro-CT) analysis demonstrated that the newly formed bone was analogous to that of autologous osteo-differentiated ASCs [164].

The capacity to develop a vascularised coral scaffold seeded with marrow-derived osteoblasts was analysed by Chen et al. [165]. Prior to the implantation, the scaffolds were in vitro incubated for two days. To obtain a vascularised biomaterial, the scaffolds were implanted under the rabbit inferior epigastric blood vessels. After two months of operation, a well-vascularised scaffold was obtained, for which new bone formation was observed by histological analysis.

Bensaïd et al. [166] compared natural coral with coral-HA, and both were seeded with MSCs. Firstly, in the natural coral scaffolds, it was observed that the presence of a pseudo-periosteal layer of MSCs involving the scaffold improved bone formation in comparison with a distribution of MSCs over the implant. Nevertheless, due to the high resorption rate of natural coral scaffolds, successful bone formation was only observed in one sheep. On the other hand, coral-HA combined with the MSCs layer and the autologous bone graft demonstrated similar new bone formation upon four weeks of implantation. Furthermore, after 14 months of implantation, the defects filled with coral-HA combined with the MSCs layer were completely replaced by new bone.

Gao et al. [167] wrapped cylindrical coral scaffolds around partially mineralised and strong osteogenic cell sheets that could be obtained from BMSCs under specific cell culture conditions. These cell sheets/scaffolds were implanted into subcutaneous pockets on the backs of mice and bone formation was studied by micro-CT scanning and histological observation. Cortical bone was formed within the cell sheet/scaffold. After eight and 12 weeks of implantation, the bone formation was 26% and 40%, respectively. Histological observation showed that neo-bone formation occurs in the manner of endochondral ossification. The authors concluded that a partially mineralised and osteogenic cell sheet could vitalise a coral scaffold for bone formation. Following a similar strategy, Geng et al. [168] combined MSCs sheets and coral particles. Coral particles were incorporated on the surface of confluent rabbit MSCs, forming a cell sheet. Posteriorly, a tubular bone graft was obtained by wrapping the cell sheet around a mandrel. The obtained bone graft was cultured in a spinner-flask bioreactor and then implanted into subcutaneous pockets on the backs of nude mice. The authors observed that following the in vitro incubation period, the bone graft still exhibited a tubular shape, sufficient radiological density, and suitable values of compressive strength. The in vivo results demonstrated that the cell sheets had a good osteogenic capacity and after eight weeks of implantation, a mature tissue with a similar mineral density as the one of the mouse spine.

In a different approach, Chen et al. [169] inserted a titanium dental implant into a coral scaffold seeded with BMSCs and then subcutaneously implanted the set into nude mice backs. Defects treated with coral carrying no cells were used as an experimental control. After two months of implantation, the local area of implantation was red and similar to native bone and, in addition, the scaffold was mostly absorbed. Also, dental

implants were fixed in the newly formed bone and surrounding the implant, new bone was formed. On the other hand, no bone formation was observed in the control scaffold.

It has been recognized that in supra-alveolar defects, periodontal and bone regeneration could be improved when using guided tissue regeneration (GTR) due to the space provision, besides their osteconductive properties [170]. Wikesjö et al. [171–174] carried out different works in which supra-alveolar periodontal defects were created in young adult beagle dogs with the aim of evaluating space provision, alveolar bone, and cementum regeneration using natural corals in combination with GTR. An histometric analysis with different parameters [defect height, defect area, membrane height, junctional epithelium, connective tissue repair, cementum regeneration, bone regeneration (height, area, and density), and biomaterial density] demonstrated that for all the evaluated parameters, no significant differences could be observed among three different step-serial sections. Thereby, representative histometric data could be obtained from a central section [172]. The combination of coral/GTR was compared with coral [173] or GTR alone [174]. At four weeks post-operation, the histopathologic and histometric analysis revealed significantly increased bone formation (height and area) at sites receiving the coral/GTR combination compared with coral or GTR alone [173,174].

Natural and Partial Transformed Corals Combined with Growth Factors

The capacity of bone tissue to repair and regenerate is in part related to the direct differentiation of MSCs into osteogenic cells. In this differentiation process, different hormones and differentiation factors play fundamental roles. The osteoclasts have the ability to activate latent TNF-β and, subsequently, during bone resorption, the active TNF-β is released, thereby promoting osteoblast and bone formation [175]. Based on this concept, Vuola et al. [176] studied the effect of adding TNF-β1 into natural coral scaffolds implanted in defects created in parietal bone of Wistar rats on bone formation, using coral scaffolds without added TNF-β1 as controls. Indeed, the presence of TNF-β1 was said to improve bone formation, but the new bone was located around the implanted material and did not fill the defect. Furthermore, the addition of the growth factor delayed bone resorption and the authors associated that with the absence of fibrous tissue ingrowth and the decrease of the number of macrophages and giant cells.

BMPs are proteins present in the bone matrix and are able to induce chondrogenesis and osteogenesis. These molecules are associated with the first signal for the beginning of MSC differentiation and enhance osteoblast differentiation and osteoblastic

differentiation. IGFs are also present in the bone matrix and play a role in bone formation. IGFs stimulate chondrogenesis and osteogenesis, as well as the synthesis of bone collagen by bone cells [175]. In this regard, Nandi et al. [177] incorporated BMP-2 or IGF-1 into HA scaffolds derived from coralline and used a rabbit model to study their potential for bone regeneration. Through an in vitro study, they observed that IGF-1 exhibited a more sustained release when compared to BMP-2. After 28 days, the release of IGF-1 and BMP-2 was 77 and 98%, respectively. The in vivo results demonstrated that the addition of growth factors improved the early-stage bone formation, though IGF-1 was demonstrated to be more effective.

Vascular endothelial growth factor (VEGF) is the best-characterized growth factor for the regulation of vascular development and angiogenesis. Since angiogenesis influences osteogenesis, VEGF is important in bone formation and remodelling [178]. Recognizing that the vascularization and osteogenesis of block grafts still remains a key problem for dentists, Du et al. [179,180] attempted to promote angiogenesis and prevascularization by seeding nano-HA (nHA)/coral blocks with angiogenic recombinant human vascular endothelial growth factor$_{165}$ (rhVEGF$_{165}$). Non-coated and coated drafts were implanted in mandibular critical-size defects using male beagle dogs as an animal model. The histological evaluation and the histomorphometric analysis revealed enhanced neovascular density and a larger quantity of new bone formation at three and eight weeks post-surgery. The results suggest that nHA/coral blocks might be satisfactory scaffolds for block grafting in critical-size mandibular defects and that additional VEGF coating via physical adsorption can promote angiogenesis in the early stage of bone healing.

Natural and Partial Transformed Corals Combined with Mesenchymal Stem Cells and Growth Factors

A bone tissue engineering strategy that combines a calcium-based scaffold and MSCs is beneficial for bone growth; however, it may lack osteoinductive properties. This can be overcome by the addition of growth factors. For instance, Xiao et al. [181] used autologous BMSCs from Beagle dogs and transfected them with adenovirus containing human BMP-2. Posteriorly, the BMP-2 expressing BMSCs were seeded onto a coral scaffold. The BMP-2-transfected BMSCs/coral scaffolds were placed in defects created in the canine medial orbital wall. The authors observed that a combined delivery of BMSCs and BMP-2 on the defect had the highest bone regeneration when compared with

the defects treated with BMSCs/coral and only coral scaffolds. In a similar procedure, Tang et al. [182] transfected autologous BMSCs from the left tibia of osteoporotic rats with human BMP-2 but, instead of seeding them onto a natural coral scaffold, they used coral-HA scaffolds. Newly formed bone was observed four weeks post-implantation, while mature bone was reported to form upon eight weeks of implantation. It is important to highlight that BMP-2 in suprahysiologic doses causes significant adverse side-effects. Decambron et al. [183] combined coral scaffolds with MSCs and/or low-doses of BMP-2 and observed that dual delivery improved bone formation and bone union when compared to a single addition of MSCs or BMP-2 to coral scaffolds. A comparison of coral scaffolds combined with MSCs and human BMP-2 and autologous bone grafts was performed by Hou et al. [184]. BMP-2 was firstly added to each coral, followed by the subsequent seeding of MSCs. The grafts were implanted in critical defects of rabbit crania. A similar bone formation was registered in the defects treated with coral/BMP-2/MSCs scaffolds (77.45 ± 0.52% in radiopacity) and with autografts (84.61 ± 0.56% in radiopacity). In addition, the osteogenesis rate in coral/BMP-2/MSCs was significantly higher compared to coral/BMP-2 scaffolds. These authors highlight an allegedly synergetic effect between MSCs and BMP-2 seeded in the coral scaffolds. More importantly, these combined scaffolds were reported to exhibit a similar behaviour to autologous grafts.

bFGF is produced by osteoblasts and stored in ECM in an active form and, thereby it regulates bone remodelling. In addition, bFGF promotes the proliferation of endothelial cells and neovascularization [185,186]. With this in mind, Zheng et al. [187] studied the feasibility of seeding mandibular condyle constructs with BMSCs onto porous coral scaffolds. The human BMSCs were transfected with bFGF gene-encoding plasmids and induced to differentiate into osteoblasts and chondroblasts. The osteogenic/chondrogenic differentiation, cell proliferation, collagen deposition, and tissue vascularization were evaluated. They observed that the transfected human BMSCs (hBMSCs) expressed bFGF and were highly proliferative. Moreover, subcutaneous transplantation of seeded coral/hydrogel hyaluran constructs into nude mice resulted in bone formation and collagen type I and type II deposition. Neovascularization was observed around newly formed bone tissue; bFGF expression was detected in implanted constructs seeded with bFGF expressing hBMSCs. Based on the encouraging results, the authors suggested that engineered porous coral constructs seeded with bFGF gene-transfected hBMSCs may be a feasible option for surgical transplantation in the temporomandibular joint.

Zhang et al. [188] prepared porous chitosan/coral composites combined with a plasmid encoding the PDGF-B gene through a freeze-drying process. PDGF-B is an important growth factor for wound healing, as well as for promoting the recruitment and proliferation of PDL and bone cells [189]. The scaffolds were evaluated in vitro by analysis of the microscopic structure and cytocompatibility. The expression of PDGF-B and ColI were detected after seeding human PDL cells in the chitosan/coral scaffold composites. The subcutaneous implantation of these scaffolds into mice revealed that the proliferation properties of hPLCs on the gene-activated scaffolds were much better than on the pure coral scaffolds. The expression of PDGF-B and ColI was also superior in gene-activated scaffolds. The results of this study suggest the porous chitosan/coral composite scaffolds combined with the PDGF-B gene as a potential construct for periodontal tissue regeneration.

Gross-Aviv et al. [190] studied the influence of the coral surface chemistry on the differentiation of MSCs. For this purpose, an aragonite matrix derived from the coral Poris lutea and a gold-coated Poris lutea were seeded with MSCs and combined or not combined with growth factors (TGF-β1 and IGF-I). An aragonite surface promoted osteogenic differentiation and, on the other hand, the gold coating that prevented the contact between the cells and the aragonite surface led to chondrogenic differentiation. The authors stated that the chondrogenic differentiation on the gold-coated scaffolds is associated with the inability of direct contact between the Ca^{2+} environment of the scaffold and the MSCs. Furthermore, the supplementation of the culture medium with the growth factors increased the influence of the surface chemistry on the cell differentiation.

Xiao et al. [191] studied the effects of osteogenic, BMP-2, and angiogenic, VEGF, factors on the repair of critical-sized bone defects in rabbit orbits. They used autologous BMSCs genetically modified to express human BMP-2 and VEGF165, which were then seeded on natural coral scaffolds. The defects were filled with coral scaffolds that had been loaded with non-transfected or transfected BMSCs with a single or combined growth factors. After four weeks of implantation in critical defects, those filled with the coral scaffolds with a combined delivery of BMP-2 and VEGF were reported to exhibit improved angiogenesis. Moreover, a maximum rate of bone formation was registered before the eighth week of implantation and a total bone-union was observed at the 16th week of implantation. The authors concluded that the presence of both BMP-2 and VEGF improved the angiogenesis and bone regeneration. Further, there was a synergetic effect between VEGF and BMP-2 during bone formation.

PRP extracted from autologous whole blood contains a wide range of autologous growth factors, namely PDGF, TGF-β, IGF-1, VEGF, and bFGF. It is beneficial for tissue healing and is being broadly used in oral and maxillofacial surgery [192,193]. With this in mind, Zhang et al. [194] studied the effect of clotting natural porous coral disks with PRP on the bone formation of marrow stromal cells (MSCs). The samples were cultured in vitro or implanted subcutaneously into nude mice. Coral scaffolds loaded with MSCs or with PRP alone were used as controls. The levels of ALP, a marker enzyme of bone formation activity, were measured for the specimens cultured in vitro for seven and 14 days, while the levels of ectopic bone formation were evaluated four and eight weeks after the operation. The in vitro results revealed that the samples from the coral/PRP/MSC group exhibited significantly higher ALP activity compared with those from the coral/MSC group or the coral/PRP group. The histomorphometric analyses of the in vivo experiments also showed higher levels of new bone and/or cartilage formation in the coral/PRP/MSC group, four and eight weeks after implantation, in comparison to the control specimens. The authors concluded that PRP could improve the ALP activity of MSCs on coral and increase ectopic bone formation.

6.2. Cuttlefish Bone

The cuttlefish, *Sepia officinalis*, is a common demersal neritic species occurring predominantly near sandy and muddy bottoms up to a depth of 200 m. CB represents approximately 9% of the cuttlefish and is a hollow structure divided by lamellae (Figure 5) [22,195,196]. Besides functioning as a skeleton, the porous structure contains liquid and gas (mainly nitrogen at a pressure of about 0.8 atm) that provides neutral buoyancy to the cuttlefish by varying its density [195,196]. Through the liquid movement into or out of the CB via osmotic forces, the volume fraction of gas in the bone changes and the cuttlefish might become more or less dense than the sea water. This buoyancy mechanism, which is almost independent of depth, confers a valuable advantage to the cuttlefish since it can maintain a fixed position in water with little effort [195,197]. This buoyancy mechanism is more stable than that conferred by the swim bladder of a fish, which leads to a state of unstable equilibrium when adapting to the depth. Indeed, if the fish rises in the sea, the swim bladder will expand and tend to push it still higher, whereas if it goes deeper in the sea, the swim bladder will be compressed and the fish will tend to sink more and more quickly [197]. To accomplish these functional and highly sophisticated requirements, the high porosity of CB enables the cuttlefish to maintain its

neutral buoyancy at a higher depth and at the same time retain enough stiffness and strength to prevent sever distortion or crushing under high hydrostatic pressures in deep water [195,198,199].

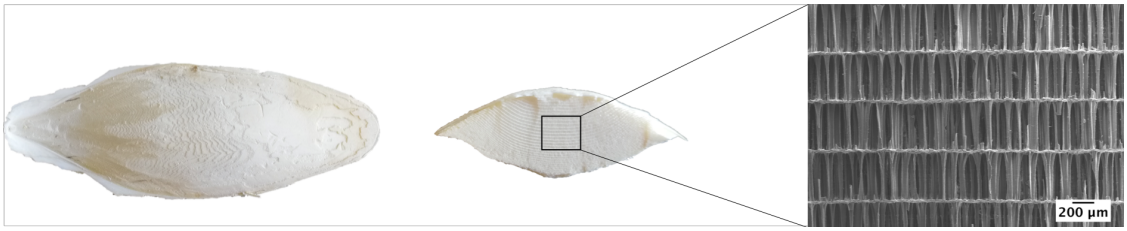

Figure 5. CB bone, its transverse section and the scanning electron microscopy of the dorsal shield and the lamellar matrix.

The dorsal shield and lamellar matrix represent the two main components of CB. The dorsal shield is highly dense and provides a rigid substrate for protecting the development of the lamellar matrix. On the other hand, the lamellar matrix has a high porosity, approximately 93%, and also manages to withstand very high hydrostatic pressure [199].

The dorsal shield is a dense and tough cover that overlays the lamellar matrix and seals off the separated chambers. It consists of a non-porous structure containing 30 to 40% by weight of organic material, β-chitin. This organic component has the ability to undergo plastic deformation, thereby increasing the toughness of the structure. It is composed of three different layers: a 1 mm thick outer calcified layer; a 0.3 mm thick transparent middle zone composed of tough, fibrous layers of sclerotized chitin; and a thin inner calcified zone [195].

The lamellar matrix is a layered, quasi-periodic microstructure composed of lamellae separated by pillars [200], which is able to resist external pressures of about 2.4 MPa [195]. The spacing of the lamellae varies between 200 and 600 µm along the CB [196], being dependent on the species [201]. Each chamber is supported by pillars that form channels with a high degree of interconnectivity, and a uniform width that progresses through the material along a sigmoidal path [199]. Its unique macroporous architecture with approximately 93% porosity is mainly composed of aragonite, which is a crystallized form of $CaCO_3$. This inorganic structure is enveloped in a thin layer of organic material primarily composed of β-chitin that represents between 3 and 4.5% of the lamellar matrix weight [195,199,202]. The presence of β-chitin is associated with initiation, organization, and inhibition of the inorganic matrix mineralization [195,202]. Moreover, the organic matrix may function as a template for the nucleation of the inorganic material, possibly

due to the interaction between the groups of the polymer and the ions in the solution phase or the nuclei of the solid phase that become more stable upon bonding [195].

CB has a unique architecture which is associated with a high ratio of compressive stiffness to weight. Indeed, under excessive compressive loading, CB can collapse in a controlled and layer-by-layer manner due to its layered structure and also to the sigmoidal shape of its pillars. In this regard, the cuttlefish can stay below the depth limit of its CB for short periods of time without significant damage. The plastic deformation of the organic component in the dorsal shield provides another important contribution to the toughness of the structure [195,199].

6.2.1. Cuttlefish Bone-Derived Bone Grafts Substitutes

CB is a worldwide available and inexpensive material with a unique porous microstructure; the pore size and pore interconnectivity of which is proven to be beneficial for bone growth and vascularization [203]. The use of CB as a bone graft substitute has been reported not only in its natural form, but also as an aragonite source, to prepare CaP materials by preserving the same porous structure after hydrothermal transformation.

Natural Cuttlefish Bone

Dogan et al. [204] studied the potential of CB as a xenograft by filling a bone defect of a rabbit with CB, demineralized bone matrix (DBM), bovine cancellous graft (BCG), and TCP. At the third post-operative week, 100% callus formation in the groups treated with CB, DBM, and TCP was observed. In the animal treated with CB, remodelling could be observed at week 6, while in the other groups, remodelling was only observed upon the twelfth week. In addition, in the group treated with CB, fibrous union started at the first post-operative week and the rate of vascularization was higher when compared to the other groups. The osteochondral union at week three resulted in an increase of the development of new bone. The defects treated with CB or with TCP exhibited the fastest remodelling. Overall, in the CB group, a high degree of vascularization and good osteogenesis and osteointegration properties were observed. Thus, CB was considered a good xenograft material.

As previously mentioned, CB is composed of a dorsal shield and lamellar matrix. Kim et al. [205] separated the CB into these two structures and studied whether the presence of small amounts of heavy metals on CB could influence its biocompatibility

and osteoblast differentiation of human MSCs. It was observed that the heavy metals did not affect the cell viability and CB allowed cell adhesion and growth. When compared to the dorsal shield, in the lamellar matrix, the cells infiltrated deeper into the structure. ALP levels increased on both the dorsal shield and lamellar matrix; however, a higher expression was observed on the dorsal shield due to the fact that confluence is achieved earlier in this material and this, consequently, resulted in earlier differentiation. Collagen type I α1 (ColIα1) and Runx2 were increased on both materials with no significant difference.

Besides being used as a scaffold, natural CB can also be milled and used to fill poly (methyl methacrylate-*co*-styrene) bone cements [206,207]. When compared with the non-filled cement, the addition of 10 and 30 wt.% of CB resulted in an increase of tensile strength and Young's modulus. Nonetheless, a cement containing 50 wt.% of CB led to a decrease in tensile strength and Young's modulus, which was associated with the formation of pores. Although the compressive strength decreased with the increase of CB content, it maintained a higher value than the minimum requirement of 70 MPa [206]. Due to the exothermic polymerization reaction, there is an increase of temperature as the reaction progresses, decreasing after a maxim value has been reached as the monomer is consumed. Due to its thermal capacity, the increase of CB content led to a decrease of the peak temperature and an increase of the time to reach that temperature, resulting in an apparent slower reaction. Furthermore, the setting time increased with the CB content, which is beneficial as it allowed enough manipulation time before setting. However, a longer setting time can cause some medical problems because pressure in the prosthesis has to be maintained until the cement sets [207]. When implanted in bone defects, the cements without CB were weakly adherent to the parietal bone, while the samples containing CB were strongly attached to the bone, an indication that osteointegration has occurred in samples containing CB [206].

Calcium Phosphate Materials Derived from Cuttlefish Bone

Being mainly composed of aragonite and having a suitable porous microstructure for bone grafting, which is preserved upon hydrothermal transformation into CaP, CB has been used as an interesting source of calcium carbonate and template for preparing CaP scaffolds or powders.

The transformation of CB into HA through a hydrothermal process was first reported by Rocha et al. [138,203,208]. Prior to the transformation, the exact aragonite content in

CB was analysed and the corresponding amount of $(NH_4)_2H_2PO_4$ was added to set the molar ratio of Ca/P = 1.67. The mixture was sealed in a polytetrafluoroethylene (Teflon) lined stainless steel autoclave and the hydrothermal treatment (HT) was conducted at 200 °C. The CB internal structure was not compromised during the HT and thereby the pore size and interconnectivity were maintained after the transformation. An AB-type carbonated HA was obtained, which is similar to the composition of human bones [136,208]. Additionally, the size of HA crystallites was similar to the size of bone-like apatite (20–50 nm) [136]. The obtained scaffolds were demonstrated to have a high thermal stability on sintering up to 1350 °C. Above 1400 °C, it was possible to observe the formation of β-TCP. Moreover, scaffolds were demonstrated to have a very good in vitro bioactivity due to the fact that when immersed in SBF, there was a rapid and evident formation of an HA layer [203]. In the presence of the scaffolds, the viability and proliferation increased, and the ALP activity was maintained at a constant value, indicating that the scaffolds were biocompatible with osteoblasts [203,208].

Different HT conditions were established by Hongmin et al. [209], who used a 0.5 M $(NH_4)_2HPO_4$ solution and a CB/$(NH_4)_2HPO_4$ weight ratio of 1/1.2, and the treatment was conducted at 180 °C for 96 h. The authors compared the in vitro and in vivo behaviour of HA scaffolds derived from CB (CBHA) and raw CB. The protein adsorption was higher on CBHA than on CB. Despite the good cell adhesion and proliferation on both CBHA and CB, CBHA demonstrated a better capacity for cell differentiation. Indeed, after 13 days of culture, ALP activity and the OC level were significantly higher on CBHA. Regarding the in vivo behaviour, both scaffolds were encapsulated in a fibrous tissue at the fourth week; however, a higher quantity of fibrous tissue and blood vessels was observed on CBHA. At week eight and contrarily, osteoblasts were found to excrete bone matrix and embed themselves to form bone lacunae. In this way, it was possible to conclude that CBHA represents an interesting osteoinductive bone graft.

As previously observed, different HT approaches can be followed to obtain CaP materials from CB. In this regard, Ivankovic et al. [200] and Kasioptas et al. [210] studied the mechanism and kinetics of the aragonite transformation into CaP scaffolds by modifying the temperature and time of the hydrothermal reaction. Ivankovic et al. [200] analysed a range of transformation temperatures from 140 to 220 °C for various time periods between 1 and 48 h. In the samples treated at 140 and 160 °C for 20 min, they observed the presence of $CaHPO_4 \cdot 2H_2O$ (brushite), a compound that preferentially precipitates at lower values of pH and temperature. A complete transformation was only

observed upon the HT at 200 °C for 24 h. At 180 °C, the transformation is not completed, even after 48 h of HT. On the other hand, the formation of $CaHPO_4$ (monetite) was reported to occur at 220 °C and above 4 h of HT. The isothermal kinetics of transformation was described by the Johnson-Mehl-Avrami (JMA) equation (Equation (1)), which is often used to describe the nucleation and growth of crystals from amorphous materials.

$$\alpha = 1 - exp[-(k^n\ (t - \tau)^n)] \quad (1)$$

In Equation (1), α represents the fraction of transformed HA; k is the rate constant; n is the Avrami exponent, associated with the nucleation type and growth dimensions; and τ is the incubation time. The rate constant increased with the increase of temperature; however, the Avrami exponent was maintained at an almost constant value and around 0.5 over the entire range of temperatures tested, indicating that the growth mechanism of HA can be defined as one-dimensional growth controlled by a diffusion process.

Alternative methods for HT can be used to produce CaP materials derived from CB. For instance, Sarin et al. [211] reported the production of BCP scaffolds from CB using a solution of phosphoric acid and 2-propanol with different concentrations of phosphoric acid from 12 to 20 wt.%. Briefly, the infiltration of the solution into the CB occurred under vacuum conditions and for 1 h. This process was followed by heat treatment at high temperatures, up to 1300 °C. The BCP scaffolds obtained with 16 wt.% of phosphoric acid preserved the initial microstructure of CB and exhibited a compressive strength of 2.38 ± 0.24 MPa that, despite being lower than the raw CB (2.74 ± 0.39 MPa), is in the range of trabecular bone. Dutta et al. [212] produced the CaP scaffolds derived from CB in ambient conditions using a de-calcification, re-calcification process followed by phosphate mineralization. $CaCO_3$ was removed from the CB structure by dipping the CB in acetic acid. The as-obtained organic matrix was re-mineralized using solutions of calcium chloride and sodium carbonate and hence amorphous calcium carbonate (ACC) was produced, due to the fact that macromolecules associated with biominerals have the capacity to stabilize ACC. Afterwards, ACC was converted into CaP by immersing the mineralized scaffold into a phosphate solution followed by a treatment with glutaraldehyde solution. Since the solubility of ACC and calcite at the working pH of 7 is high, there was a complete phase conversion, not to HA, but instead to brushite, the formation of which is favoured at this pH.

In addition to being converted into porous CaP scaffolds preserving the internal structure, CB can also be used to produce CaP powder [213,214] or granules [215]. Lee et al. [213] mixed CB that was previously calcined, consisting of pure CaO phase, with phosphoric acid, to synthesize CaP. Different ratios between CB and phosphoric acid from 1:1.0 to 1:1.7 were tested. HA and β-TCP were obtained at 1:1.2 and 1:1.7 ratios, respectively. The samples heat treated at 900 °C were entirely crystalized. CBHA granules with a size varying from 200–500 μm were obtained by HT at 200 °C for 24 h. Besides being non-toxic, the CBHA granules enabled a higher cell density and improved cell differentiation capacity in comparison to pure HA granules. This could be justified not only by the higher surface roughness and surface area of CBHA that are beneficial for cell proliferation and adhesion, but also because CBHA contains some mineral ions, like magnesium, which play fundamental roles in the binding of cell-surface receptors and ligand proteins that, consequently, can enhance cell attachment. The in vivo results were in agreement with the in vitro tests and CBHA had a significantly higher percentage of bone formation and more multi-nucleated giant cells, fibroblasts, osteoblast-like cells, and connective tissue and micro blood vessels [215]. Furthermore, Kim et al. [214] produced a porous composite scaffold by solvent casting and particulate leaching using CBHA powder and PCL. CBHA powder, obtained by HT at 200 °C for 24 h, and PCL were mixed with salt particles (200–300 μm) that acted as a porogen. The introduction of CBHA into the PCL scaffolds improved the compressive strength. Regarding the in vitro tests, the addition of CBHA improved the viability, adhesion, and proliferation. In the in vivo studies, it was demonstrated that CBHA/PCL scaffolds improved the bone formation.

Doped – Calcium Phosphate Materials Derived from Cuttlefish Bone

The inorganic part of the human bone consists of carbonated HA with trace amounts of other ions like Na^+, Mg^{2+}, Zn^{2+}, Sr^{2+}, F^-, and silicon. Therefore, the incorporation of the aforementioned ions into the CaP matrix has been used to improve the biological performance of the material. With this in mind, Kannan et al. [216] and Kim et al. [217] incorporated F^- and silicon (Si) ions into the CBHA structure, respectively.

F^- is an important element for bone and dental growth. It is involved in the prevention and treatment of dental caries. The incorporation of F^- ions into the HA structure stimulates the osteoblast proliferation and differentiation and improves the mineral deposition in cancellous bone [218–220]. Two different levels of F^- substitutions (46 and

85%) on the OH^- sites via HT at 200 °C for 24 h were studied by Kannan et al. [216]. For the HT, a required volume of $(NH_4)_2HPO_4$ was added to the CB samples setting a Ca/P molar ratio of 10/6 and F^- was added by the NH_4F solution at 1 M or 2 M. A nano-sized AB-type carbonated apatite with precise control of F^- content was obtained. For a substitution of 85%, the lattice parameters were typical for fluorapatite, leading to a contraction along the a-axis.

Silicon represents an important trace element in bone, as it is associated with bone growth. The incorporation of Si in HA materials modifies their surface by creating a more electronegative surface, generating a finer structure, and also increasing the solubility. Furthermore, Si-substituted materials have been demonstrated to improve the bioactive behaviour and increase the bone formation in vivo [96,220]. Kim et al. [217] synthesized Si-substituted CBHA using hydrothermal and solvothermal methods. Firstly, CB and $(NH_4)_2HPO_4$ were placed in an autoclave for HT at 200 °C for 6 h. Subsequently, CB was immersed in a solution of silicon acetate ($Si(CH_3COO)_4$) saturated with acetone and solvothermal treatment took place at 200 °C for 12 h. In the final step, CB was again mixed with a $(NH_4)_2HPO_4$ solution and the HT occurred at 200 °C for 12 h. The Si content of the samples was about 0.77 wt.%. Regarding the in vitro results, the presence of an Si–OH layer on the biomaterial surface was associated with the improvement of cell adhesion and proliferation on the Si-substituted CBHA. Moreover, the incorporation of Si enhanced cell density and consequently improved cell differentiation, which was observed by the ALP activity and expression of Runx2, ColIα1, and OC. According to the in vitro results, the in vivo tests demonstrated that bone formation was higher on Si-substituted CBHA than on CBHA.

Composite Materials Derived from Cuttlefish Bone

CaP scaffolds obtained from CB are normally brittle and exhibit low strength, thereby limiting the application of these materials as bone grafts. In order to improve the compressive strength, some authors investigated the coating of these scaffolds with polymers like PCL [221–224], polyvinyl alcohol [222], and collagen [225].

CBHA scaffolds were obtained through an HT and PCL was incorporated into the scaffold structure under vacuum to remove the air from the pores and allow a complete impregnation of the polymer into the structure [221–224]. Kim et al. [221] reported the coating with 1, 5, and 10% of PCL of CBHA scaffolds. The PCL layer obtained by the coating with 1% PCL could hardly be observed and the roughness of the sample was

similar to the uncoated one. Coating with 5% PCL led to the formation of a thin PCL layer that covered the entire surface. When further increasing the amount of PCL to 10%, a thicker layer was formed and the number of clogged pores increased, thereby decreasing the porosity. Nonetheless, Milovac et al. [223] coated the scaffolds with 20% PCL, and although roughness and porosity noticeably decreased, they reported that such a coating allowed the maintenance of the number of pores and their interconnectivity. Through an SBF assay, it was possible to observe the formation of an apatite layer on the PCL-coated scaffold [222]. The compressive strength decreased with the HT due to a more extensive degradation of the organic matter that provides the mechanical support of the structure; however, with the exception of the coating with 1% PCL, the compressive strength improved with the PCL coating, as reported in Table 2. The coated scaffolds did not exhibit any cytotoxicity and cells were able to adhere and proliferate, and it was also demonstrated that penetration of the cells happened through the entire depth of the scaffold [221,224]. The cell proliferation was higher for the sample coated with 5 and 10% PCL. However, for the sample coated with 10% PCL, the cell proliferation decreased after six days of culture due to the reduction of porosity and the consequent lower surface area available for cell adhesion [222]. The ALP activity increased on the scaffolds coated with 5, 10, and 20% PCL [221,224]. The expression of ALP, Runx2, and ColIα1 significantly improved with the coating of 10% PCL, since the cells reached the confluence earlier, which consequently beneficiated the differentiation of cells [221]. The scaffolds coated with 20% PCl exhibited a higher level of collagen production, suggesting that the PCL coating improved cell adhesion and consequently induced higher levels of collagen secretion [223].

Siddiqi et al. [222] reported the coating with 5% of PVA of CBHA. The addition of 5% PVA improved the mechanical strength to 0.95 MPa compared to the raw CB (0.61 MPa) and the hydrothermally-transformed CBHA scaffold (0.38 MPa). The coating with PVA did not modify the viability and the adhesion and proliferation capacity of CBHA scaffolds.

Table 2. Compressive strength of raw CB, CBHA, and the different percentages of PCL coating on CBHA.

Ref	Compressive Strength (MPa)					
	Raw CB	CBHA	CBHA1%PCL	CBHA5%PCL	CBHA10%PCL	CBHA20%PCL
[221]	1.63 ± 0.13	1.11 ± 0.26	1.25 ± 0.56	2.32 ± 0.44	3.67 ± 0.46	—
[222]	0.609	0.376	—	1.376	—	—
[223]	0.46 ± 0.06	0.15 ± 0.09	—	—	—	0.88 ± 0.11

Alternatively to the production of CBHA through HT and a posterior coating with polymer, *Sukul et al.* [225] modified the raw CB with HA and collagen (CB-HA-COL). To this end, CB was immersed in SBF solution to form an HA layer and samples were subsequently coated with collagen through the freeze-drying method. The modification of the CB surface with HA and collagen resulted in lower values of pore size (80–100 μm) and porosity (~84%), but still, these values have been reported as beneficial in bone tissue engineering. On the other hand, the coating enhanced the compressive strength from 2.00 ± 0.40 MPa for raw CB to 2.71 ± 0.16 MPa for CB-HA-COL. The coated scaffolds promoted cell adhesion and proliferation and showed higher levels of ALP expression.

7. Conclusions

The earlier industrial revolution, in addition to the innovations in agricultural production and distribution, enabled nutritional diversity and consistency to large numbers of people, increasing the survival rate. The progresses in medicine, namely related to the understanding and control of infectious and parasitic diseases, some of the common causes of death, and improvements in clinical practice, in addition to the noticeable changes in public health that occurred from the late 19th century and physical activity, have led to a gradual and remarkable increase in human life expectancy at birth. Not surprisingly, postponing death to old ages came together with several problematic health consequences related to aging, including degenerative diseases such as cancers and diseases of the circulatory system, as well as the brittleness and breakage of bones weakened by osteoporosis, especially for older women.

The increased incidence of degenerative diseases such as osteoarthritis, especially in cases of excessive sedentary behaviour, and bone tumour resections demands for suitable bone grafts. Although the autologous bone graft is the gold standard clinical material for bone regeneration because of its advantages in terms of osteoconduction and osteoinduction, the limited availability and donor site morbidity are the most obvious drawbacks related to this option. A bone allograft is an alternative source, being the second most used option for orthopaedic procedures due to the availability in various forms and large quantities. But the main limitations include reduced osteoinductivity that may lead to inferior healing as compared with the use of autologous grafts, and to

potential risks of the immune response. Xenografts are abundant, but the potential rejection by the host remains and cannot be discarded.

The shortcomings of the biologically-derived bone grafts and the increasing demand for bone repair materials constitute the main driving forces for the continuous search of synthetic bone graft substitutes. This article reviews the state of the art of synthetic bone graft materials fabricated from synthetic calcium phosphate powders or resulting from the total or partial hydrothermal transformation of aragonite marine-derived porous structures such as corals and cuttlefish bones. Tailor-made porous structures can also be made by using additive manufacturing techniques. Doping the calcium phosphate materials with selected doses of other elements enhances the biological performance of the inorganic materials. On the other hand, combining the inorganic components with suitable biopolymers is a very promising strategy for obtaining multifunctional bone graft materials. Furthermore, applying tissue engineering principles by suitably combining growth factors and cells is a method employed for developing synthetic bone grafts with in vivo performances that compete with autografts.

Author Contributions: Both authors have contributed to this review article. J.M.F.F. conceived and designed the main structure of the article and did the specific literature survey and analysis about corals. A.S.N. is a PhD student doing research on synthetic bone graft substitutes based on calcium phosphates and on the use of CB for biomedical applications. Her PhD work programme was also conceived and designed by J.M.F.F., and aims at developing porous scaffolds following two different approaches: (i) the hydrothermal transformation of CB into biphasic calcium phosphates while preserving its unique porous structure; and (ii) the hydrothermal synthesis of biphasic calcium phosphate powders and their use for preparing highly concentrated and extrudable pastes suitable for the fabrication of tailor-made porous scaffolds by robocasting. A.S.N. was in charge of performing most of the literature survey and analysis, and of elaborating the first draft of the parts more closely related to her PhD work programme, as well of integrating the spare contributes received from the supervisor into a single document. The supervisor conducted the final check of and provided refinements to the entire document.

Acknowledgments: This work was developed within the scope of the project CICECO-Aveiro Institute of Materials, POCI-01-0145-FEDER-007679 (FCT Ref. UID /CTM /50011/2013), University of Aveiro, financed by national funds through the FCT/MEC, Portugal, and when appropriate, co-financed by FEDER under the PT2020 Partnership Agreement. Ana S. Neto is grateful to AdvaMTech, the PhD Program on Advanced Materials and Processing for the PhD grant, PD/BD/114132/2015, founded by the Portuguese Foundation for Science and Technology (FCT).

References

1. Baron, R. Anatomy and Ultrastructure of Bone—Histogenesis, Growth and Remodeling. [Updated 2008 May 13]. In *Endotext [Internet]*; De Groot, L.J., Chrousos, G., Dungan, K., Feingold, K.R., Grossman, A., Hershman, J.M., Koch, C., Korbonits, M., McLachlan, R., New, M., et al., Eds.; MDText.com, Inc.: South Dartmouth, MA, USA, 2000.
2. Jee, W.S.S. Integrated Bone Tissue Physiology: Anatomy and Physiology. In *Bone Mechanics Handbook*; Cowin, S.C., Ed.; CRC Press: Boca Raton, FL, USA, 2001; Volume 2, ISBN 0849345626.
3. Hadjidakis, D.J.; Androulakis, I.I. Bone remodeling. *Ann. N. Y. Acad. Sci.* **2006**, *1092*, 385–396.
4. Dimitriou, R.; Jones, E.; McGonagle, D.; Giannoudis, P. V Bone regeneration: Current concepts and future directions. *BMC Med.* **2011**, *9*, 66, doi:10.1186/1741-7015-9-66.
5. Wang, P.; Zhao, L.; Liu, J.; Weir, M.D.; Zhou, X.; Xu, H.H.K. Bone tissue engineering via nanostructured calcium phosphate biomaterials and stem cells. *Bone Res.* **2014**, *2*, 14017, doi:10.1038/boneres.2014.17.
6. Nandi, S.K.; Roy, S.; Mukherjee, P.; Kundu, B.; De, D.; Basu, D. Orthopaedic applications of bone graft & graft substitutes: A review. *Indian J. Med. Res.* **2010**, *132*, 15–30.
7. Sen, M.K.; Miclau, T. Autologous iliac crest bone graft: Should it still be the gold standard for treating nonunions? *Injury* **2007**, *38* (Suppl. 1), S75–S80.
8. Zimmermann, G.; Moghaddam, A. Allograft bone matrix versus synthetic bone graft substitutes. *Injury* **2011**, *42*, S16–S21.
9. Ravaglioli, A.; Krajewski, A. *Bioceramics*; Chapman & Hall: London, UK, 1992; ISBN 978-94-010-5032-6.
10. Wong, J.Y.; Bronzino, J.D. *Biomaterials*; CRC Press: Boca Raton, FL, USA, 2007; ISBN 9781405116244.
11. Ratner, B.D.; Hoffman, A.S.; Schoen, F.J.; Lemons, J.E. Biomaterials Science: An Evolving Multidisciplinary Endeavor. In *Biomaterials Science: An Introduction to*

Materials in Medicine; Academic Press: Waltham, MA, USA, 2013 ISBN 0080500145.

12. O'Brien, F.J. Biomaterials & scaffolds for tissue engineering. *Mater. Today* **2011**, *14*, 88–95.
13. Goel, A.; Kapoor, S.; Rajagopal, R.R.; Pascual, M.J.; Kim, H.W.; Ferreira, J.M.F. Alkali-free bioactive glasses for bone tissue engineering: A preliminary investigation. *Acta Biomater.* **2012**, *8*, 361–372.
14. Wang, M. Developing bioactive composite materials for tissue replacement. *Biomaterials* **2003**, *24*, 2133–2151.
15. Basha, R.Y.; T.S., S.K.; Doble, M. Design of biocomposite materials for bone tissue regeneration. *Mater. Sci. Eng. C* **2015**, *57*, 452–463.
16. Turnbull, G.; Clarke, J.; Picard, F.; Riches, P.; Jia, L.; Han, F.; Li, B.; Shu, W. 3D bioactive composite scaffolds for bone tissue engineering. *Bioact. Mater.* **2017**, *3*, 278–314.
17. Tanner, K.E. Bioactive composites for bone tissue engineering. *Procedings Inst. Mech. Eng. Part H* **2010**, *224*, 1359–1372.
18. García-Gareta, E.; Coathup, M.J.; Blunn, G.W. Osteoinduction of bone grafting materials for bone repair and regeneration. *Bone* **2015**, *81*, 112–121.
19. Roseti, L.; Parisi, V.; Petretta, M.; Cavallo, C.; Desando, G.; Bartolotti, I.; Grigolo, B. Scaffolds for Bone Tissue Engineering: State of the art and new perspectives. *Mater. Sci. Eng. C* **2017**, *78*, 1246–1262.
20. Bose, S.; Vahabzadeh, S.; Bandyopadhyay, A. Bone tissue engineering using 3D printing. *Mater. Today* **2013**, *16*, 496–504.
21. Green, D.W.; Lai, W.F.; Jung, H.S. Evolving marine biomimetics for regenerative dentistry. *Mar. Drugs* **2014**, *12*, 2877–2912.
22. Zhang, X.; Vecchio, K.S. Conversion of natural marine skeletons as scaffolds for bone tissue engineering. *Front. Mater. Sci.* **2013**, *7*, 103–117.
23. Gong, T.; Xie, J.; Liao, J.; Zhang, T.; Lin, S.; Lin, Y. Nanomaterials and bone regeneration. *Bone Res.* **2015**, *3*, 15029, doi:10.1038/boneres.2015.29.
24. Boskey, A.L. Mineralization of bones and teeth. *Elements* **2007**, *3*, 385–391.

25. Young, M.F. Bone matrix proteins: Their function, regulation, and relationship to osteoporosis. *Osteoporos. Int.* **2003**, *14* (Suppl. 3), S35–S42.

26. Reznikov, N.; Shahar, R.; Weiner, S. Bone hierarchical structure in three dimensions. *Acta Biomater.* **2014**, *10*, 3815–3826.

27. Habraken, W.; Habibovic, P.; Epple, M.; Bohner, M. Calcium phosphates in biomedical applications: Materials for the future? *Mater. Today* **2016**, *19*, 69–87.

28. Boskey, A.L. Bone composition: Relationship to bone fragility and antiosteoporotic drug effects. *Bonekey Rep.* **2013**, *2*, 447, doi:10.1038/bonekey.2013.181.

29. Orgel, J.P.R.O.; Miller, A.; Irving, T.C.; Fischetti, R.F.; Hammersley, A.P.; Wess, T.J. The in situ supermolecular structure of type I collagen. *Structure* **2001**, *9*, 1061–1069.

30. Rho, J.; Kuhn-Spearing, L.; Zioupos, P. Mechanical properties and the hierarchical structure of bone. *Med. Eng. Phys.* **1998**, *20*, 92–102.

31. Sroga, G.E.; Vashishth, D. Effects of Bone Matrix Proteins on Fracture and Fragility in Osteoporosis. *Biophys. Chem.* **2005**, *257*, 2432–2437.

32. Raisz, L.G. Physiology and pathophysiology of bone remodeling. *Clin. Chem.* **1999**, *45*, 1353–1358.

33. Barry, F.P.; Murphy, J.M. Mesenchymal stem cells: Clinical applications and biological characterization. *Int. J. Biochem. Cell Biol.* **2004**, *36*, 568–584.

34. Marolt, D.; Knezevic, M.; Novakovic, G.V. Bone tissue engineering with human stem cells. *Stem Cell Res. Ther.* **2010**, *1*, 1–10.

35. Pountos, I.; Corscadden, D.; Emery, P.; Giannoudis, P.V. Mesenchymal stem cell tissue engineering: Techniques for isolation, expansion and application. *Injury* **2007**, *38* (Suppl. 4), S23–S33.

36. Florencio-Silva, R.; Sasso; Da Silva, G.R.; Sasso-Cerri, E.; Simões, M.J.; Cerri, P.S. Biology of Bone Tissue: Structure, Function, and Factors That Influence Bone Cells. *BioMed Res. Int.* **2015**, *2015*, 1–17.

37. Caetano-Lopes, J.; Canhão, H.; Fonseca, J.E. Osteoblasts and bone formation. *Acta Reumatol. Port.* **2007**, *32*, 103–110.

38. Yavropoulou, M.P.; Yovos, J.G. Osteoclastogenesis—Current knowledge and future

perspectives. *J. Musculoskelet. Neuronal Interact.* **2008**, *8*, 204–16.

39. Väänänen, K. Mechanism of osteoclast mediated bone resorption—Rationale for the design of new therapeutics. *Adv. Drug Deliv. Rev.* **2005**, *57*, 959–971.
40. Kini, U.; Nandeesh, B.N. Physiology of Bone Formation, Remodeling, and Metabolism. In *Radionuclide and Hybrid Bone Imaging*; **Springer: Berlin, Germany,** 2012; pp. 29–57, ISBN 9783642023996.
41. Bonewald, L.F. The amazing osteocyte. *J. Bone Miner. Res.* **2011**, *26*, 229–238.
42. Kapinas, K.; Delany, A.M. MicroRNA biogenesis and regulation of bone remodeling. *Arthritis Res. Ther.* **2011**, *13*, 220, doi:10.1186/ar3325.
43. Niedźwiedzki, T.; Filipowska, J. Bone remodeling in the context of cellular and systemic regulation: The role of osteocytes and the nervous system. *J. Mol. Endocrinol.* **2015**, *55*, R23–R36.
44. Pogoda, P.; Priemel, M.; Rueger, J.M.; Amling, M. Bone remodeling: New aspects of a key process that controls skeletal maintenance and repair. *Osteoporos. Int.* **2005**, *16* (Suppl. 2), S18–S24.
45. Thomlinson, R. *Population Dynamics. Causes and Consequences of World Demographic Change, 2nd ed.*; Random House: New York, NY, USA, 1976.
46. National Research Council. *Preparing for an Aging World: The Case for Cross-National Research*; National Academy Press: Washington, DC, USA, 2001.
47. Preston, S.; Haines, M. *Fatal Years- Child Mortality in Late Nineteenth-Century America*; Princeton University Press: Princeton, NJ, USA, 1991.
48. McKeown, T. *The Role of Medicine- Dream, Mirage, or Nemesis?*; Princeton University Press: Princeton, NJ, USA, 1979.
49. Howse, K. *Increasing Life Expectancy and the Compression of Morbidity: A Critical Review of the Debate*; Oxford Working Paper Number 206. Oxford Institute of Ageing: Oxford, UK, 2006.
50. Wang, W.; Yeung, K.W.K. Bone grafts and biomaterials substitutes for bone defect repair: A review. *Bioact. Mater.* **2017**, *2*, 224–247.
51. Oryan, A.; Alidadi, S.; Moshiri, A.; Maffulli, N. Bone regenerative medicine: Classic options, novel strategies, and future directions. *J. Orthop. Surg. Res.* **2014**, *9*, 18,

doi:10.1186/1749-799X-9-18.

52. Moore, W.R.; Graves, S.E.; Bain, G.I. Synthetic bone graft substitutes. *ANZ J. Surg.* **2001**, *71*, 354–361.

53. Albrektsson, T.; Johansson, C. Osteoinduction, osteoconduction and osseointegration. *Eur. Spine J.* **2001**, *10*, 96–101.

54. Legeros, R.Z.; Craig, R.G. Strategies to affect bone remodeling: Osteointegration. *J. Bone Miner. Res.* **1993**, *8* (Suppl. 2), S583–S596.

55. Blokhuis, T.J.; Arts, J.J.C. Bioactive and osteoinductive bone graft substitutes: Definitions, facts and myths. *Injury* **2011**, *42* (Suppl. 2), S26–S29.

56. James, R.; Deng, M.; Laurencin, C.T.; Kumbar, S.G. Nanocomposites and bone regeneration. *Front. Mater. Sci.* **2011**, *5*, 342–357.

57. Griffin, K.S.; Davis, K.M.; McKinley, T.O.; Anglen, J.O.; Chu, T.M.G.; Boerckel, J.D.; Kacena, M.A. Evolution of Bone Grafting: Bone Grafts and Tissue Engineering Strategies for Vascularized Bone Regeneration. *Clin. Rev. Bone Miner. Metab.* **2015**, *13*, 232–244.

58. Delloye, C.; Cornu, O.; Druez, V.; Barbier, O. Bone allografts: What they can offer and what they cannot. *J. Bone Jt. Surg. Br.* **2007**, *89–B*, 574–580.

59. Barend, H. Mr. Job van Meekeren (1611–1666) and Surgery of the Hand. *Plast. Reconstr. Surg.* **1988**, *82*, 539–546.

60. Crapo, P.M.; Gilbert, T.W.; Badylak, S.F. An overview of tissue and whole organ decellularization processes. *Biomaterials* **2011**, *32*, 3233–3243.

61. Gilbert, T.W. Strategies for tissue and organ decellularization. *J. Cell. Biochem.* **2012**, *113*, 2217–2222.

62. Stone, K. Bone Xenografts. Patent US 20030074065A1, 17 April 2003.

63. Tehrani, A.H. *Exploring Methods of Preparing Functional Cartilage-Bone Xenografts for Joint Repair*; Queensland University of Technology: Queensland, Australia, 2015.

64. Kheir, E.; Stapleton, T.; Shaw, D.; Jin, Z.; Fisher, J.; Ingham, E. Development and characterization of an acellular porcine cartilage bone matrix for use in tissue engineering. *J. Biomed. Mater. Res. Part A* **2011**, *99*, 283–294.

65. Gardin, C.; Ricci, S.; Ferroni, L.; Guazzo, R.; Sbricoli, L.; De Benedictis, G.; Finotti, L.; Isola, M.; Bressan, E.; Zavan, B. Decellularization and delipidation protocols of bovine bone and pericardium for bone grafting and guided bone regeneration procedures. *PLoS ONE* **2015**, *10*, 1–26.

66. Keane, T.J.; Londono, R.; Turner, N.J.; Badylak, S.F. Consequences of ineffective decellularization of biologic scaffolds on the host response. *Biomaterials* **2012**, *33*, 1771–1781.

67. Shibuya, N.; Jupiter, D.C. Bone Graft Substitute: Allograft and Xenograft. *Clin. Podiatr. Med. Surg.* **2015**, *32*, 21–34.

68. Rhee, S.-H.; Chung, C.-P.; Park, Y.-J. Method for Preparing a Prion-Free Bone Grafting Substitute. Patent WO2007132952A1, 12 May 2006.

69. Cho, J.S.; Kim, H.S.; Um, S.H.; Rhee, S.H. Preparation of a novel anorganic bovine bone xenograft with enhanced bioactivity and osteoconductivity. *J. Biomed. Mater. Res. Part B Appl. Biomater.* **2013**, *101*, 855–869.

70. Jensen, T.; Schou, S.; Stavropoulos, A.; Terheyden, H.; Holmstrup, P. Maxillary sinus floor augmentation with Bio-Oss or Bio-Oss mixed with autogenous bone as graft in animals: a systematic review. *Int. J. Oral Maxillofac. Surg.* **2012**, *41*, 114-120, doi:10.1016/j.ijom.2011.08.010.

71. Stavropoulos, A. Deproteinized Bovine Bone Xenograft. In *Musculoskeletal Tissue Regeneration*; Pietrzak, W.S., Ed.; Humana Press Totowa, NI, USA, 2008; ISBN 978-1-58829-909-3.

72. Bhatt, R.A.; Rozental, T.D. Bone Graft Substitutes. *Hand Clin.* **2012**, *28*, 457–468.

73. Soucacos, P.N.; Johnson, E.O.; Babis, G. An update on recent advances in bone regeneration. *Injury* **2008**, *39* (Suppl. 2), S1–S4.

74. Perez, R.A.; Seo, S.J.; Won, J.E.; Lee, E.J.; Jang, J.H.; Knowles, J.C.; Kim, H.W. Therapeutically relevant aspects in bone repair and regeneration. *Mater. Today* **2015**, *18*, 573–589.

75. Mouriño, V.; Boccaccini, A.R. Bone tissue engineering therapeutics: Controlled drug delivery in three-dimensional scaffolds. *J. R. Soc. Interface* **2010**, *7*, 209–227.

76. Hench, L.L.; Polak, J.M. Third Generation Biomedical Materials. *Science* **2002**, *295*,

1014–1017.

77. Henkel, J.; Woodruff, M.A.; Epari, D.R.; Steck, R.; Glatt, V.; Dickinson, I.C.; Choong, P.F.M.; Schuetz, M.A.; Hutmacher, D.W. Bone Regeneration Based on Tissue Engineering Conceptions—A 21st Century Perspective. *Bone Res.* **2013**, *1*, 216–248.

78. Stevens, M.M. Biomaterials for bone tissue engineering. *Mater. Today* **2008**, *11*, 18–25.

79. Shrivats, A.R.; McDermott, M.C.; Hollinger, J.O. Bone tissue engineering: State of the union. *Drug Discov. Today* **2014**, *19*, 781–786.

80. Cortizo, M.S.; Belluzo, M.S. Biodegradable Polymers for Bone Tissue Engineering. In *Industrial Applications of Renewable Biomass Products Past, Present and Future*; Goyanes, S.N., D'Accorso, N.B., Eds.;Spring: Berlin, Germany, 2017; ISBN 978-3-319-61287-4.

81. Sabir, M.I.; Xu, X.; Li, L. A review on biodegradable polymeric materials for bone tissue engineering applications. *J. Mater. Sci.* **2009**, *44*, 5713–5724.

82. Echave, M.C.; Sanchez, P.; Pedraz, J.L.; Orive, G. Progress of gelatin-based 3D approaches for bone regeneration. *J. Drug Deliv. Sci. Technol.* **2017**, *42*, 63–74.

83. Solchaga, L.A.; Dennis, J.E.; Goldberg, V.M.; Caplan, A.I. Hyaluronic acid-based polymers as cell carriers for tissue-engineered repair of bone and cartilage. *J. Orthop. Res.* **1999**, *17*, 205–213.

84. Cheung, H.Y.; Lau, K.T.; Lu, T.-P.; Hui, D. A critical review on polymer-based bio-engineered materials for scaffold development. *Compos. Part B* **2007**, *38*, 291–300.

85. Georgopoulou, A.; Kaliva, M.; Vamvakaki, M.; Chatzinikolaidou, M. Osteogenic potential of pre-osteoblastic cells on a chitosan-graft-polycaprolactone copolymer. *Materials* **2018**, *11*, 1–14.

86. Shirani, K.; Nourbakhsh, M.S.; Rafienia, M. Electrospun polycaprolactone/gelatin/bioactive glass nanoscaffold for bone tissue engineering. *Int. J. Polym. Mater. Polym. Biomater.* **2018**, 1–9, doi:10.1080/00914037.2018.1482461.

87. Fonseca, A.C.; Coelho, J.F.J.; Gil, M.H.; Simões, P.N. Poly(ester amide)s based on

l-lactic acid oligomers and glycine: The role of the central unit of the l-lactic acid oligomers and their molecular weight in the poly(ester amide)s properties. *Polym. Bull.* **2014**, *71*, 3085–3109.

88. Fonseca, A.C.; Gil, M.H.; Simões, P.N. Biodegradable poly(ester amide)s—A remarkable opportunity for the biomedical area: Review on the synthesis, characterization and applications. *Prog. Polym. Sci.* **2014**, *39*, 1291–1311.
89. Stakleff, K.S.; Lin, F.; Smith Callahan, L.A.; Wade, M.B.; Esterle, A.; Miller, J.; Graham, M.; Becker, M.L. Resorbable, amino acid-based poly(ester urea)s crosslinked with osteogenic growth peptide with enhanced mechanical properties and bioactivity. *Acta Biomater.* **2013**, *9*, 5132–5142.
90. Li, S.; Xu, Y.; Yu, J.; Becker, M.L. Enhanced osteogenic activity of poly(ester urea) scaffolds using facile post-3D printing peptide functionalization strategies. *Biomaterials* **2017**, *141*, 176–187.
91. Marzec, M.; Kucińska-Lipka, J.; Kalaszczyńska, I.; Janik, H. Development of polyurethanes for bone repair. *Mater. Sci. Eng. C* **2017**, *80*, 736–747.
92. Dorozhkin, S.V. Calcium Orthophosphates as Bioceramics: State of the Art. *J. Funct. Biomater.* **2010**, *1*, 22–107.
93. Dorozhkin, S. Bioceramics of calcium orthophosphates. *Biomaterials* **2010**, *31*, 1465–1485.
94. Dorozhkin, S.V. Calcium Apatites and Other Calcium Orthophosphates. In *Calcium Orthophosphates: Applications in Nature, Biology and Medicine*; CRC Press: Boca Raton, FL, USA, 2012; pp. 1–151, ISBN 9814316628.
95. Bohner, M. Design of ceramic-based cements and putties for bone graft substitution. *Eur. Cells Mater.* **2010**, *20*, 1–12.
96. Boanini, E.; Gazzano, M.; Bigi, A. Ionic substitutions in calcium phosphates synthesized at low temperature. *Acta Biomater.* **2010**, *6*, 1882–1894.
97. Marques, C.F.; Lemos, A.; Vieira, S.I.; Da Cruz E Silva, O.A.B.; Bettencourt, A.; Ferreira, J.M.F. Antibiotic-loaded Sr-doped porous calcium phosphate granules as multifunctional bone grafts. *Ceram. Int.* **2016**, *42*, 2706–2716.
98. Marques, C.F.; Matos, A.C.; Ribeiro, I.A.C.; Gonçalves, L.M.; Bettencourt, A.;

Ferreira, J.M.F. Insights on the properties of levofloxacin-adsorbed Sr- and Mg-doped calcium phosphate powders. *J. Mater. Sci. Mater. Med.* **2016**, *27*, 1–12.

99. Torres, P.M.C.; Marote, A.; Cerqueira, A.R.; Calado, A.J.; Abrantes, J.C.C.; Olhero, S.; da Cruz e Silva, O.A.B.; Vieira, S.I.; Ferreira, J.M.F. Injectable MnSr-doped brushite bone cements with improved biological performance. *J. Mater. Chem. B* **2017**, *5*, 2775–2787.

100. Bracci, B.; Torricelli, P.; Panzavolta, S.; Boanini, E.; Giardino, R.; Bigi, A. Effect of Mg^{2+}, Sr^{2+}, and Mn^{2+} on the chemico-physical and in vitro biological properties of calcium phosphate biomimetic coatings. *J. Inorg. Biochem.* **2009**, *103*, 1666–1674.

101. Luo, X.; Barbieri, D.; Davison, N.; Yan, Y.; De Bruijn, J.D.; Yuan, H. Zinc in calcium phosphate mediates bone induction: In vitro and in vivo model. *Acta Biomater.* **2014**, *10*, 477–485.

102. Cruz, R.; Calasans-Maia, J.; Sartoretto, S.; Moraschini, V.; Rossi, A.M.; Louro, R.S.; Granjeiro, J.M.; Calasans-Maia, M.D. Does the incorporation of zinc into calcium phosphate improve bone repair? A systematic review. *Ceram. Int.* **2018**, *44*, 1240–1249.

103. Vincent, J.F. V Biomimetics in architectural design. *Intell. Build. Int.* **2016**, *8*, 138–149.

104. Mano, J.F.; Sousa, R.A.; Boesel, L.F.; Neves, N.M.; Reis, R.L. Bioinert, biodegradable and injectable polymeric matrix composites for hard tissue replacement: State of the art and recent developments. *Compos. Sci. Technol.* **2004**, *64*, 789–817.

105. Li, X.; Wang, Y.; Wang, Z.; Qi, Y.; Li, L.; Zhang, P.; Chen, X.; Huang, Y. Composite PLA/PEG/nHA/Dexamethasone Scaffold Prepared by 3D Printing for Bone Regeneration. *Macromol. Biosci.* **2018**, 18, 1800068, doi: 10.1002/mabi.201800068.

106. Rakovsky, A.; Gotman, I.; Rabkin, E.; Gutmanas, E.Y. β-TCP–polylactide composite scaffolds with high strength and enhanced permeability prepared by a modified salt leaching method. *J. Mech. Behav. Biomed. Mater.* **2014**, *32*, 89–98.

107. Mavis, B.; Demirtas, T.T.; Gümüsderelioglu, M.; Gündüz, G.; Çolak, Ü. Synthesis , characterization and osteoblastic activity of polycaprolactone nanofibers coated with biomimetic calcium phosphate. *Acta Biomater.* **2009**, *5*, 3098–3111.

108. Patil, T.; Saha, S.; Biswas, A. Preparation and Characterization of HAp Coated Chitosan-Alginate PEC Porous Scaffold for Bone Tissue Engineering. *Macromol. Symp.* **2017**, 376 1600205, doi:10.1002/masy.201600205.

109. Motealleh, A.; Eqtesadi, S.; Pajares, A.; Miranda, P. Enhancing the mechanical and in vitro performance of robocast bioglass scaffolds by polymeric coatings : Effect of polymer composition. *J. Mech. Behav. Biomed. Mater.* **2018**, *84*, 35–45.

110. Li, W.; Nooeaid, P.; Roether, J.A.; Schubert, D.W.; Boccaccini, A.R. Preparation and characterization of vancomycin releasing PHBV coated 45S5 Bioglass® -based glass—Ceramic scaffolds for bone tissue engineering. *J. Eur. Ceram. Soc.* **2014**, *34*, 505–514.

111. Canal, C.; Khurana, K.; Gallinetti, S.; Bhatt, S.; Pulpytel, J.; Arefi-Khonsari, F.; Ginebra, M.-P. Design of calcium phosphate scaffolds with controlled simvastatin release by plasma polymerisation. *Polymer* **2016**, *92*, 170–178.

112. Roohani-Esfahani, S.-I.; Nouri-khorasani, S.; Lu, Z.; Appleyard, R.; Zreiqat, H. The influence hydroxyapatite nanoparticle shape and size on the properties of biphasic calcium phosphate scaffolds coated with hydroxyapatite-PCL composites. *Biomaterials* **2010**, *31*, 5498–5509.

113. Shi, Y.; Liu, J.; Yu, L.; Zhong, L.Z.; Jiang, B.H. β-TCP scaffold coated with PCL as biodegradable materials for dental applications. *Ceram. Int.* **2018**, 44, 15086-15091.

114. Bose, S.; Roy, M.; Bandyopadhyay, A. Recent advances in bone tissue engineering scaffolds. *Trends Biotechnol.* **2012**, *30*, 546–554.

115. Tang, W.; Lin, D.; Yu, Y.; Niu, H.; Guo, H.; Yuan, Y.; Liu, C. Bioinspired trimodal macro/micro/nano-porous scaffolds loading rhBMP-2 for complete regeneration of critical size bone defect. *Acta Biomater.* **2016**, *32*, 309–323.

116. Miranda, P.; Saiz, E.; Gryn, K.; Tomsia, A.P. Sintering and robocasting of b-tricalcium phosphate scaffolds for orthopaedic applications. *Acta Biomater.* **2006**, *2*, 457–466.

117. Smay, J.E.; Cesarano, J.; Lewis, J.A. Colloidal inks for directed assembly of 3-D periodic structures. *Langmuir* **2002**, *18*, 5429–5437.

118. Sa, M.-W.; Kim, J.Y. Fabrication and evaluation of 3D β-TCP scaffold by novel direct-write assembly method. *J. Mech. Sci. Technol.* **2015**, *29*, 5369–5376.

119. Houmard,M.;Fu,Q.;Genet,M.;Saiz,E.;Tomsia,A.P.Onthestructural,mechanical,andbiodegradation properties of HA/β-TCP robocast scaffolds. *J. Biomed. Mater. Res. Part B* **2013**, *101*, 1233–1242.

120. Dellinger, J.G.; Cesarano, J., III; Jamison, R.D. Robotic deposition of model hydroxyapatite scaffolds with multiple architectures and multiscale porosity for bone tissue engineering. *J. Biomed. Mater. Res. Part A* **2007**, *82*, 383–394.

121. Miranda, P.; Pajares, A.; Saiz, E.; Tomsia, A.P.; Guiberteau, F. Mechanical properties of calcium phosphate scaffolds fabricated by robocasting. *J. Biomed. Mater. Res. Part A* **2008**, *85*, 218–227.

122. Marques, C.F.; Perera, F.H.; Marote, A.; Ferreira, S.; Vieira, S.I.; Olhero, S.; Miranda, P.; Ferreira, J.M.F. Biphasic calcium phosphate scaffolds fabricated by direct write assembly: Mechanical, anti-microbial and osteoblastic properties. *J. Eur. Ceram. Soc.* **2017**, *37*, 359–368.

123. Del Rosario, C.; Rodríguez-Évora, M.; Reyes, R.; Delgado, A.; Évora, C. BMP-2, PDGF-BB, and bone marrow mesenchymal cells in a macroporous β-TCP scaffold for critical-size bone defect repair in rats. *Biomed. Mater.* **2015**, *10*, 045008, doi:10.1088/1748-6041/10/4/045008.

124. Hong, S.J.; Jeong, I.; Noh, K.T.; Yu, H.S.; Lee, G.S.; Kim, H.W. Robotic dispensing of composite scaffolds and in vitro responses of bone marrow stromal cells. *J. Mater. Sci. Mater. Med.* **2009**, *20*, 1955–1962.

125. Maazouz, Y.; Montufar, E.B.; Guillem-Marti, J.; Fleps, I.; Öhman, C.; Persson, C.; Ginebra, M.P. Robocasting of biomimetic hydroxyapatite scaffolds using self-setting inks. *J. Mater. Chem. B* **2014**, *2*, 5378–5386.

126. Touri, M.; Moztarzadeh, F.; Osman, N.A.A.; Dehghan, M.M.; Mozafari, M. 3D–printed biphasic calcium phosphate scaffolds coated with an oxygen generating system for enhancing engineered tissue survival. *Mater. Sci. Eng. C* **2018**, *84*, 236–242.

127. Eqtesadi, S.; Motealleh, A.; Miranda, P.; Pajares, A.; Lemos, A.; Ferreira, J.M.F. Robocasting of 45S5 bioactive glass scaffolds for bone tissue engineering. *J. Eur. Ceram. Soc.* **2014**, *34*, 107–118.

128. Eqtesadi, S.; Motealleh, A.; Wendelbo, R.; Ortiz, A.L.; Miranda, P. Reinforcement

with reduced graphene oxide of bioactive glass scaffolds fabricated by robocasting. *J. Eur. Ceram. Soc.* **2017**, *37*, 3695–3704.

129. Olhero, S.M.; Fernandes, H.R.; Marques, C.F.; Silva, B.C.G.; Ferreira, J.M.F. Additive manufacturing of 3D porous alkali-free bioactive glass scaffolds for healthcare applications. *J. Mater. Sci.* **2017**, *52*, 12079–12088.

130. Stanciuc, A.M.; Sprecher, C.M.; Adrien, J.; Roiban, L.I.; Alini, M.; Gremillard, L.; Peroglio, M. Robocast zirconia-toughened alumina scaffolds: Processing, structural characterisation and interaction with human primary osteoblasts. *J. Eur. Ceram. Soc.* **2018**, *38*, 845–853.

131. Kim, S.-K. *Marine Biomaterials: Characterization, Isolation and Applications*; CRC Press: New York, NY, USA, 2013; ISBN 9781466505650.

132. Ben-Nissan, B. Introduction to marine biomaterials. Discovery and development of marine biomaterials. In *Functional Marine Biomaterials Properties and Applications*; Elsevier, 2015; ISBN 9781845694708.

133. Roy, D.M.; Linnehan, S.K. Hydroxyapatite formed from coral skeletal carbonate by hydrothermal exchange. *Nature* **1974**, *247*, 220–222.

134. Zhang, X.; Takahashi, T.; Vecchio, K.S. Development of bioresorbable Mg-substituted tricalcium phosphate scaffolds for bone tissue engineering. *Mater. Sci. Eng. C* **2009**, *29*, 2003–2010.

135. Zhang, X.; Jiang, F.; Groth, T.; Vecchio, K.S. Preparation, characterization and mechanical performance of dense β-TCP ceramics with/without magnesium substitution. *J. Mater. Sci. Mater. Med.* **2008**, *19*, 3063–3070.

136. Demers, C.; Hamdy, C.R.; Corsi, K.; Chellat, F.; Tabrizian, M.; Yahia, L. Natural coral exoskeleton as a bone graft substitute: A review. *Biomed. Mater. Eng.* **2002**, *12*, 15–35.

137. Rocha, J.H.G.; Lemos, A.F.; Kannan, S.; Agathopoulos, S.; Ferreira, J.M.F. Hydroxyapatite scaffolds hydrothermally grown from aragonitic cuttlefish bones. *J. Mater. Chem.* **2005**, *15*, 5007–5011.

138. Green, D.; Howard, D.; Yang, X.; Kelly, M.; Oreffo, R.O.C. Natural marine sponge fiber skeleton: A biomimetic scaffold for human osteoprogenitor cell attachment, growth, and differentiation. *Tissue Eng.* **2003**, *9*, 1159–1166.

139. Vecchio, K.S.; Zhang, X.; Massie, J.B.; Wang, M.; Kim, C.W. Conversion of bulk seashells to biocompatible hydroxyapatite for bone implants. *Acta Biomater.* **2007**, *3*, 910–918.

140. Vecchio, K.S.; Zhang, X.; Massie, J.B.; Wang, M.; Kim, C.W. Conversion of sea urchin spines to Mg-substituted tricalcium phosphate for bone implants. *Acta Biomater.* **2007**, *3*, 785–793.

141. Ruppert, E.E.; Fox, R.S.; Barnes, R.D. *Invertebrate Zoology: A Functional Evolutionary Approach*, 7th ed.; Cengage Learning: Belmont, CA, USA, 2003; ISBN 9780030259821 .

142. About Coral Reefs. [Updated 2014. August 14], NOAA Coral Reef Conservation Program National Oceanic and Atmospheric Administration, U.S. Department of Commerce.

143. Julia, V.; Maharani, D.A.; Kartasasmita, R.E.; Latief, B.S. The use of coral scaffold in oral and maxillofacial surgery: A review. *J. Int. Dent. Med. Res.* **2016**, *9*, 427–435.

144. Damien, E.; Revell, P.A. Coralline hydroxyapatite bone graft substitute: A review of experimental studies and biomedical applications. *J. Appl. Biomater. Biomech.* **2004**, *2*, 65–73.

145. Elsinger, E.C.; Leal, L. Coralline hydroxyapatite bone graft substitutes. *J. Foot Ankle Surg.* **1996**, *35*, 396–399.

146. Okamura, T.; Uemura, N.; Baba, S.; Yasuda, N.; Yamashiro, H.; Imai, K.; Nishikawa, T.; Shimizu, H.; Shida, M.; Tominaga, K.; Tanaka, A. Montipora digitata Exoskeleton Derived Aragonite Particles are useful Scaffold for Tissue-engineered Vascular Graft in Vitro. *Nano Biomed.* **2017**, *9*, 105–111.

147. Sergeeva, N.S.; Britaev, T.A.; Sviridova, I.K.; Akhmedova, S.A.; Kirsanova, V.A.; Popov, A.A.; Antokhin, A.I.; Frank, G.A.; Kaprin, A.D. Scleractinium coral aquaculture skeleton: A possible 3D scaffold for cell cultures and bone tissue engineering. *Bull. Exp. Biol. Med.* **2014**, *156*, 504–508.

148. Puvaneswary, S.; Balaji Raghavendran, H.R.; Syuhada Ibrahim, N.S.; Murali, M.R.; Mahmood Merican, A.; Kamarul, T. A comparative study on morphochemical properties and osteogenic cell differentiation within bone graft and coral graft culture

systems. *Int. J. Med. Sci.* **2013**, *10*, 1608–1614.

149. Mangano, C.; Iaculli, F.; Piattelli, A.; Mangano, F.; Shibli, J.A.; Perrotti, V.; Iezzi, G. Clinical and Histologic Evaluation of Calcium Carbonate in Sinus Augmentation: A Case Series. *Int. J. Periodontics Restor. Dent.* **2014**, *34*, e43–e49.

150. Gunn, J.M.; Rekola, J.; Hirvonen, J.; Aho, A.J. Comparison of the osteoconductive properties of three particulate bone fillers in a rabbit model: Allograft, calcium carbonate (Biocoral®) and S53P4 bioactive glass. *Acta Odontol. Scand.* **2013**, *71*, 1238–1242.

151. Koëter, S.; Tigchelaar, S.J.; Farla, P.; Driessen, L.; Van Kampen, A.; Buma, P. Coralline hydroxyapatite is a suitable bone graft substitute in an intra-articular goat defect model. *J. Biomed. Mater. Res. Part B Appl. Biomater.* **2009**, *90*, 116–122.

152. Devecioğlu, D.; Tözüm, T.F.; Şengün, D.; Nohutcu, R.M. Biomaterials in Periodontal Regenerative Surgery: Effects of Cryopreserved Bone, Commercially Available Coral, Demineralized Freeze-dried Dentin, and Cementum on Periodontal Ligament Fibroblasts and Osteoblasts. *J. Biomater. Appl.* **2004**, *19*, 107–120.

153. Zhang, Y.; Yin, Q.S.; Xia, H.; Ai, F.Z.; Jiao, Y.P.; Chen, X.Q. Determination of antibacterial properties and cytocompatibility of silver-loaded coral hydroxyapatite. *J. Mater. Sci. Mater. Med.* **2010**, *21*, 2453–2462.

154. Mahanani, E.S.; Bachtiar, I.; Ana, I.D. Human mesenchymal stem cells behavior on synthetic coral scaffold. *Key Eng. Mater.* **2016**, *696*, 205–211.

155. Manassero, M.; Viateau, V.; Deschepper, M.; Oudina, K.; Logeart-Avramoglou, D.; Petite, H.; Bensidhoum, M. Bone Regeneration in Sheep Using Acropora Coral, a Natural Resorbable Scaffold, and Autologous Mesenchymal Stem Cells. *Tissue Eng. Part A* **2013**, *19*, 1554–1563.

156. Decambron, A.; Manassero, M.; Bensidhoum, M.; Lecuelle, B.; Logeart-Avramoglou, D.; Petite, H.; Viateau, V. A comparative study of tissue-engineered constructs from Acropora and Porites coral in a large animal bone defect model. *Bone Jt. Res.* **2017**, *6*, 208–215.

157. Viateau, V.; Manassero, M.; Sensébé, L.; Langonné, A.; Marchat, D.; Logeart-Avramoglou, D.; Petite, H.; Bensidhoum, M. Comparative study of the osteogenic ability of four different ceramic constructs in an ectopic large animal model. *J. Tissue*

Eng. Regen. Med. **2016**, *10*, E177–E187.

158. Vuola, J.; Taurio, R.; Göransson, H.; Asko-Seljavaara, S. Compressive strength of calcium carbonate and hydroxyapatite implants after bone-marrow-induced osteogenesis. *Biomaterials* **1998**, *19*, 223–227.

159. Yuan, J.; Cui, L.; Zhang, W.J.; Liu, W.; Cao, Y. Repair of canine mandibular bone defects with bone marrow stromal cells and porous β-tricalcium phosphate. *Biomaterials* **2007**, *28*, 1005–1013.

160. Kon, E.; Muraglia, A.; Corsi, A.; Bianco, P.; Marcacci, M.; Martin, I.; Boyde, A.; Ruspantini, I.; Chistolini, P.; Rocca, M.; et al. Autologous bone marrow stromal cells loaded onto porous hydroxyapatite ceramic accelerate bone repair in critical-size defects of sheep long. *J. Biomed. Mater. Res.* **2000**, *49*, 328–337.

161. Yuan, J.; Zhang, W.J.; Liu, G.; Wei, M.; Qi, Z.L.; Liu, W.; Cui, L.; Cao, Y.L. Repair of Canine Mandibular Bone Defects with Bone Marrow Stromal Cells and Coral. *Tissue Eng. Part A* **2010**, *16*, 1385–1394.

162. Birk, R.Z.; Abramovitch-Gottlib, L.; Margalit, I.; Aviv, M.; Forti, E.; Geresh, S.; Vago, R. Conversion of adipogenic to osteogenic phenotype using crystalline porous biomatrices of marine origin. *Tissue Eng.* **2006**, *12*, 21–31.

163. Cui, L.; Liu, B.; Liu, G.; Zhang, W.; Cen, L.; Sun, J.; Yin, S.; Liu, W.; Cao, Y. Repair of cranial bone defects with adipose derived stem cells and coral scaffold in a canine model. *Biomaterials* **2007**, *28*, 5477–5486.

164. Liu, G.; Zhang, Y.; Liu, B.; Sun, J.; Li, W.; Cui, L. Bone regeneration in a canine cranial model using allogeneic adipose derived stem cells and coral scaffold. *Biomaterials* **2013**, *34*, 2655–2664.

165. Chen, F.; Chen, S.; Tao, K.; Feng, X.; Liu, Y.; Lei, D.; Mao, T. Marrow-derived osteoblasts seeded into porous natural coral to prefabricate a vascularised bone graft in the shape of a human mandibular ramus: Experimental study in rabbits. *Br. J. Oral Maxillofac. Surg.* **2004**, *42*, 532–537.

166. Bensaïd, W.; Oudina, K.; Viateau, V.; Potier, E.; Bousson, V.; Blamchat, C.; Sedel, L.; Guillemin, G.; Petite, H. De Novo Reconstruction of Functional Bone by Tissue Engineering in the Metatarsal Sheep Model. *Tissue Eng.* **2005**, *11*, 814–824.

167. Gao, Z.; Chen, F.; Zhang, J.; He, L.; Cheng, X.; Ma, Q.; Mao, T. Vitalisation of

tubular coral scaffolds with cell sheets for regeneration of long bones: A preliminary study in nude mice. *Br. J. Oral Maxillofac. Surg.* **2009**, *47*, 116–122.

168. Geng, W.; Ma, D.; Yan, X.; Liu, L.; Cui, J.; Xie, X.; Li, H.; Chen, F. Engineering tubular bone using mesenchymal stem cell sheets and coral particles. *Biochem. Biophys. Res. Commun.* **2013**, *433*, 595–601.

169. Chen, F.; Ouyang, H.; Feng, X.; Gao, Z.; Yang, Y.; Zou, X.; Liu, T.; Zhao, G.; Mao, T. Anchoring Dental Implant in Tissue-Engineered Bone Using Composite Scaffold: A Preliminary Study in Nude Mouse Model. *J. Oral Maxillofac. Surg.* **2005**, *63*, 586–591.

170. Sculean, A.; Nikolidakis, D.; Schwarz, F. Regeneration of periodontal tissues: Combinations of barrier membranes and grafting materials—Biological foundation and preclinical evidence: A systematic review. *J. Clin. Periodontol.* **2008**, *35*, 106–116.

171. Koo, K.-T.; Polimeni, G.; Albandar, J.M.; Wikesjo, U.M.E. Periodontal repair in dogs : Examiner reproducibility in the supraalveolar periodontal defect model. *J. Clin. Periodontol.* **2004**, 31, 439–442.

172. Koo, K.; Polimeni, G.; Albandar, J.M.; Wikesjö, U.M.E. Periodontal Repair in Dogs : Analysis of Histometric Assessments in the Supraalveolar Periodontal Defect Model. *J. Periodontol.* **2004**, *75*, 1688–1693.

173. Koo, K.-T.; Polimeni, G.; Qahash, M.; Kim, C.K.; Wikesjö, U.M.E. Periodontal repair in dogs: Guided tissue regeneration enhances bone formation in sites implanted with a coral-derived calcium carbonate biomaterial. *J. Clin.* **2005**, 32, 104–110.

174. Wikesjö, U.M.E.; Lim, W.H.; Razi, S.S.; Sigurdsson, T.J.; Lee, M.B.; Tatakis, D.N.; Hardwick, W.R. Periodontal Repair in Dogs : A Bioabsorbable Calcium Carbonate Coral Implant Enhances Space Provision for Alveolar Bone Regeneration in Conjunction with Guided Tissue Regeneration. *J. Periodontol.* **2003**, 74, 957–964.

175. Rose, F.R.a.J.; Hou, Q.; Oreffo, R.O.C. Delivery systems for bone growth factors—The new players in skeletal regeneration. *J. Pharm. Pharmacol.* **2004**, *56*, 415–427.

176. Vuola, J.; Böhling, T.; Göransson, H.; Puolakkainen, P. Transforming growth factor β released from natural coral implant enhances bone growth at calvarium of mature

rat. *J. Biomed. Mater. Res.* **2002**, *59*, 152–159.

177. Nandi, S.K.; Kundu, B.; Mukherjee, J.; Mahato, A.; Datta, S.; Balla, V.K. Converted marine coral hydroxyapatite implants with growth factors: In vivo bone regeneration. *Mater. Sci. Eng. C* **2015**, *49*, 816–823.

178. Hu, K.; Olsen, B.R. The roles of vascular endothelial growth factor in bone repair and regeneration. *Bone* **2016**, *91*, 30–38.

179. Du, B.; Gao, Y.; Deng, Y.; Zhao, Y.; Lai, C.; Guo, Z.; Rong, M.; Zhou, L. Local delivery of rhVEGF165 through biocoated nHA/coral block grafts in critical-sized dog mandible defects: A histological study at the early stages of bone healing. *Int. J. Clin. Exp. Med.* **2015**, *8*, 4940–4953.

180. Du, B.; Liu, W.; Deng, Y.; Li, S.; Liu, X.; Gao, Y.; Zhou, L. Angiogenesis and bone regeneration of porous nano-hydroxyapatite/coralline blocks coated with rhVEGF165in critical-size alveolar bone defects in vivo. *Int. J. Nanomed.* **2015**, *10*, 2555–2565.

181. Xiao, C.; Zhou, H.; Ge, S.; Tang, T.; Hou, H.; Lou, M.; Fan, X. Repair of orbital wall defects using biocoral scaffolds combined with bone marrow stem cells enhanced by human bone morphogenetic protein-2 in a canine model. *Int. J. Mol. Med.* **2010**, *26*, 517–525.

182. Tang, Y.; Tang, W.; Lin, Y.; Long, J.; Wang, H.; Liu, L.; Tian, W. Combination of bone tissue engineering and BMP-2 gene transfection promotes bone healing in osteoporotic rats. *Cell Biol. Int.* **2008**, *32*, 1150–1157.

183. Decambron, A.; Fournet, A.; Bensidhoum, M.; Manassero, M.; Sailhan, F.; Petite, H.; Logeart-Avramoglou, D.; Viateau, V. Low-dose BMP-2 and MSC dual delivery onto coral scaffold for critical-size bone defect regeneration in sheep. *J. Orthop. Res.* **2017**, *35*, 2637–2645.

184. Hou, R.; Chen, F.; Yang, Y.; Cheng, X.; Gao, Z.; Yang, H.O.; Wu, W.; Mao, T. Comparative study between coral-mesenchymal stem cells-rhBMP-2 composite and auto-bone-graft in rabbit critical-sized cranial defect model. *J. Biomed. Mater. Res. Part A* **2007**, *80*, 85–93.

185. Canalis, E.; Centrella, M.; McCarthy, T. Effects of basic fibroblast growth factor on bone formation in vitro. *J. Clin. Investig.* **1988**, *81*, 1572–1577.

186. Nagai, H.; Tsukuda, R.; Mayahara, H. Effects of Basic Fibroblast Growth Factor (bFGF) on Bone Formation in Growing Rats. *Bone* **1995**, *16*, 367–373.

187. Zheng, Y.-H.; Su, K.; Jian, Y.-T.; Kuang, S.-J.; Zhang, Z.-G. Basic fibroblast growth factor enhances osteogenic and chondrogenic differentiation of human bone marrowmesenchymal stem cells in coral scaffold constructs. *J. Tissue Eng. Regen. Med.* **2011**, *5*, 540–550.

188. Zhang, Y.; Wang, Y.; Shi, B.; Cheng, X. A platelet-derived growth factor releasing chitosan/coral composite scaffold for periodontal tissue engineering. *Biomaterials* **2007**, *28*, 1515–1522.

189. Nevins, M.; Camelo, M.; Nevins, M.L.; Schenk, R.K.; Lynch, S.E. Periodontal Regeneration in Humans Using Recombinant Human Platelet- Derived Growth Factor-BB (rhPDGF-BB) and Allogenic Bone. *J. Periodontol.* **2003**, *74*, 1282–1292.

190. Gross-Aviv, T.; Vago, R. The role of aragonite matrix surface chemistry on the chondrogenic differentiation of mesenchymal stem cells. *Biomaterials* **2009**, *30*, 770–779.

191. Xiao, C.; Zhou, H.; Liu, G.; Zhang, P.; Fu, Y.; Gu, P.; Hou, H.; Tang, T.; Fan, X. Bone marrow stromal cells with a combined expression of BMP-2 and VEGF-165 enhanced bone regeneration. *Biomed. Mater.* **2011**, *6*, 015013, doi:10.1088/1748-6041/6/1/015013.

192. Oyama, T.; Nishimoto, S.; Tsugawa, T.; Shimizu, F. Efficacy of Platelet-Rich Plasma in Alveolar Bone Grafting. *J. Oral Maxillofac. Surg.* **2004**, *62*, 555–558.

193. Sammartino, G.; Tia, M.; Marenzi, G.; Espedito Di Lauro, A.; D'Agostino, E.; Claudio, P.P. Use of autologous Platelet-Rich Plasma (PRP) in periodontal defect treatment after extraction of impacted mandibular third molars. *J. Oral Maxillofac. Surg.* **2005**, *63*, 766–770.

194. Zhang, S.; Mao, T.; Chen, F. Influence of platelet-rich plasma on ectopic bone formation of bone marrow stromal cells in porous coral. *Int. J. Oral Maxillofac. Surg.* **2011**, *40*, 961–965.

195. Birchall, J.D.; Thomas, N.L. On the architecture and function of cuttlefish bone. *J. Mater. Sci.* **1983**, *18*, 2081–2086.

196. Denton, E.J.; Gilpin-Brown, J.B. Buoyancy of the Cuttlefish. *Nature* **1959**, *184*,

1330–1331.

197. Denton, E.J.; Howarth, J. The osmotic mechanism of cuttlebone. *J. Mar. Biol. Assoc. U. K.* **1961**, *41*, 351–363.

198. Cadman, J.; Zhou, S.; Chen, Y.; Li, W.; Appleyard, R.; Li, Q. Characterization of cuttlebone for a biomimetic design of cellular structures. *Acta Mech. Sin.* **2010**, *26*, 27–35.

199. Cadman, J.; Zhou, S.; Chen, Y.; Li, Q. Cuttlebone: Characterisation, Application and Development of Biomimetic Materials. *J. Bionic Eng.* **2012**, *9*, 367–376.

200. Ivankovic, H.; Tkalcec, E.; Orlic, S.; Ferrer, G.G.; Schauperl, Z. Hydroxyapatite formation from cuttlefish bones: Kinetics. *J. Mater. Sci. Mater. Med.* **2010**, *21*, 2711–2722.

201. Sherrard, K.M. Cuttlebone morphology limits habitat depth in eleven species of Sepia (Cephalopoda: Sepiidae). *Biol. Bull.* **2000**, *198*, 404–414.

202. Falini, G.; Fermani, S. Chitin Mineralization. *Tissue Eng.* **2004**, *10*, 1–6.

203. Rocha, J.H.G.; Lemos, A.F.; Agathopoulos, S.; Valério, P.; Kannan, S.; Oktar, F.N.; Ferreira, J.M.F. Scaffolds for bone restoration from cuttlefish. *Bone* **2005**, *37*, 850–857.

204. Dogan, E.; Okumus, Z. Cuttlebone used as a bone xenograft in bone healing. *Vet. Med.* **2014**, *59*, 254–260.

205. Kim, B.-S.; Kim, J.S.; Sung, H.-M.; You, H.-K.; Lee, J. Cellular attachment and osteoblast differentiation of mesenchymal stem cells on natural cuttlefish bone. *J. Biomed. Mater. Res. Part A* **2012**, *100A*, 1673–1679.

206. García-Enriquez, S.; Guadarrama, H.E.R.; Reyes-González, I.; Mendizábal, E.; Jasso-Gastinel, C.F.; García-Enriquez, B.; Rembao-Bojórquez, D.; Pane-Pianese, C. Mechanical performance and in vivo tests of an acrylic bone cement filled with bioactive Sepia officinalis cuttlebone. *J. Biomater. Sci. Polym. Ed.* **2010**, *21*, 113–125.

207. Jasso-Gastinel, C.F.; Reyes-Gonzalez, I.; Enriquez, S.G.; Flores, J.; Mijares, E.M. Acrylic bone cements modified with bioactive filler. *Macromol. Symp.* **2009**, *283–284*, 159–166.

208. Rocha, J.H.G.; Lemos, A.F.; Agathopoulos, S.; Kannan, S.; Valério, P.; Ferreira, J.M.F. Hydrothermal growth of hydroxyapatite scaffolds from aragonitic cuttlefish bones. *J. Biomed. Mater. Res. Part A* **2006**, *77*, 160–168.

209. Hongmin, L.; Wei, Z.; Xingrong, Y.; Jing, W.; Wenxin, G.; Jihong, C.; Xin, X.; Fulin, C. Osteoinductive nanohydroxyapatite bone substitute prepared via in situ hydrothermal transformation of cuttlefish bone. *J. Biomed. Mater. Res. Part B Appl. Biomater.* **2015**, *103B*, 816–824.

210. Kasioptas, A.; Geisler, T.; Putnis, C.V.; Perdikouri, C.; Putnis, A. Crystal growth of apatite by replacement of an aragonite precursor. *J. Cryst. Growth* **2010**, *312*, 2431–2440.

211. Sarin, P.; Lee, S.J.; Apostolov, Z.D.; Kriven, W.M. Porous biphasic calcium phosphate scaffolds from cuttlefish bone. *J. Am. Ceram. Soc.* **2011**, *94*, 2362–2370.

212. Dutta, A.; Fermani, S.; Arjun Tekalur, S.; Vanderberg, A.; Falini, G. Calcium phosphate scaffold from biogenic calcium carbonate by fast ambient condition reactions. *J. Cryst. Growth* **2011**, *336*, 50–55.

213. Lee, S.J.; Lee, Y.C.; Yoon, Y.S. Characteristics of calcium phosphate powders synthesized from cuttlefish bone and phosphoric acid. *J. Ceram. Process. Res.* **2007**, *8*, 427–430.

214. Kim, B.S.; Yang, S.S.; Lee, J. A polycaprolactone/cuttlefish bone-derived hydroxyapatite composite porous scaffold for bone tissue engineering. *J. Biomed. Mater. Res. Part B* **2014**, *102*, 943–951.

215. Kim, B.S.; Kang, H.J.; Yang, S.S.; Lee, J. Comparison of in vitro and in vivo bioactivity: Cuttlefish-bone-derived hydroxyapatite and synthetic hydroxyapatite granules as a bone graft substitute. *Biomed. Mater.* **2014**, *9*, 025004, doi:10.1088/1748-6041/9/2/025004.

216. Kannan, S.; Rocha, J.H.G.; Agathopoulos, S.; Ferreira, J.M.F. Fluorine-substituted hydroxyapatite scaffolds hydrothermally grown from aragonitic cuttlefish bones. *Acta Biomater.* **2007**, *3*, 243–249.

217. Kim, B.S.; Yang, S.S.; Yoon, J.H.; Lee, J. Enhanced bone regeneration by silicon-substituted hydroxyapatite derived from cuttlefish bone. *Clin. Oral Implant. Res.* **2015**, *00,* 1–8.

218. Fahami, A.; Beall, G.W.; Betancourt, T. Synthesis, bioactivity and zeta potential investigations of chlorine and fluorine substituted hydroxyapatite. *Mater. Sci. Eng. C* **2016**, *59*, 78–85.

219. Komlev, V.S.; Barinov, S.M.; Girardin, E.; Oscarsson, S.; Rosengren, Å.; Rustichelli, F.; Orlovskii, V.P. Porous spherical hydroxyapatite and fluorhydroxyapatite granules: Processing and characterization. *Sci. Technol. Adv. Mater.* **2003**, *4*, 503–508.

220. Ratnayake, J.T.B.; Mucalo, M.; Dias, G.J. Substituted hydroxyapatites for bone regeneration: A review of current trends. *J. Biomed. Mater. Res. Part B* **2017**, *105B*, 1285–1299.

221. Kim, B.S.; Kang, H.J.; Lee, J. Improvement of the compressive strength of a cuttlefish bone-derived porous hydroxyapatite scaffold via polycaprolactone coating. *J. Biomed. Mater. Res. Part B* **2013**, *101*, 1302–1309.

222. Siddiqi, S.A.; Manzoor, F.; Jamal, A.; Tariq, M.; Ahmad, R.; Kamran, M.; Chaudhry, A.; Rehman, I.U. Mesenchymal stem cell (MSC) viability on PVA and PCL polymer coated hydroxyapatite scaffolds derived from cuttlefish. *RSC Adv.* **2016**, *6*, 32897–32904.

223. Milovac, D.; Gallego Ferrer, G.; Ivankovic, M.; Ivankovic, H. PCL-coated hydroxyapatite scaffold derived from cuttlefish bone: Morphology, mechanical properties and bioactivity. *Mater. Sci. Eng. C* **2014**, *34*, 437–445.

224. Milovac, D.; Gamboa-Martínez, T.C.; Ivankovic, M.; Gallego Ferrer, G.; Ivankovic, H. PCL-coated hydroxyapatite scaffold derived from cuttlefish bone: In vitro cell culture studies. *Mater. Sci. Eng. C* **2014**, *42*, 264–272.

225. Sukul, M.; Min, Y.K.; Lee, B.T. Collagen-hydroxyapatite coated unprocessed cuttlefish bone as a bone substitute. *Mater. Lett.* **2016**, *181*, 156–160.

Chapter 2

Surface functionalization of cuttlefish bone derived biphasic calcium phosphate scaffolds with polymeric coatings

Surface functionalization of cuttlefish bone-derived biphasic calcium phosphate scaffolds with polymeric coatings

Ana S. Neto[a], Ana C. Fonseca[b], J.C.C. Abrantes[a,c], Jorge F. J. Coelho[b], José M.F. Ferreira[a]

[a] Department of Materials and Ceramic Engineering / CICECO – Aveiro Institute of Materials, University of Aveiro, 3810-193 Aveiro, Portugal

[b] CEMMPRE, Department of Chemical Engineering, University of Coimbra, Rua Sílvio Lima-Pólo II, 3030-790 Coimbra, Portugal

[c] UIDM, ESTG, Polytechnique Institute of Viana do Castelo, 4900 Viana do Castelo, Portugal

Materials Science & Engineering C 105 (2019) 110014

doi: 10.1016/j.msec.2019.110014

Abstract

Cuttlefish bone (CB) has been explored as biomaterial in the bone tissue-engineering field due to its unique porous structure and capacity of the aragonite mineral to be hydrothermally converted into calcium phosphates (CaPs). In the present study, undoped and ion (Sr^{2+}, Mg^{2+} and/or Zn^{2+}) doped biphasic calcium phosphate (BCP) scaffolds were prepared by hydrothermal transformation (HT, 200 ºC, 24 h) of CB. The obtained scaffolds were sintered and then coated with two commercial polymers, poly(ε-caprolactone) (PCL) or poly(DL-lactide) (PDLA), and with two synthesized ones, a poly(ester amide) (PEA) or a poly(ester urea) (PEU) in order to improve their compressive strength. The scaffolds were characterized by X-ray diffraction (XRD) coupled with structural Rietveld refinement, Fourier transform infrared (FTIR) spectroscopy, and scanning electron microscopy (SEM). The results demonstrate that CB could be entirely transformed into BCPs in the presence or absence of doping elements. The initial CB structure was preserved and the polymeric coatings did not jeopardize the interconnected porous structure. Furthermore, the polymeric coatings enhanced the compressive strength of the scaffolds. The *in vitro* bio-mineralization upon immersing the scaffolds into simulated body fluid (SBF) demonstrated the formation of bone-like apatite surface layers in both uncoated and coated scaffolds. Overall, the produced scaffolds exhibit promising properties for bone tissue engineering applications.

Keywords: Cuttlefish bone; Hydrothermal transformation; Biphasic calcium phosphate; Ion doping; Polymeric coatings

1. Introduction

Bone is the second most transplanted tissue worldwide. Autografts, still considered the gold standard due to their optimal osteogenic, osteoinductive and osteoconductive properties, have multiple drawbacks, including the donor site morbidity and their limited availability [1]. In the last decades, bone tissue engineering has been regarded as a promising alternative to the current bone grafting approaches. It involves the use of porous 3D scaffolds that provide a suitable environment and architecture during bone regeneration and development [2].

Calcium phosphates (CaPs) are some of the most used materials for bone graft strategies due to their close resemblance with the mineral component of the bone [3]. Nowadays, biphasic calcium phosphates (BCP) are regarded with much interest [4,5]. Being a combination of a more stable phase, hydroxyapatite (HA), and a more soluble one, β-tricalcium phosphate (β-TCP), BCP biomaterials are often preferred for bone remodeling processes for enabling tailoring an adequate equilibrium between resorption/solubilization [6,7]. Certain ions existing in bone composition, such as strontium (Sr^{2+}), magnesium (Mg^{2+}) and zinc (Zn^{2+}) can be incorporated into the crystalline structure of CaPs in single or combined ways and might favorably influence their biological behaviors upon implantation [8]. Sr^{2+} is present in bone in considerable quantities, mainly at regions with high levels of metabolic turnover. It enhances bone formation while depressing bone resorption by inducing the proliferation of pre-osteoblasts and its differentiation and increasing the apoptosis of osteoclast [9,10]. On the other hand, Mg^{2+} is intimately related to the mineralization of the calcified tissues. Furthermore, Mg^{2+} influences osteoblast and osteoclast activity and, thereby, the bone metabolism and bone growth [9,10]. Zn^{2+} plays an important role in bone development and growth [9,10]. In addition, Zn^{2+} is a trace element recognized for its antioxidant and anti-inflammatory properties, with beneficial therapeutic effects in different diseases like atherosclerosis, neurodegeneration, immunologic disorders and cancer [11].

Despite all the above mentioned advantages, CaP materials are associated with poor mechanical properties (brittleness, fracture strength) thereby, limiting their use under load-bearing applications [3,12]. Bone is a typical natural composite, combining CaPs and natural polymers [13,14]. As matrices for engineered composites, synthetic polymers offer several advantages in comparison to natural polymers, since their properties can be tailored and their mechanical properties and degradation rates are more predictable and

reproducible. Polyesters, such as polylactic acid (PLA) and poly(ε-caprolactone) (PCL), are the most commonly used synthetic polymer in bone tissue engineering. These polymers are biocompatible, non-cytotoxic and demonstrated to have suitable degradation rates [15,16]. Alternatively, α-amino acid based poly(ester amide) (PEA) and poly(ester urea) (PEU) belong to a class of synthetic polymers with promising properties in biomedical field. Indeed, these polymers can combine the biodegradability of polyesters and the mechanical and thermal behavior of polyamides [17,18]. The presence of the α-amino acids in the PEA and PEU's structure improves cell-material interactions and provides the polymers with the ability to be degraded by enzymes. Additionally, if α-amino acids with reactive pendant groups (–OH, $–NH_2$, –COOH, –SH) are used, the further post-functionalization of the polymers with moieties of interest is possible [19]. For instance, a PEU based on tyrosine was used to attach osteogenic growth peptide or bone morphogenetic protein-2 as a way to improve osteogenic differentiation [20,21]. PEAs and PEUs can be prepared with a myriad of structures, allowing tailoring their properties to a specific application [19].

Scaffolds for bone tissue engineering must be biocompatible and, thereby, cells must be able to adhere to their surfaces and proliferate. They should have an interconnected porous structure with pore sizes > 100 μm for enabling cell adhesion and proliferation, nutrient/waste transportation and bone ingrowth. The mechanical properties should ideally be similar to those of host bone, and the degradation rate should match the rate of new bone formation [22]. Marine skeletons, mainly composed by aragonite ($CaCO_3$), have been explored as an attractive source to obtain CaP scaffolds *via* a hydrothermal treatment (HT) [23]. Cuttlefish bone (CB), the hard tissue in cuttlefish, is a widely available and inexpensive material. It is composed by an internal lamellar matrix and a dorsal shield. The lamellar matrix has a quasi-periodic microstructure organized by lamellae supported by pillars, which form channels with an elevated degree of interconnectivity. This unique architecture has a porosity of approximately 93% and pore sizes varying between 200 and 600 μm [24]. In this regard, among the different marine skeletons, CB is one of the most studied materials for bone grafts. Rocha et al. [25,26] were the first ones to obtain CB-derived HA scaffolds *via* HT. The original structure was fully preserved in the HA scaffolds and the *in vitro* and *in vivo* studies demonstrated their osteoinductive properties, promoting excellent cell adhesion, proliferation and differentiation [25–27]. To improve the biological performance, fluorine (F^-) [28] and silicon (Si^{4+}) [29] were incorporated into the obtained scaffolds. On the other hand, and

recognizing the brittleness of the HA scaffolds derived from CB, Milovac et al. [30,31] and Kim et al. [32] coated the scaffolds with PCL and observed the improvement of mechanical and biological behaviors. In order to have an effective improvement of the mechanical properties, Milovac et al. [31] coated the scaffolds with a 20% (w/v) of PCL solution. But considering the slow degradation of PCL, Rogina et al. [33] coated HA scaffolds derived from CB with a combination of PCL and PLA. Through the combination of these two polymers, it was possible to reduce the polymer thickness and improve the mechanical properties.

The present work aims at obtaining *via* HT CB-derived BCP scaffolds incorporating different doping ions (Sr^{2+}, Mg^{2+} and Zn^{2+}) in various combinations. The surface of the scaffolds was further functionalized with PCL, poly(DL-lactide) (PDLA), PEA and PEU coatings by using vacuum impregnation. The chemical composition, morphological properties and mechanical properties were examined. The capacity of coated scaffolds to induce the precipitation of a calcium phosphate layer on its surface was investigated.

2. Materials and methods

2.1. Preparation of non-doped and doped BCP scaffolds derived from CB

Di-ammonium hydrogen phosphate [$(NH_4)_2HPO_4$, Panreac AppliChem, Spain] was used as precursor for phosphorous (P). Nitrate salts were adopted as precursors for the cationic (Sr^{2+}, Mg^{2+}, Zn^{2+}) dopants, namely, Strontium nitrate, $Sr(NO_3)_2$, Magnesium nitrate hexahydrate, $Mg(NO_3)_2\ 6H_2O$, and zinc nitrate hexahydrate, $Zn(NO_3)_2\ 6H_2O$, all from Sigma-Aldrich, Germany. CBs obtained from cuttlefish, *Sepia officinalis*, were used as calcium source. In order to evaluate the exact amount of water, organic matter and $CaCO_3$, raw CB samples were subjected to differential and gravimetric thermal analyses (DTA/TG, Labsys Setaram TG- DTA/DSC, France), using a heating rate of 10 °C min^{-1}. The exact content of $CaCO_3$ was determined and taken into account upon mixing with the required amounts of the other reagents. The lamella of raw CB was firstly cut into small pieces, washed with water, and dried before being used as starting materials for the preparation of non-doped and doped BCP scaffolds derived from the CB. The CB pieces with a known amount of $CaCO_3$ were mixed with the required amount and concentration of the phosphorous (P) precursor solution to obtain the desired non-doped BCP composition. For the doped scaffolds, an additional solution containing the required

propositions of the cationic nitrate precursor salts was also prepared and mixed with the phosphorous solution. Four different doped compositions with a fixed Sr^{2+} content (6 mol%, BCP-6Sr), alone or in various combinations with other doping ions (2 mol% Mg^{2+}, BCP-6Sr2Mg; 2 mol% Zn^{2+}, BCP-6Sr2Zn; and 2 mol% Mg^{2+} + 2 mol% Zn^{2+}, BCP-6Sr2Mg2Zn) were prepared.

The reacting solutions and the CB pieces were then sealed in poly (tetrafluorethylene) (PTFE) lined stainless steel autoclaves and placed at 200 ºC for 24 h in the oven. The obtained scaffolds were washed with distilled water and dried in an oven at 40 ºC. Afterwards, the scaffolds were heat treated at 700 ºC with a heating rate of 0.5 ºC· min^{-1} for 1 h to eliminate the organic material and, then, sintered at 1200 ºC for 2 h, using a heating rate of 2 ºC min^{-1}.

2.2. Polymeric coatings

BCP scaffolds were coated with two of the most used polymers in the biomedical field, PCL (CAPATM6800 M_n = 80.000 g mol^{-1}) or PDLA (PURASORB® PDL 20, M_w = 47,365 g mol^{-1}), purchased from Perstorp Specialty Chemicals AB (Perstorp, Sweden) and Corbion Purac (Amsterdam, The Netherlands), respectively. In addition, PEA or PEU, which were synthesized in the laboratory (see Supporting information for the synthesis details and chemical characterization of the polymers, Figures S1 and S2), were also used for the coating of BCP scaffolds. Both PCL and PDLA were dissolved in dichloromethane (Sigma-Aldrich, Germany) at concentrations of 5% and 3% (w/v), respectively. On the other hand, PEA and PEU were dissolved in chloroform (Fisher Scientific, United Kingdom) at a concentration of 5% (w/v). The addition of 1 ml of *N*, *N*′-dimethylformamide (Sigma-Aldrich, Germany) was required to improve the dissolution of these polymers.

The prepared scaffolds were dipped in the polymer solutions under partial vacuum for approximately 5 min. The vacuum allows the removal of air from the pores and ensures that the polymer solution can be easily impregnated into the porous structure. The coated samples were dried in an oven overnight and were, posteriorly, placed at room temperature (RT) for more 7 days to eliminate the remaining organic solvent.

2.3. Characterization

The crystalline phases of all the synthesized (non-doped and doped) CB-derived BCP scaffolds were identified by X-ray diffraction (XDR) using a High Resolution X-ray

Diffractometer (PANalytical X'Pert PRO) with Cu Kα radiation (λ = 1.5406 Å) produced at 40 mA and 45 kV. Data were collected in the 2θ range between 10º and 100º with a 2θ- step size of 0.0260º per second. The Rietveld refinements were performed using the software TOPAS 5.0 (Bruker AXS, Karlsruhe, Germany) with the fundamental parameters. To identify the crystalline phases, it was used the ICDD card numbers of # 04-015-7545 for HA and # 04-006-9376 for β-TCP.

Inductively couple plasma (ICP) spectrometry (ICP-OES Jobin Yvon Activa M., USA) was used for the elemental analysis of Sr, Mg and Zn. Before analyses, the powders were dissolved in 2% nitric acid (HNO_3).

The identification of the characteristic functional groups and structural characterization was obtained by Fourier transform infrared (FTIR) spectroscopy using a FTIR Bruker Tensor 27 equipped with a Golden Gate Single Reflection Diamond ATR. The data are collected over the spectral range of 400–4000 cm^{-1} using a total of 256 scans and a spectral resolution of 4 cm^{-1} having the sample placed directly over the diamond crystal and pressed.

The ^1H NMR spectra of the PEA and PEU was obtained at 25 °C on a Bruker Avance 400 MHz Spectrometer (Billerica, Massachusetts, EUA) using a 5 mm broadband NMR probe, in DMSO-*d*6. Tetramethylsilane was used as the internal standard.

The interconnectivity of the CB microstructure was assessed by micro computed tomography (μ-CT, Bruker) using an exposure time of 800 ms, energy of 50 kV and intensity of 200 μA. The NRecon software was used for the reconstruction of cross-section images. The microstructure and morphology of the raw CB scaffolds, and after hydrothermal transformation, without and with the polymeric coatings were observed by scanning electron microscopy (SEM, Hitachi SU-70, Hitachi High-Technologies Europe, GmbH, Germany).

Density measurements using the buoyancy (Archimedes') method was employed to analyze whether the porosity changes after transformation and how it was affected by the polymeric coating. Thus, raw CB and the hydrothermally transformed and sintered scaffolds, without and with the polymeric coatings were immersed in distilled water in accordance with the European Standard EN 993-1. The scaffolds density was calculated using the following equation:

$$\rho_{scaffold} = \frac{m_1}{m_3 - m_2} \times \rho_w$$

where $\rho_{scaffold}$ and ρ_w are respectively the densities of the scaffold and of water in g cm^{-3}; m_1 is the weight of the dried scaffold (g), m_2 is the weight of the scaffold suspended in water (g), and m_3 the weight of the water saturated scaffold measured in air (g). By knowing the mineralogical phase compositions and, if applicable, the percentage of adsorbed polymer in each sample, it is possible to calculate the theoretical density of the scaffold and, then, its porosity.

The compression tests were carried out in using a universal testing machine (AG-IS10kN, Shimadzu, Kyoto, Japan) by applying perpendicularly to the lamella a maximum load of 200 N to cubic shape scaffolds with approximately 3 mm side at a constant crosshead speed of 0.5 mm min^{-1} under dry ambient conditions.

2.4. *In vitro* bio-mineralization

The *in vitro* bio-mineralization capacity of the scaffolds was analyzed by immersion of the uncoated and coated scaffolds in simulated body fluid (SBF) at 37 ºC in an orbital shaker for 3, 7 and 14 days. The SBF solution was prepared accordingly to the international standard ISO 23317. The *in vitro* bio-mineralization tests were performed according to a unified procedure described elsewhere [34] using a standard area per mL of SBF solution of 0.5 cm^2 mL^{-1}. After each soaking period, the samples were removed from SBF solution, gently rinsed with distilled water and then left to dry in a desiccator. Once dried, the scaffolds were analyzed by SEM to observe the bioactive layer deposited onto their surfaces.

2.5. Statistical analysis

The experiments were performed in triplicated and the values are expressed as mean ± standard deviation. The statistical analysis was performed using one-way analysis of variance (ANOVA). $P < 0.05$ was considered statistically significant.

3. Results

3.1. Thermal analysis

The results of the thermal analysis (DTA and TG) of raw CB are shown in Figure 1. The TG curve revealed a weight loss of 1.02% up to 150 ºC associated with water evaporation. The weight loss between 150 ºC and 500 ºC due to the burning of the organic

matter was about 4.49% and is associated with two exothermic peaks (DTA curve) at 285 and 430 ºC. Lastly, the weight loss of 38.64% over 500–1000 ºC was due to the decomposition of aragonite into calcium oxide. This thermal transformation is also responsible for the strong endothermic peak centered at 844 ºC.

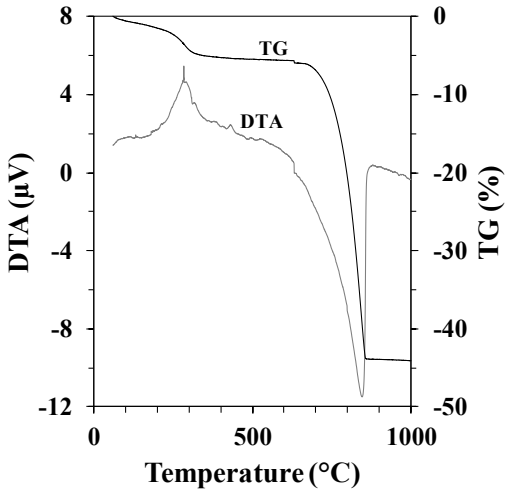

Figure 1. Thermal analysis of raw CB.

3.2. Chemical and structural characterization

The XRD patterns of the HT scaffolds sintered at 1200 ºC are displayed in Figure 2. The crystalline phases identified indicated the presence of HA (# 04-015-7245) and β-TCP (# 04-006-9376). Although all the synthesized compositions exhibited the same phases (HA and β-TCP), their propositions were dependent on the doping combinations. When Sr^{2+} is incorporated alone in the crystalline lattice all the peaks are shifted to lower angles. On the other hand, when Sr^{2+} is incorporated along with Mg^{2+} or Zn^{2+} in the crystalline lattice, there is an intensity enhancement and a shift to higher angles of the peaks corresponding to the β-TCP phase, while the HA peaks are shifted in the opposite direction. The concomitant incorporation of Sr^{2+}, Mg^{2+} and Zn^{2+} in the crystalline structure results in a slight overall shift of all the peaks to higher angles. The quantitative phase analysis data determined by Rietveld refinement (wt%) for all compositions are summarized in Table 1.

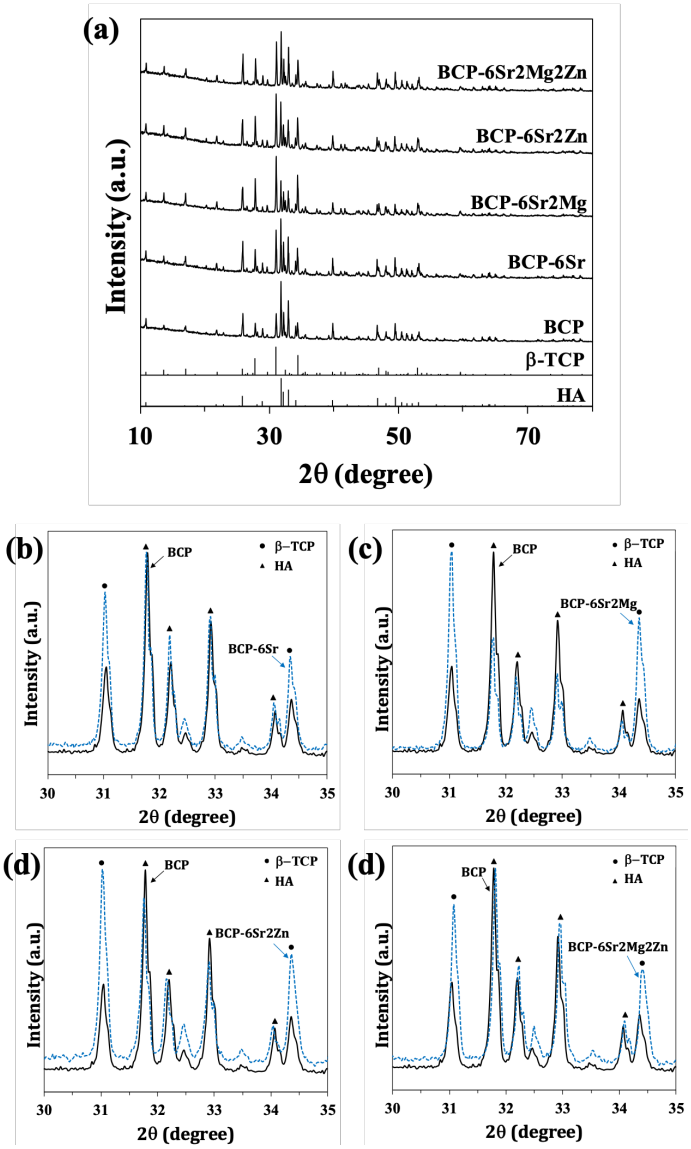

Figure 2. XRD patterns of BCP, BCP-6Sr, BCP-6Sr2Mg, BCP-6Sr2Zn and BCP-6Sr2Mg2Zn scaffolds sintered at 1200ºC. The diffraction pattern of β-TCP and HA standards, ICDD PDF 04-006-9376 and 04-015-7245, respectively, are also present for comparison purpose. Zoomed area within the 2θ range from 30-35º of the main HA and β-TCP peaks to show the effects of **(a)** Sr^{2+}, **(b)** Sr^{2+} and Mg^{2+}, **(c)** Sr^{2+} and Zn^{2+} and **(d)** Sr^{2+}, Mg^{2+} and Zn^{2+} co-doping on the shift of the XRD peaks in comparison with undoped BCP.

Table 1. Quantitative analysis obtained by Rietveld refinement of the different CB derived compositions

Sample	wt.% of composition obtained by Rietveld refinement	
	HA	β-TCP
BCP	47.75	52.25
BCP-6Sr	49.23	50.77
BCP-6Sr2Mg	29.45	70.55
BCP-6Sr2Zn	33.00	67.00
BCP-6Sr2Mg2Zn	47.85	52.15

The contents of the doping elements (Sr, Mg and Zn) in the BCP scaffolds were determined by ICP analysis. The experimentally measured values reported in Table 2 reveal that they are significantly below to the planned ones.

Table 2. Planned and experimentally obtained molar concentrations of Sr, Mg and Zn in the BCP compositions.

Sample	Concentration of Sr, Mg and Zn (mol%)					
	Planned compositions			ICP elemental analysis		
	Sr	Mg	Zn	Sr	Mg	Zn
BCP	0	0	0	0.9	0.29	0.02
BCP-6Sr	6	0	0	2.6	0.32	0.02
BCP-6Sr2Mg	6	2	0	1.8	0.51	0.03
BCP-6Sr2Zn	6	0	2	1.8	0.31	0.80
BCP-6Sr2Mg2Zn	6	2	2	1.8	0.37	0.68

The FTIR spectra of the uncoated and coated (with different polymers) BCP scaffolds are shown in Figure 3. All the uncoated scaffolds exhibit similar spectra with the characteristic vibrational modes of –PO4 and –OH groups. The band at 475 cm^{-1} is associated to doubly degenerate $v2$ O–P–O bending. The bands at 550 and 600 cm^{-1} correspond to the PO4 tetrahedra $v4$ mode and 1020 and 1087 cm^{-1} represent the peaks for the $v3$ mode. The bands at 940 and 960 cm^{-1} denote the $v1$ non-degenerate P–O symmetry stretching mode. The typical stretching and vibrational modes of –OH group should appear at 630 and 3575 cm^{-1} [35]. Nevertheless, the band at 630 cm^{-1} appears with a low intensity while the peak at 3575 cm^{-1} did not appear at all. Overall, the FTIR spectra of the polymeric coated scaffolds appear as superpositions of individual BCP and polymer (PCL, PDLA, PEA or PEU) spectra. In FTIR spectra of the PCL coated samples the band at 1720 cm^{-1} is due to the stretching vibrations of the C–O group in the ester linkage. The bands at 1460, 1390 and 1367 cm^{-1} correspond to the CH_2 bending modes, and the 2942 and 2895 cm^{-1} ones are ascribed to the CH_2 to the stretching mode. In addition, the bands at 1234, 1107 and 1042 cm^{-1} correspond to the stretching vibrations of the C–O–C group of the ester linkage. The bands located at 1290 and 1160 cm^{-1} are associated with the stretching of the C–C and C–O bonds of the ester group in the crystalline and amorphous phase, respectively [36]. The FTIR spectra of the PDLA coated samples exhibit the characteristic PDLA bands, although of low intensity. This can be understood considering that the coating was deposited from a relatively low concentrated [3% (w/v)] PDLA solution, which results in a lower percentage of polymeric coating. At

1745 cm^{-1} is observed the stretching vibration of the C–O groups of the ester linkage. The peaks at 2998 and 2940 cm^{-1} correspond to the stretching vibrations of the C–CH_3 and CH groups, respectively. The band at 1180 cm^{-1} is ascribed to the stretching vibration of the C–O–C group and the CH_3 asymmetric deformation and symmetric wagging is observed at 1448 and 1375 cm^{-1}, respectively. The band located at 1043 cm^{-1} is associated with stretching of the C–O bond and CH bending [37]. The FTIR spectra of PEA coated scaffolds show characteristic PEA peaks with the ester and amide linkages. The peak at 3300 cm^{-1} corresponds to the stretching vibration of the N–H group of the amide linkage. The bands at 2890 and 2930 cm^{-1} correspond to the symmetric and asymmetric stretching vibrations, respectively, of the CH_2 groups. The stretching vibration of the C–O group of the ester linkage appears at 1740 cm^{-1}. At 1650 and 1540 cm^{-1} is possible to identify the bands ascribed to the amide I and II groups, respectively [38–40]. Lastly, the characteristic bands of PEU with the ester and urea linkages are observed in the PEU coated scaffolds. The band at 3390 cm^{-1} corresponds to the stretching vibration of the N–H groups of the urea linkage. At 1565 cm^{-1} is identified the band corresponding to both the bending of the N–H group and of the stretching of the C–N group of the urea linkage. The vibration of the C–O group of the ester and urea are identified at 1740 and 1625 cm^{-1}, respectively.

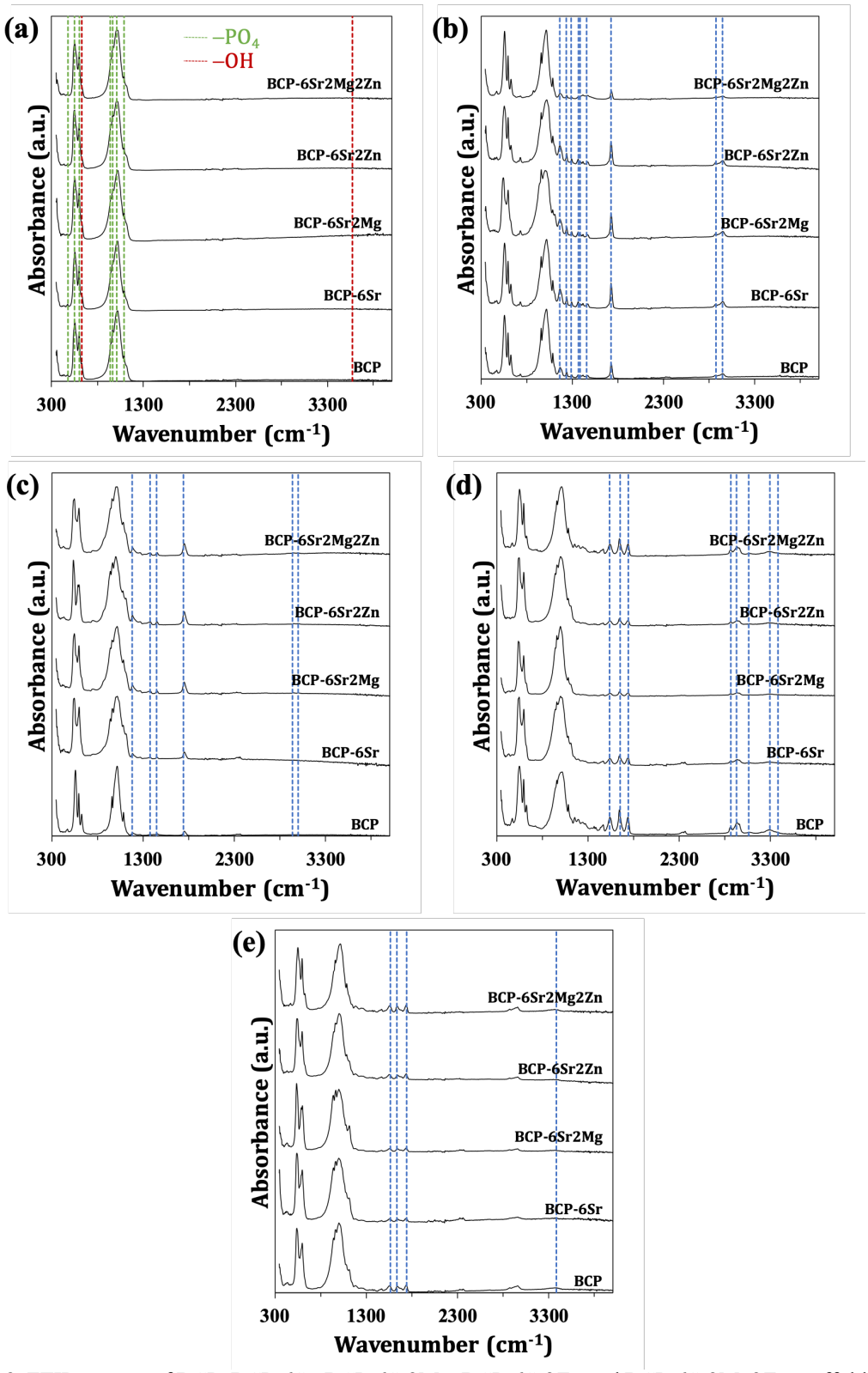

Figure 3. FTIR spectra of BCP, BCP-6Sr, BCP-6Sr2Mg, BCP-6Sr2Zn and BCP-6Sr2Mg2Zn scaffolds **(a)** without polymer; and coated with **(b)** PCL; **(c)** PLA; **(d)** PEA; **(e)** PEU. The green and red lines correspond to the –PO4 and –OH groups, respectively. The blue lines correspond to the characteristic peaks of each polymer.

3.3. Microstructure

The unique CB architecture was observed by μ-CT and SEM (Figure 4).

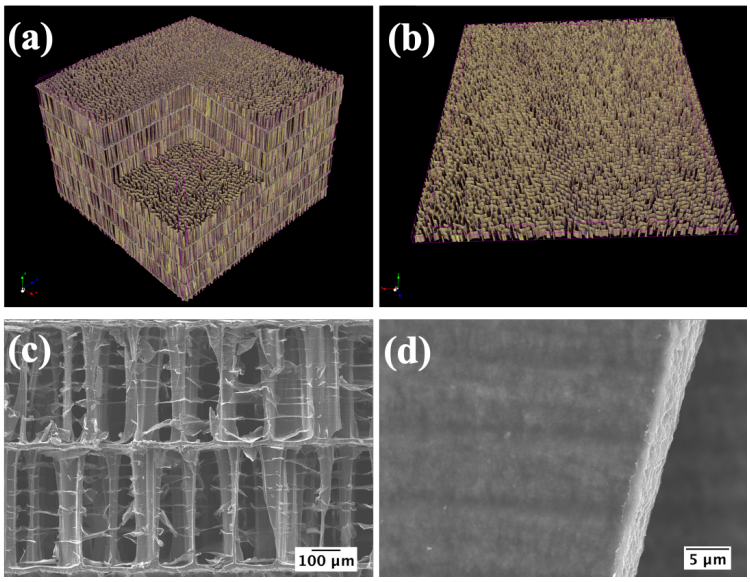

Figure 4. Microstructure of raw CB. **(a, b)** μ-CT images highlighting the interconnectivity and sigmoidal path of the pillars; SEM micrographs **(c)** showing the presence of β-chitin and **(d)** the detail of the pillar wall.

The structure comprised by lamellae is supported by numerous pillars generating chambers with a height of approximately 400μm. These chambers are separated by walls with a thickness of approximately 10 μm. Furthermore, the pillars create an interconnected porosity with widths between 100 and 260 μm that progress through the material in a sigmoidal path. Moreover, it is evident the coating of the lamellar matrix with organic material, β-chitin. This interconnected porous structure was retained in all the compositions after HT and sintering (Figure 5). Under a higher magnification, it is possible to observe the formation of CaP crystals and the morphological characteristics did not modify in the presence of the doping elements.

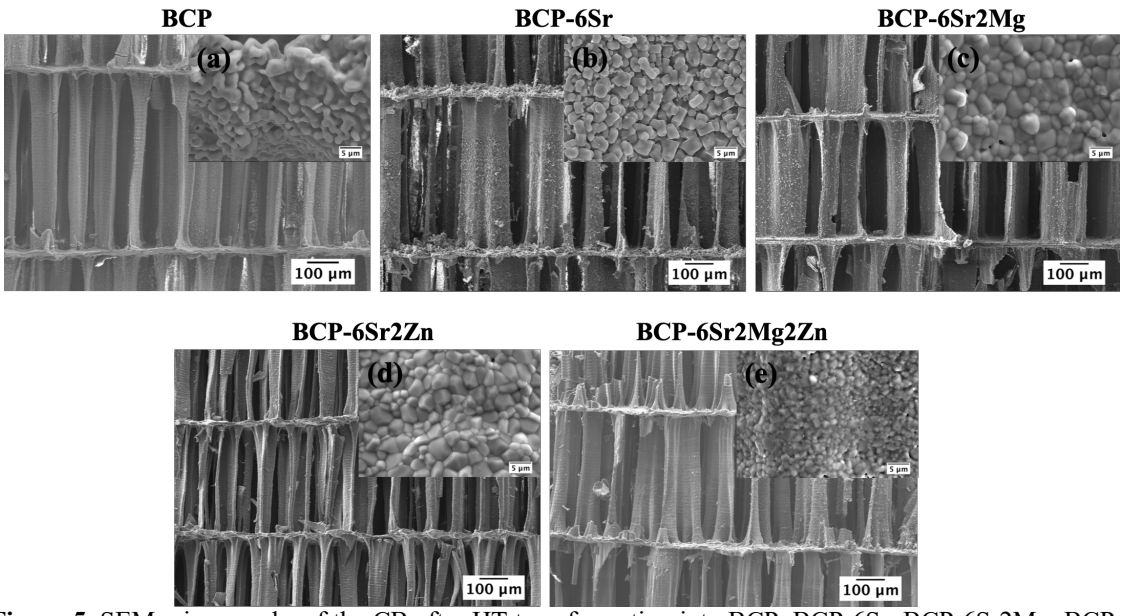

Figure 5. SEM micrographs of the CB after HT transformation into BCP, BCP-6Sr, BCP-6Sr2Mg, BCP-6Sr2Zn and BCP-6Sr2Mg2Zn. Zoomed SEM micrographs of the **(a)** BCP, **(b)** BCP-6Sr, **(c)** BCP-6Sr2Mg, **(d)** BCP-6Sr2Zn and **(e)** BCP-6Sr2Mg2Zn.

The morphology of the scaffolds from all BCP compositions after coating with the different polymers was also observed by SEM (Figure 6). It is possible to observe that the surfaces of the scaffolds have been effectively covered with polymer layers, with most of the pores remaining unclogged. Moreover, it is possible to infer that the various polymers tested have different interactions with the inorganic matrix (Figure 7a). These interactions could be a consequence of the viscosity of the polymeric solutions used for the coating (Figure 7b). It was registered lower and similar viscosities for the 5% (w/v) PEA and PEU solutions. Higher and also similar viscosity curves were obtained for the 5% (w/v) PCL and 3% (w/v) PDLA solutions. The highest viscosity curve was achieved with the 5% (w/v) PDLA solution.

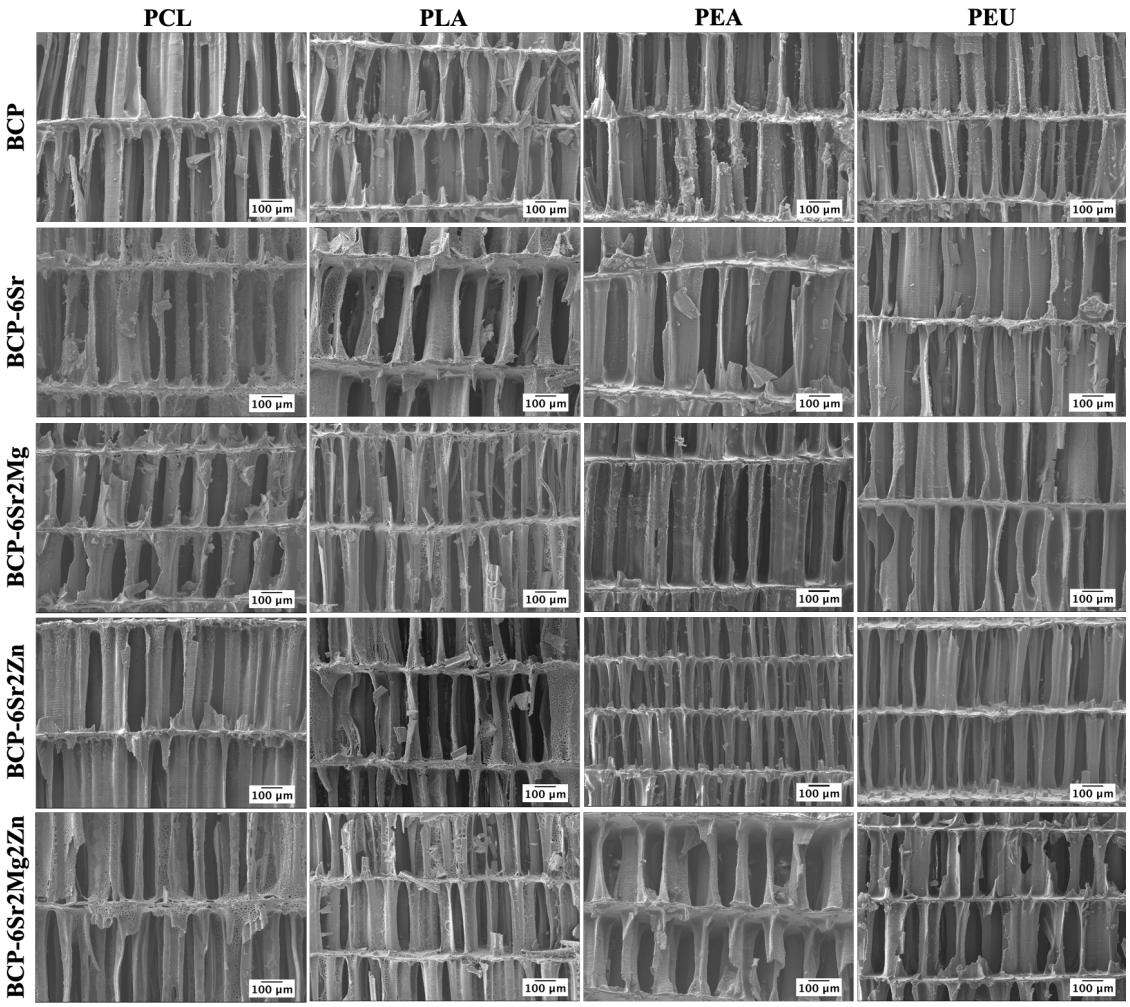

Figure 6. SEM micrographs of the coated CB derived scaffolds (BCP BCP-6Sr, BCP-6Sr2Mg, BCP-6Sr2Zn and BCP-6Sr2Mg2Zn) with the different polymers (PCL, PLA, PEA and PEU).

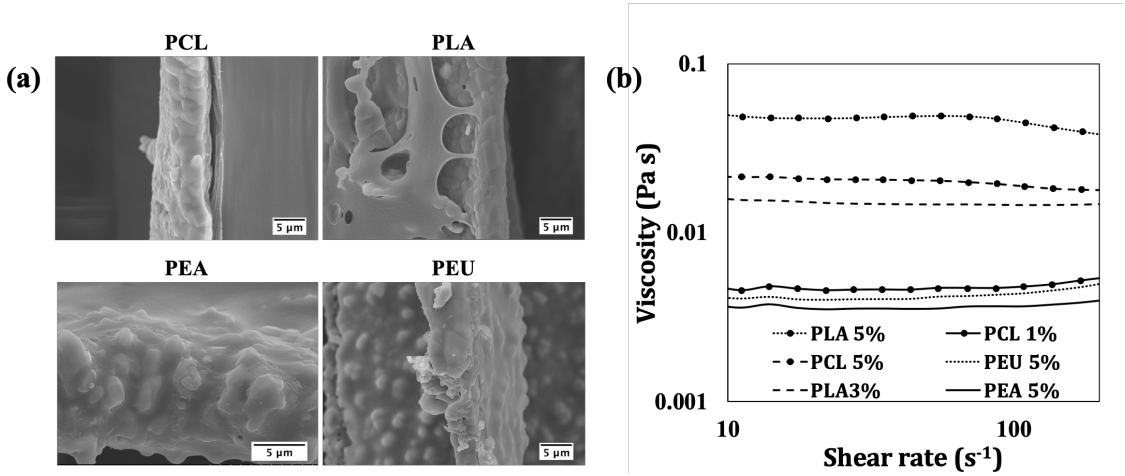

Figure 7. (a) SEM micrographs highlighting the interactions between the CB derived scaffolds and the different polymers. **(b)** Viscosity as a function of shear rate of the polymeric solutions.

3.4. Porosity and mechanical properties

The porosity data reported in Table 3 reveal that the hydrothermal transformation and sintering processes did not affect the porous fraction of the scaffolds, as expected. The average percentages of porosity measured all the scaffolds are within the range of 92–93%, being very similar to that of raw CB (92.85 ± 0.36%). The polymeric coatings induced slight decreases in porosity, with the higher and similar porosities being registered for the scaffolds coated with PDLA, PEA or PEU. Porosity values slightly below 90% were measured for the scaffolds coated with PCL.

Table 3. Porosities (%) of raw CB and of the CB-derived BCP scaffolds, uncoated and coated with polymer solutions containing 5 (w/v %), expect for PLA in which the concentration was reduced to 3 (w/v %).

Polymer	Raw CB	BCP	BCP-6Sr	BCP-6Sr2Mg	BCP-6Sr2Zn	BCP-6Sr2Mg2Zn
–	92.85±0.36	92.73±0.27	92.56±0.35	92.85±0.50	92.85±0.54	92.76±0.26
PCL	–	89.56±0.66	89.04±0.15	89.66±0.37	89.27±0.52	89.27±0.08
PDLA*	–	90.94±0.54	90.67±0.59	91.17±0.62	91.83±0.14	91.54±0.10
PEA	–	91.27±0.03	90.61±0.12	90.86±0.36	90.74±0.56	90.78±0.02
PEU	–	91.28±0.23	91.20±0.17	90.68±0.24	90.78±0.22	91.28±0.24

The values of compressive strength (CS) and Young's modulus (YM) calculated from the maximum mechanical stress reached during the deformation period are summarized in Table 4. The CS of the raw CB (1.63 ± 0.07 MPa) was drastically reduced by about 8 times after HT and sintering for BCP, BCP-6Sr and BCP-6Sr2Zn, and by about 4 times for the other compositions (BCP-6Sr2Mg, BCP-6Sr2Mg2Zn).

Table 4. Compressive strength (first row, MPa) and Young's modulus (second row, MPa) of the raw CB and the CB-derived BCP scaffolds uncoated and coated with polymer solutions containing 5 (w/v %), expect for PLA in which the concentration was reduced to 3 (w/v %).

Polymer	Raw CB	BCP	BCP-6Sr	BCP-6Sr2Mg	BCP-6Sr2Zn	BCP-6Sr2Mg2Zn
–	1.63±0.07	0.21±0.02	0.20±0.02	0.40±0.02	0.20±0.01	0.36±0.02
	2.76±0.58	0.33±0.03	0.27±0.02	0.51±0.09	0.21±0.01	0.52±0.05
PCL	–	0.62±0.06	1.42±0.06	1.28±0.12	0.67±0.07	0.46±0.04
	–	1.22±0.24	2.10±0.29	2.22±0.31	1.29±0.08	0.66±0.05
PDLA	–	0.70±0.02	0.63±0.04	0.96±0.07	0.63±0.10	0.61±0.05
	–	1.26±0.16	0.98±0.16	1.35±0.17	1.01±0.22	1.01±0.13
PEA	–	0.31±0.05	0.36±0.02	0.30±0.03	0.25±0.04	0.20±0.01
	–	0.40±0.07	0.51±0.12	0.51±0.16	0.44±0.10	0.35±0.09
PEU	–	0.93±0.13	1.73±0.25	1.12±0.10	0.94±0.06	1.05±0.12
	–	1.31±0.23	2.61±1.01	1.57±0.20	1.59±0.23	1.54±0.18

Despite the differences in CS between the raw and the hydrothermally transformed CB, both types of scaffolds exhibit similar stress-strain behaviors with the microstructure collapsing layer-by-layer (Figure 8), instead of a catastrophic failure.

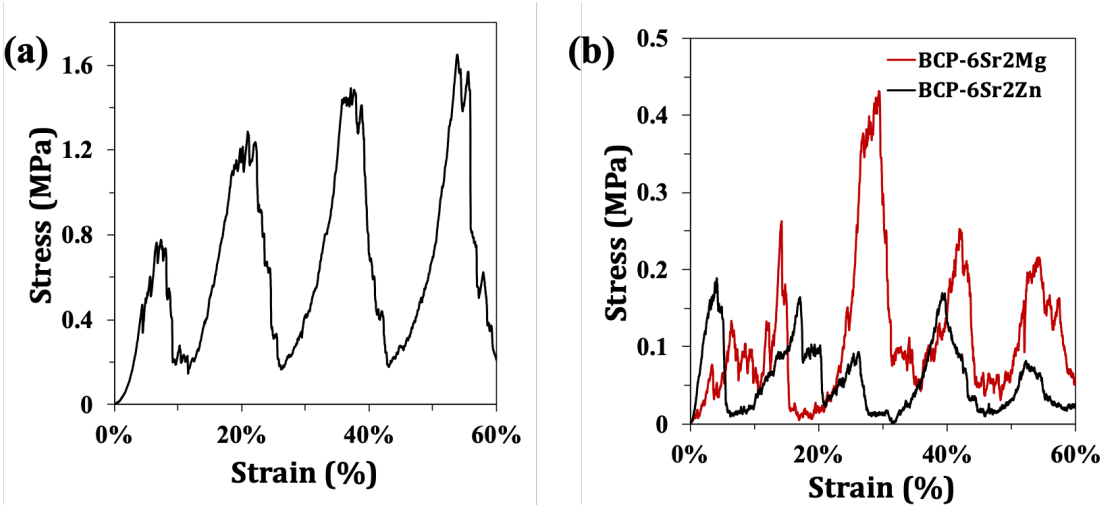

Figure 8. Compressive strength of **(a)** raw CB and **(b)** the higher (BCP-6Sr2Mg, red line) and lower (BCP-6Sr2Zn, black line) obtained results after HT and sintering.

The polymeric coatings significantly improved the CS, partially recovering the initial composite nature of the porous structures. The stress-strain plots displayed in Figure 9 show that scaffolds undergo deformation but without the occurrence of a total collapse of the CB layers. In general, the higher values of CS and YM were achieved for the scaffolds coated with PEU. On the other hand, the lowest values were registered for the scaffolds coated with PEA. For instance, BCP-6Sr2Zn scaffolds improved the CS by almost 5 times from 0.20 ± 0.01 MPa to 0.97 ± 0.06 MPa after the coating with PEU.

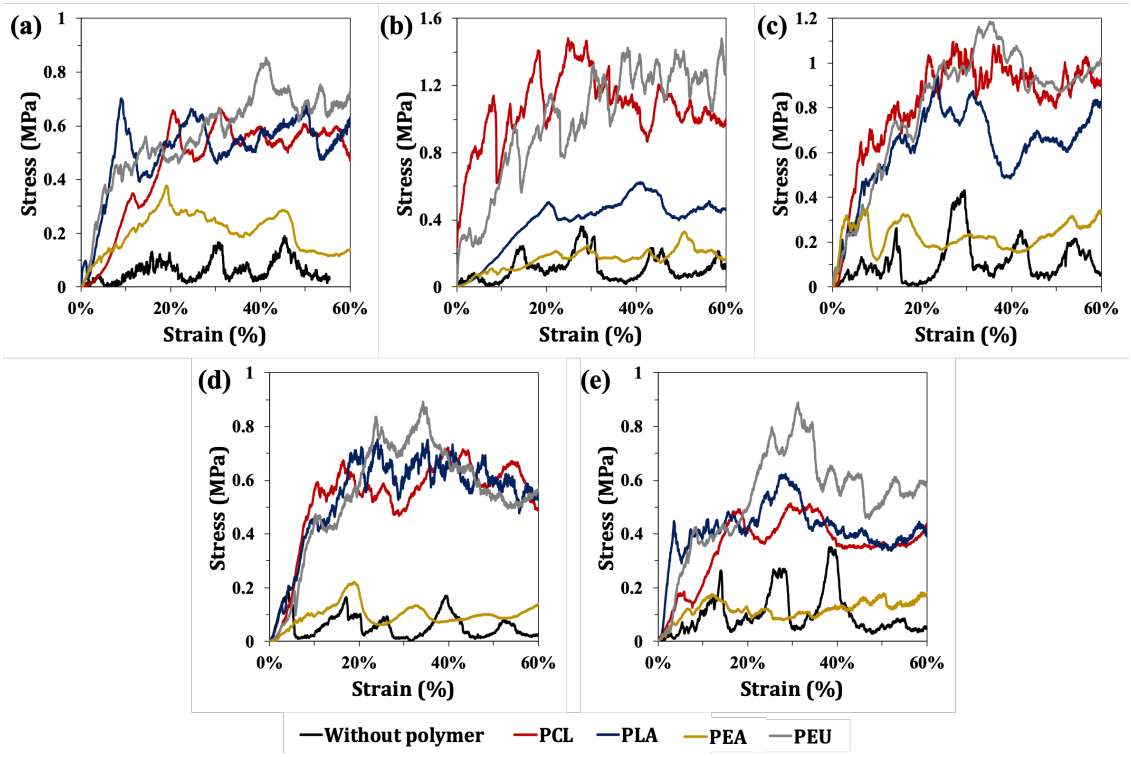

Figure 9. Representative result of the compressive strength of CB derived scaffolds after HT and coated with PCL, PLA, PEA or PEU: **(a)** BCP scaffolds; **(b)** BCP-6Sr scaffolds; **(c)** BCP-6Sr2Mg scaffolds; **(d)** BCP-6Sr2Zn scaffolds; **(e)** BCP-6Sr2Mg2Zn scaffolds.

3.5. *In vitro* bio-mineralization

The *in vitro* bio-mineralization occurred after immersion the scaffolds into SBF solution was analyzed by SEM (Figure 10) After 14 days of incubation, all the scaffolds compositions exhibited the deposition of isolated or aggregated calcium phosphate microspheres, characteristic from the apatite developed *in vitro*. Despite knowing that the mineralization process is affected by the nature of the polymer, it was observed similar mineralizations for the different polymeric coating with exception of the scaffolds coated with PEA. The EDS analysis of the obtained particles showed presence of Ca, P and O and small quantities of Na, Mg and Cl, characteristic of the natural apatite of the human bone.

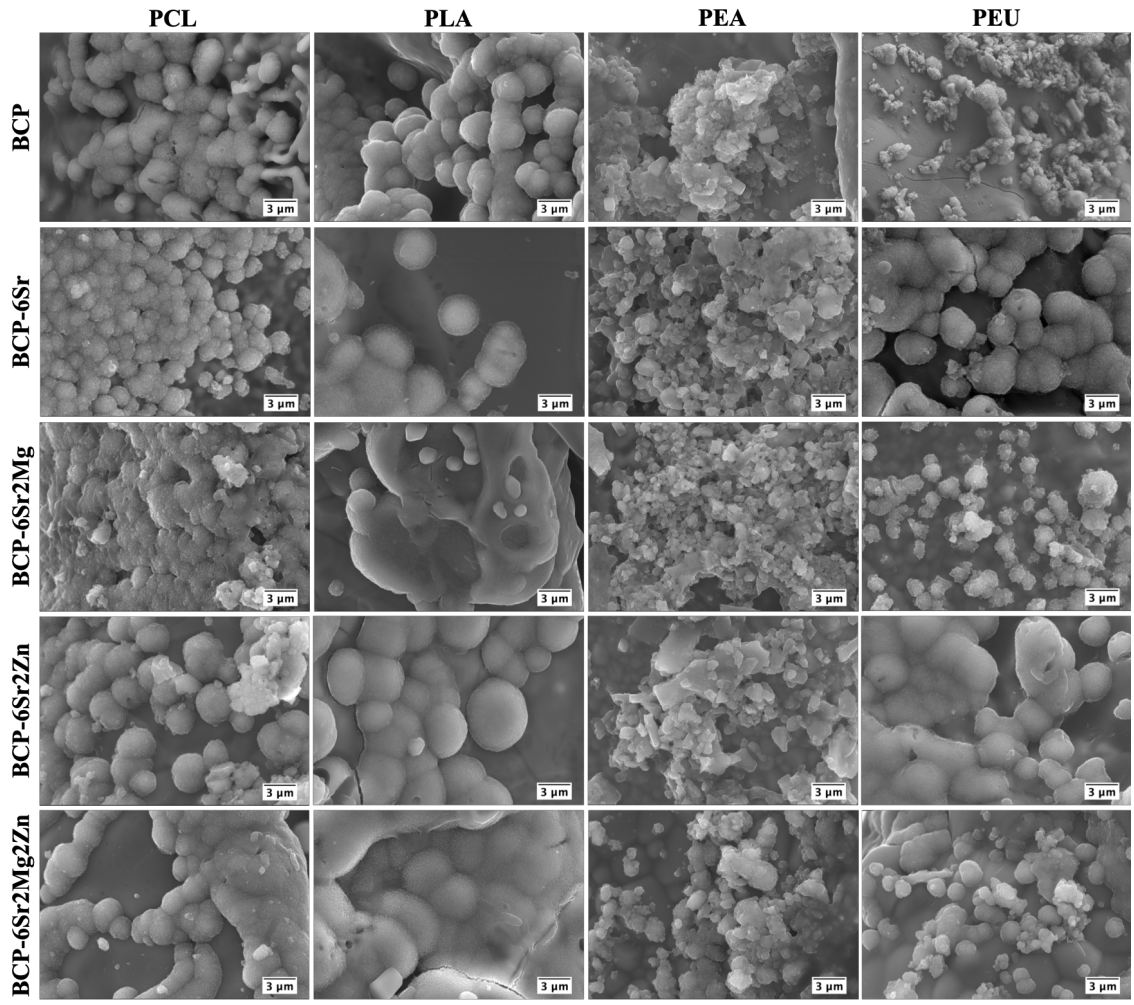

Figure 10 SEM micrographs of the different coated CB after soaking in SBF solution for 14 days.

4. Discussion

In this study, we obtained undoped and ion (Sr^{2+}, Mg^{2+} and Zn^{2+}) doped BCP scaffolds derived from CB. Different polymers (PCL, PDLA, PEA and PEU) were used for the polymeric coating in order to achieve better mechanical properties.

Rocha et al. [26] were the first authors to report the transformation of CB into HA scaffolds by HT. Since then, the research works have been mainly focused on the transformation of CB into HA scaffolds. Nevertheless, it is recognized that BCP (HA + β-TCP) biomaterials enable to obtain a better balance between resorption and solubilization and, consequently, ensuring the stability of the material while promoting bone ingrowth. In this vein, Sarin et al. [41] attempted to produced BCP scaffolds derived from CB by immersion the raw CB into a phosphoric acid solution, but only a partial conversion extent was achieved, as the final product presented a significant amount of CaO (~6.4 wt%). This is not desired as the remaining CaO will react with the

physiological fluid after implantation forming calcium hydroxide and creating a cytotoxic high pH environment [42,43]. In the present work, a complete transformation of CB into a BCP scaffold was achieved for both undoped and doped scaffolds. Accordingly, beyond HA and β-TCP, no other crystalline phases were observed by XRD (Figure 2) and the Rietveld refinement (Table 1). The obtained FTIR spectra of the samples revealed the presence of the $–PO_4$ groups and a very small content of –OH groups, which might be a consequence of the absence of –OH group in the β-TCP phase, or the occurrence of a partial de-hydroxylation of HA at 1200 ºC. But the very low content of –OH groups in biological apatites is also well recognized [44]. Regarding the volatile nature of carbonates and the sintering temperature of the scaffolds (1200 °C), the carbonate peaks in apatites (872, 1412, 1458 and 1547 cm^{-1} did not appear in the FTIR spectra of all the samples [26]. The FTIR data are therefore in good agreement with the XRD results (Figure 2).

The incorporation of doping elements into the crystalline lattices of CaP has been adopted as a strategy to improve the biological performance of CB-derived scaffolds. Kannan et al. [28] and Kim et al. [29] studied the incorporation of F^- and Si^{4+} respectively. This work was more ambitious aiming at the concomitant incorporation of some essential ions (Sr^{2+}, Mg^{2+} and Zn^{2+}) into the BCP structure. Although the diffraction patterns of all the samples are more or less coincident with HA and β-TCP, the effects of doping with ions having different radii are reflected in the shifts observed in the XRD peaks. For instance, the incorporation of Sr^{2+} into the crystal lattice (BCP-6Sr) resulted in a slight shift to lower angles. This is consistent with an increase in the lattice parameters, as expected from the partial replacement of Ca^{2+} (0.99 Å) by the larger size ion (Sr^{2+} 1.20 Å) in the lattice sites of HA and β-TCP [45]. This is a clear indication that Sr^{2+} has been effectively incorporated in both crystalline phases [45–50]. The incorporation of Sr^{2+} together with Mg^{2+} (BCP-6Sr2Mg) or with Zn^{2+} (BCP-6Sr2Zn) resulted in shifts of the HA and β-TCP peaks to lower and higher angles, respectively. The slight shift of the β-TCP peaks to higher angles means that the smaller Mg^{2+} (0.69 Å) and Zn^{2+} (0.74 Å) ions were preferentially incorporated in the β-TCP phase. This is not much surprising considering these smaller ions tend to enhance the stability of β-TCP, which has been extensively reported, particularly for Mg^{2+} [48,49,51,52]. Moreover, in the presence of Mg^{2+} or Zn^{2+} there is an intensity enhancement of the β-TCP peaks. This confirms the preference of these doping ions for occupying lattice positions in the β-TCP phase, enhancing its stability. Under these circumstances, the Sr^{2+} ions that can almost equally

be accommodated in any of the crystalline lattices (HA or β-TCP) will compete with the Ca^{2+} ions replaced in the β-TCP phase for available positions in the crystalline lattice of HA. The resulting increase in the lattice parameters of HA explains the observed shift of the XRD peaks to lower angles. On the other hand, the incorporation of Sr^{2+} together with Mg^{2+} and Zn^{2+} (BCP-6Sr2Mg2Zn) resulted in an apparent slight shift of all the peaks to higher angles, what is somehow surprising. Despite the shifts of the XRD peaks, the elementary analysis shown in Table 2 demonstrates that doping elements encounter some difficulties in entering the lattice structure to replace calcium, attributed to ionic size mismatches.

An interconnected porous structure is a crucial parameter for cell proliferation, vascularization and nutrient supply. Thereby, such interconnected porous structure is beneficial for bone growth [22]. Recognizing the optimal pore size and interconnectivity of the CB, a significant number of research works [25–32,41,53,54] demonstrated that the initial CB structure could be preserved. Following the same principle, in this work it was observed by SEM (Figure 4 and Figure 5) that the HT and the ionic substitutions did not jeopardize the internal structure of CB. Moreover, the increasing surface roughness after the HT and sintering is beneficial for bone growth because it influences not only the cell adhesion and migration but also the production of extracellular matrix [55].

Raw CB is a composite with an inorganic phase ($CaCO_3$) and an organic phase (β-chitin) that covers the inorganic matrix [24]. However, the organic part is removed upon HT and sintering. The elimination of the organic component is intrinsically related to the decrease in the mechanical properties observed for all the different scaffold compositions (Figure 7 and Table 4). In raw CB, the β-chitin is responsible for the redistribution of the compressive stress and dissipate the mechanical energy during deformation, increasing the resilience and toughness of the composite material, thereby, hindering the propagation of cracks [31]. Thus, β-chitin plays an important role in conferring to the CB the functional and highly sophisticated features that enable cuttlefish maintaining its neutral buoyancy at high depths, while retaining enough stiffness and strength to prevent sever distortion or crushing under the high hydrostatic pressures in deep water [56–58]. The elimination of the organic matter during the HT and sintering processes severely degrades the mechanical properties of CB.

To overcome this drawback and improving the mechanical properties of CB-derived HA scaffolds, Milovac et al. [31] and Kim et al. [32] impregnated them with PCL solutions, which were then evaporated to leave coatings deposited in the porous cell walls.

A coating of the CB- derived HA scaffolds with a combination of PCL and PLA was studied by Rogina et al. [33].

The polymeric coatings applied to CB-derived BCP scaffolds aimed at improving their mechanical properties. Besides PCL or PDLA (two of the most widely used polymers in the biomedical field), coatings based on PEA or PEU (polymers with an increasing relevance for biomedical applications [19]) were also investigated in the present work. The presence of the polymers in the coated scaffolds was confirmed by FTIR through their characteristic peaks appearing superposed with those of BCP peaks. Importantly, the polymeric coatings had no significant negative impact on the porosity (Table 3), except in the case of the most viscous 5% (w/v) PDLA solution (Figure S3). Accordingly, a more diluted solution [3% (w/v)] was adopted for further coatings with this polymer. Under this condition, the porosity values of PDLA coated scaffolds were similar to the PEA and PEU coated scaffolds. The lowest value of porosity (~89%) registered for scaffolds coated with PCL from a 5% (w/v) solution, which can also be attributed to its relatively high viscosity, limiting the solution runoff from the pores. The 5% (w/v) PEA and PEU solutions exhibited the lower viscosities, being able to penetrate into the intrinsic porosity of cell walls and easily runoff, forming thinner coating layers in comparison to PCL and PDLA. For instance, a reduction in the concentration of the PCL solution to 1% (w/v) (Figure S4) was required to achieve viscosity curves similar to the ones corresponding to the 5% (w/v) PEA and PEU solutions. The specific interactions between the functional groups of the different polymers and the CaP substrates are also likely to play an important role in determining the features of the coatings. The –COOH groups present in all polymers exhibit a high affinity for calcium. In addition to –COOH group, the PEA and PEU polymers exhibit –NH_2 as terminal groups, which have chemical affinity towards phosphorous [59]. These affinities could justify also the enhanced interactions of the PEA and PEU with the CaP scaffolds.

Regarding the mechanical properties, the coating significantly improved the CS. The vacuum impregnation allowed an efficient filling of the defects, thus mitigating the crack propagation in the scaffolds. In this vein, instead of a layer-by-layer collapse, it was observed a deformation of the scaffolds with small and less pronounced cracks. Regarding the PCL coated scaffolds, the results are in agreement with those of Kim et al. [32]. The authors obtained an improvement of the mechanical properties by 2.09-fold upon the coating with 5% PCL. In our study, the mechanical properties of the BCP scaffolds coated with 5% PCL improved 2.95-fold. Although the CS values registered for

the scaffolds coated with PEA are generally lower, the stress-deformation curves are more stable. This feature can be attributed to a better interaction between the PEA and the inorganic matrix (Figure 8). The higher values of mechanical strength were registered with PEU coating. For instance, an improvement by 4.70-fold was obtained for the BCP-6Sr2Zn scaffolds. Typically, the values of CS and YM of human trabecular bone vary between 0.1 and 16 MPa and between 50 and 500 MPa, respectively [60]. Thus, the CS and YM registered for our composite scaffolds are respectively above, and below, the lower limits of the ranges reported for trabecular bone. These relatively low values are understandable considering the intrinsically high porosity of the scaffolds. Further enhancements of mechanical properties are likely achievable by repeating the dipping process, while taking care for do not excessively compromising the porosity.

The material capacity to bond the natural bone upon implantation is normally evaluated by immersion in SBF solution, which is recognized as a powerful technique to predicting the bioactivity of a material [61]. The apatite formation on the polymeric coated scaffolds is dependent on the functional group on the polymer surface. Negatively charged groups, like $–COO^–$, strongly induced apatite formation as they bind to Ca^{2+}, which promote the apatite nucleation and growth. On the other hand, the apatite formation in the presence of positive groups, like $–NH_3^+$, is significantly lower [62]. The four used polymers originate –COOH groups during hydrolysis. However, for PEA the pH drop is very small because $–NH_2$ groups are also formed, being a well-known advantage of these polymers. As consequence, a lower concentration of –COOH is available for complexation with Ca^{2+} and less amount of apatite is formed.

5. Conclusions

Raw CB was, for the first time, completely hydrothermally con- verted into undoped and ion (Sr^{2+}, Mg^{2+} and/or Zn^{2+}) doped BCP scaffolds while maintaining their internal structure. This transformation and the subsequent heat treatment removed the organic (β-chitin) phase matrix existing in the raw CB, negatively affecting the mechanical properties of the scaffolds. To overcome this problem, different polymers (PCL, PDLA, PEA or PEU) were used to coat the scaffolds. The polymers did enhance the mechanical properties of the scaffolds. However, PEU was generally more effective in upgrading the com- pressive strength to values registered for human trabecular bone (0.93–1.73 MPa). Moreover, after the polymeric coating the scaffolds exhibited a good *in vitro* bioactivity

in SBF. These scaffolds are worthy of further investigation as potential candidates for bone tissue engineering applications.

Acknowledgments: This work was developed within the scope of the project CICECO- Aveiro Institute of Materials, FCT Ref. UID/CTM/50011/2019, financed by national funds through the FCT/MCTES. Ana S. Neto acknowledges to AdvaMTech, the PhD Program on Advanced Materials and Processing for the PhD grant, PD/BD/114132/2015, founded by the Portuguese Foundation for Science and Technology (FCT). The authors are very thankful to Dias de Sousa - Instrumentação Analítica e Científica, S.A., Setúbal, Portugal, for doing the μ-CT analysis of our samples.

Supporting Information

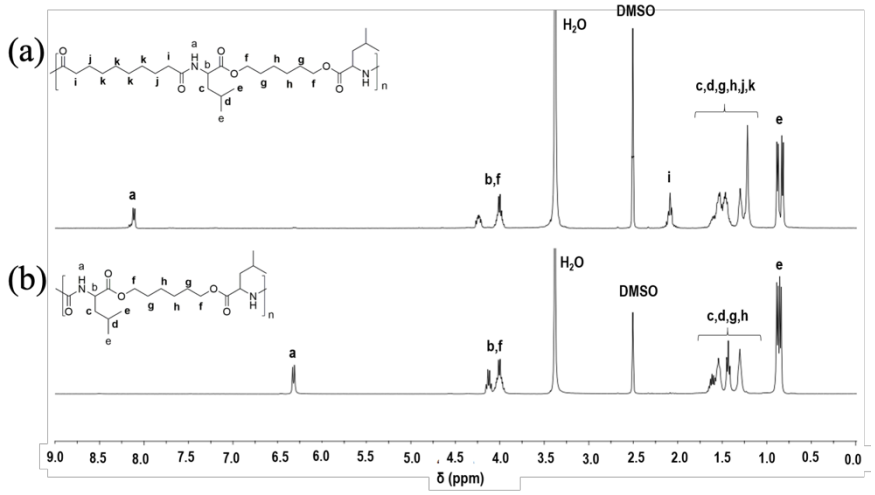

Figure S1 ^{1}H NMR spectra of (a) PEA and (b) PEU.

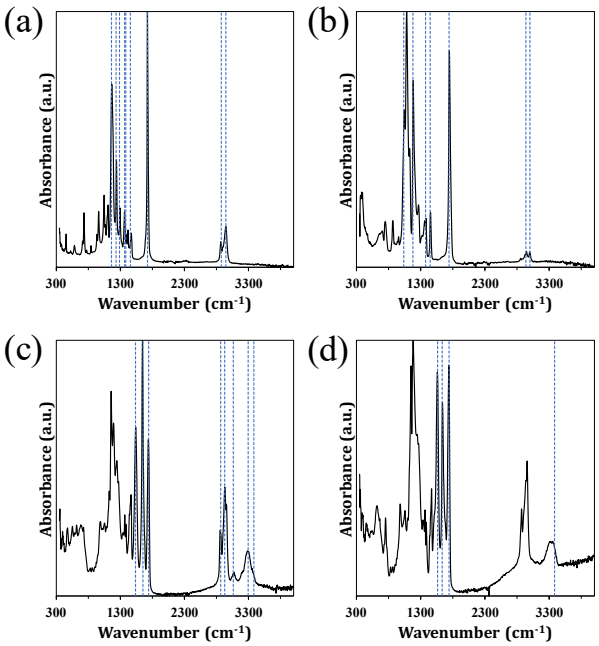

Figure S2 FTIR spectra of the polymers used for the coating: (a) PCL; (b) PDLA; (c) PEA; (d) PEU.

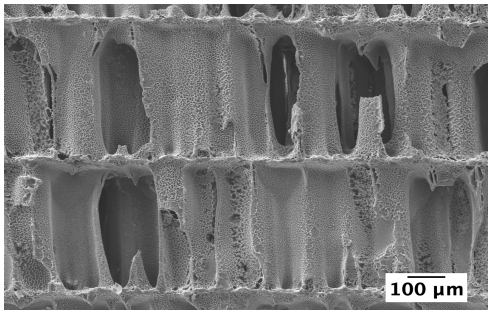

Figure S3 Polymeric coating with a 5% (w/v) PDLA solution.

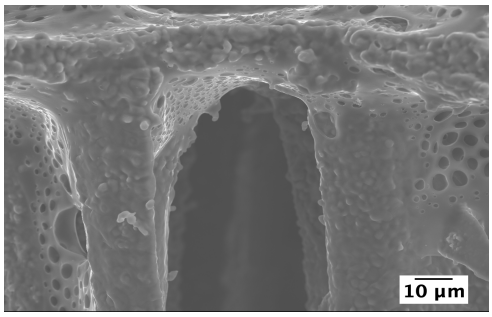

Figure S4 Polymeric coating with a 1% (w/v) PCL solution.

References

[1] M.K. Sen, T. Miclau, Autologous iliac crest bone graft: should it still be the gold standard for treating nonunions? Injury. 38 (Suppl. 1) (2007) S75–S80, https://doi.org/10.1016/j.injury.2007.02.012.

[2] L. Roseti, V. Parisi, M. Petretta, C. Cavallo, G. Desando, I. Bartolotti, B. Grigolo, Scaffolds for bone tissue engineering: state of the art and new perspectives, Mater. Sci. Eng. C. 78 (2017) 1246–1262, https://doi.org/10.1016/j.msec.2017.05.017.

[3] S.V. Dorozhkin, Calcium orthophosphates as bioceramics: state of the art, J. Funct. Biomater. 1 (2010) 22–107, https://doi.org/10.3390/jfb1010022.

[4] R.Z. Legeros, Calcium phosphate materials in restorative dentistry: a review, Adv. Dent. Res. 2 (1988) 164–180, https://doi.org/10.1177/08959374880020011101.

[5] J.M. Bouler, P. Pilet, O. Gauthier, E. Verron, Biphasic calcium phosphate ceramics for bone reconstruction: a review of biological response, Acta Biomater. 53 (2017) 1–12, https://doi.org/10.1016/j.actbio.2017.01.076.

[6] C. Castellani, G. Zanoni, S. Tangl, M. Van Griensven, H. Redl, Biphasic calcium phosphate ceramics in small bone defects: potential influence of carrier substances and bone marrow on bone regeneration, Clin. Oral Implants Res. 20 (2009) 1367–1374, https://doi.org/10.1111/j.1600-0501.2009.01760.x.

[7] S.E.Lobo,T.L.Arinzeh,Biphasiccalciumphosphateceramicsforboneregeneration and tissue engineering applications, Materials (Basel). 3 (2010) 815–826, https://doi.org/10.3390/ma3020815.

[8] E. Boanini, M. Gazzano, A. Bigi, Ionic substitutions in calcium phosphates synthesized at low temperature, Acta Biomater. 6 (2010) 1882–1894, https://doi.org/10.1016/j.actbio.2009.12.041.

[9] E.A.Botchwey,S.R.Pollack,E.M.Levine,C.T.Laurencin,Bonetissueengineeringin a rotating bioreactor, J. Biomed. Mater. Res. - Part A. 55 (2001) 242–253, https://doi.org/10.1016/j.micinf.2011.07.011.Innate.

[10] E. O'Neill, G. Awale, L. Daneshmandi, O. Umerah, K.W.H. Lo, The roles of ions on bone regeneration, Drug Discov. Today 23 (2018) 879–890, https://doi.org/10.1016/j.drudis.2018.01.049.

[11] A.S. Prasad, Zinc is an antioxidant and anti-inflammatory agent: its role in human health, Front. Nutr. 1 (2014) 1–10, https://doi.org/10.3389/fnut.2014.00014.

[12] A.R.Shrivats, M.C.McDermott, J.O.Hollinger, Bone tissue engineering: state of the union, Drug Discov. Today 19 (2014) 781–786, https://doi.org/10.1016/j.drudis. 2014.04.010.

[13] R.Y. Basha, S.K. T.S., M. Doble, Design of biocomposite materials for bone tissue regeneration, Mater. Sci. Eng. C. 57 (2015) 452–463. doi:https://doi.org/10.1016/ j.msec.2015.07.016.

[14] K.E. Tanner, Bioactive composites for bone tissue engineering, Procedings Inst. Mech. Eng. H. 224 (2010) 1359–1372, https://doi.org/10.1243/ 09544119JEIM823.

[15] M.I. Sabir, X. Xu, L. Li, A review on biodegradable polymeric materials for bone tissue engineering applications, J. Mater. Sci. 44 (2009) 5713–5724, https://doi. org/10.1007/s10853-009-3770-7.

[16] M.S. Cortizo, M.S. Belluzo, Biodegradable polymers for bone tissue engineering, in: S.N. Goyanes, N.B. D'Accorso (Eds.), Ind, Appl. Renew. Biomass Prod. Past, Present Futur, 2017, https://doi.org/10.1007/978-3-319-61288-1.

[17] A. Rodriguez-Galan, L. Franco, J. Puiggali, Degradable poly(ester amide)s for biomedical applications, Polymers (Basel). 3 (2011) 65–99, https://doi.org/10.3390/ polym3010065.

[18] A.C. Fonseca, J.F.J. Coelho, M.H. Gil, P.N. Simões, Poly(ester amide)s based on l-lactic acid oligomers and glycine: the role of the central unit of the l-lactic acid oligomers and their molecular weight in the poly(ester amide)s properties, Polym. Bull. 71 (2014) 3085–3109, https://doi.org/10.1007/s00289-014-1239-6.

[19] A.C. Fonseca, M.H. Gil, P.N. Simões, Biodegradable poly(ester amide)s - a remarkable opportunity for the biomedical area: review on the synthesis, characterization and applications, Prog. Polym. Sci. 39 (2014) 1291–1311, https://doi.org/ 10.1016/j.progpolymsci.2013.11.007.

[20] K.S. Stakleff, F. Lin, L.A. Smith Callahan, M.B. Wade, A. Esterle, J. Miller, M. Graham, M.L. Becker, Resorbable, amino acid-based poly(ester urea)s cross- linked with osteogenic growth peptide with enhanced mechanical properties and bioactivity, Acta Biomater. 9 (2013) 5132–5142, https://doi.org/10.1016/j.actbio. 2012.08.035.

[21] S. Li, Y. Xu, J. Yu, M.L. Becker, Enhanced osteogenic activity of poly(ester urea) scaffolds using facile post-3D printing peptide functionalization strategies, Biomaterials. 141 (2017) 176–187, https://doi.org/10.1016/j.biomaterials.2017. 06.038.

[22] F.J.O'Brien,Biomaterials&scaffoldsfortissueengineering,Mater.Today14(2011) 88–95, https://doi.org/10.1016/S1369-7021(11)70058-X.

[23] X.Zhang, K.S.Vecchio, Conversion of natural marine skeletons as scaffolds for bone tissue engineering, Front. Mater. Sci. 7 (2013) 103–117, https://doi.org/10.1007/ s11706-013-0204-x.

[24] J.D. Birchall, N.L. Thomas, On the architecture and function of cuttlefish bone, J. Mater. Sci. 18 (1983) 2081–2086, https://doi.org/10.1007/BF00555001.

[25] J.H.G. Rocha, A.F. Lemos, S. Agathopoulos, S. Kannan, P. Valério, J.M.F. Ferreira, Hydrothermal growth of hydroxyapatite scaffolds from aragonitic cuttlefish bones, J. Biomed. Mater. Res. - Part A. 77 (2006) 160–168, https://doi.org/10.1002/jbm. a.30566.

[26] J.H.G. Rocha, A.F. Lemos, S. Agathopoulos, P. Valério, S. Kannan, F.N. Oktar, J.M.F. Ferreira, Scaffolds for bone restoration from cuttlefish, Bone. 37 (2005) 850–857, https://doi.org/10.1016/j.bone.2005.06.018.

[27] L. Hongmin, Z. Wei, Y. Xingrong, W. Jing, G. Wenxin, C. Jihong, X. Xin, C. Fulin, Osteoinductive nanohydroxyapatite bone substitute prepared via in situ hydrothermal transformation of cuttlefish bone, J. Biomed. Mater. Res. - Part B Appl. Biomater. 103B (2015) 816–824, https://doi.org/10.1002/jbm.b.33261.

[28] S. Kannan, J.H.G. Rocha, S. Agathopoulos, J.M.F. Ferreira, Fluorine-substituted hydroxyapatite scaffolds hydrothermally grown from aragonitic cuttlefish bones, Acta Biomater. 3 (2007) 243–249, https://doi.org/10.1016/j.actbio.2006.09.006.

[29] B.S. Kim, S.S. Yang, J.H. Yoon, J. Lee, Enhanced bone regeneration by silicon-substituted hydroxyapatite derived from cuttlefish bone, Clin. Oral Implants Res. 00 (2015) 1–8, https://doi.org/10.1111/clr.12613.

[30] D. Milovac, T.C. Gamboa-Martínez, M. Ivankovic, G. Gallego Ferrer, H. Ivankovic, PCL-coated hydroxyapatite scaffold derived from cuttlefish bone: in vitro cell culture studies, Mater. Sci. Eng. C. 42 (2014) 264–272, https://doi.org/10.1016/j. msec.2014.05.034.

[31] D. Milovac, G. Gallego Ferrer, M. Ivankovic, H. Ivankovic, PCL-coated hydroxyapatite scaffold derived from cuttlefish bone: morphology, mechanical properties and bioactivity, Mater. Sci. Eng. C. 34 (2014) 437–445, https://doi.org/10.1016/j. msec.2014.05.034.

[32] B.S.Kim,H.J.Kang,J.Lee,Improvementofthecompressivestrengthofacuttlefish bone-derived porous hydroxyapatite scaffold via polycaprolactone coating, J. Biomed. Mater. Res. - Part B. 101 (2013) 1302–1309, https://doi.org/10.1002/jbm. b.32943.

[33] A. Rogina, M. Antunovic, D. Milovac, Biomimetic design of bone substitutes based on cuttlefish bone-derived hydroxyapatite and biodegradable polymers, J. Biomed. Mater. Res. - Part B. 107B (2018) 197–204.

[34] A.C. Popa, G.E. Stan, M.A. Husanu, I. Mercioniu, L.F. Santos, H.R. Fernandes, J.M.F. Ferreira, Bioglass implant-coating interactions in synthetic physiological fluids with varying degrees of biomimicry, Int. J. Nanomedicine 12 (2017) 683–707, https://doi.org/10.2147/IJN.S123236.

[35] S. Raynaud, E. Champion, D. Bernache-Assollant, P. Thomas, Calcium phosphate apatites with variable Ca/P atomic ratio I. Synthesis, characterisation and thermal stability of powders, Biomaterials. 23 (2002) 1065–1072, https://doi.org/10.1016/ S0142-9612(01)00218-6.

[36] A. Elzubair, C.N. Elias, J.C.M. Suarez, H.P. Lopes, M.V.B. Vieira, The physical characterization of a thermoplastic polymer for endodontic obturation, J. Dent. 34 (2006) 784–789, https://doi.org/10.1016/j.jdent.2006.03.002.

[37] D. Mao, Q. Li, D. Li, Y. Chen, X. Chen, X. Xu, Fabrication of 3D porous poly(lactic acid)-based composite scaffolds with tunable biodegradation for bone tissue engineering, Mater. Des. 142 (2018) 1–10, https://doi.org/10.1016/j.matdes.2018. 01.016.

[38] X.Pang, C.C.Chu, Synthesis, characterization and biodegradation of functionalized amino acid-based poly(ester amide)s, Biomaterials. 31 (2010) 3745–3754, https:// doi.org/10.1016/j.biomaterials.2010.01.027.

[39] D.J. Skrovanek, S.E. Howe, P.C. Painter, M.M. Coleman, Hydrogen bonding in polymers: infrared temperature studies of an amorphous polyamide, Macromolecules. 18 (1985) 1676–1683.

[40] B. Kaczmarczyk, S.E. Danuta, Hydrogen bonds in poly(ester amide)s and their model compounds, Polymer (Guildf). 36 (1995) 5019–5025, https://doi.org/10.1016/0032-3861(96)81631-4.

[41] P. Sarin, S.J. Lee, Z.D. Apostolov, W.M. Kriven, Porous biphasic calcium phosphate scaffolds from cuttlefish bone, J. Am. Ceram. Soc. 94 (2011) 2362–2370, https://doi.org/10.1111/j.1551-2916.2011.04404.x.

[42] F.A. Guiotti, M.C. Kuga, M.A.H. Duarte, A. Sant'Anna Júnior, G. Faria, Effect of calcium hydroxide dressing on push-out bond strength of endodontic sealers to root canal dentin, Braz. Oral Res. 28 (2014) 1–6, https://doi.org/10.1590/S1806-83242014.50000002.

[43] A.R.Butt, S.Ejaz, J.C.Baron, M.Ikram, S.Ali, S. Applications, CaO nanoparticles as a potential drug delivery agent for biomedical applications, Diget J. Nomaterials Biostructures. 10 (2015) 799–809.

[44] J.D. Pasteris, B. Wopenka, J.J. Freeman, K. Rogers, E. Valsami-Jones, J.A.M. Van Der Houwen, M.J. Silva, Lack of OH in nanocrystalline apatite as a function of degree of atomic order: implications for bone and biomaterials, Biomaterials. 25 (2004) 229–238, https://doi.org/10.1016/S0142-9612(03)00487-3.

[45] A.Bigi, E.Boanini, C.Capuccini, M.Gazzano, Strontium-substituted hydroxyapatite nanocrystals, Inorganica Chim. Acta. 360 (2007) 1009–1016, https://doi.org/10.1016/j.ica.2006.07.074.

[46] C.Capuccini, P.Torricelli, E.Boanini, M.Gazzano, R.Giardino, A.Bigi, Interaction of Sr-doped hydroxyapatite nanocrystals with osteoclast and osteoblast-like cells, J. Biomed. Mater. Res. - Part A. 89 (2009) 594–600, https://doi.org/10.1002/jbm.a. 31975.

[47] U. Thormann, S. Ray, U. Sommer, T. ElKhassawna, T. Rehling, M. Hundgeburth, A. Henß, M. Rohnke, J. Janek, K.S. Lips, C. Heiss, G. Schlewitz, G. Szalay, M. Schumacher, M. Gelinsky, R. Schnettler, V. Alt, Bone formation induced by strontium modified calcium phosphate cement in critical-size metaphyseal fracture defects in ovariectomized rats, Biomaterials. 34 (2013) 8589–8598, https://doi.org/10.1016/j.biomaterials.2013.07.036.

[48] C.F. Marques, A. Lemos, S.I. Vieira, O.A.B. Da Cruz, E Silva, A. Bettencourt, J.M.F. Ferreira, Antibiotic-loaded Sr-doped porous calcium phosphate granules as

multifunctional bone grafts, Ceram. Int. 42 (2016) 2706–2716. doi:https://doi.org/10.1016/j.ceramint.2015.11.001.

[49] C.F. Marques, S. Olhero, J.C.C. Abrantes, A. Marote, S. Ferreira, S.I. Vieira, J.M.F. Ferreira, Biocompatibility and antimicrobial activity of biphasic calcium phosphate powders doped with metal ions for regenerative medicine, Ceram. Int. 43 (2017) 15719–15728, https://doi.org/10.1016/j.ceramint.2017.08.133.

[50] B. Bracci, P. Torricelli, S. Panzavolta, E. Boanini, R. Giardino, A. Bigi, Effect of Mg2+, Sr2+, and Mn2+ on the chemico-physical and in vitro biological proper- ties of calcium phosphate biomimetic coatings, J. Inorg. Biochem. 103 (2009) 1666–1674, https://doi.org/10.1016/j.jinorgbio.2009.09.009.

[51] C.F. Marques, A.C. Matos, I.A.C. Ribeiro, L.M. Gonçalves, A. Bettencourt, J.M.F. Ferreira, Insights on the properties of levofloxacin-adsorbed Sr- and Mg- doped calcium phosphate powders, J. Mater. Sci. Mater. Med. 27 (2016) 1–12, https://doi.org/10.1007/s10856-016-5733-2.

[52] M. Frasnelli, V.M. Sglavo, Effect of Mg2+doping on beta-alpha phase transition in tricalcium phosphate (TCP) bioceramics, Acta Biomater. 33 (2016) 283–289, https://doi.org/10.1016/j.actbio.2016.01.015.

[53] H. Ivankovic, G. Gallego Ferrer, E. Tkalcec, S. Orlic, M. Ivankovic, Preparation of highly porous hydroxyapatite from cuttlefish bone, J. Mater. Sci. Mater. Med. 20 (2009) 1039–1046, https://doi.org/10.1007/s10856-008-3674-0.

[54] X. Li, Y. Zhao, Y. Bing, Y. Li, N. Gan, Z. Guo, Z. Peng, Biotemplated syntheses of macroporous materials for bone tissue engineering scaffolds and experiments in vitro and vivo biotemplated syntheses of macroporous materials for bone tissue engineering scaffolds and experiments in vitro and vivo, ACS Appl. Mater. Interfaces 5 (2013) 5557–5562, https://doi.org/10.1021/am400779e.

[55] P. Wang, L. Zhao, J. Liu, M.D. Weir, X. Zhou, H.H.K. Xu, Bone tissue engineering via nanostructured calcium phosphate biomaterials and stem cells, Bone Res. 2 (2014) 14017, https://doi.org/10.1038/boneres.2014.17.

[56] H. Ivankovic, E. Tkalcec, S. Orlic, G.G. Ferrer, Z. Schauperl, Hydroxyapatite formation from cuttlefish bones: kinetics, J. Mater. Sci. Mater. Med. 21 (2010) 2711–2722, https://doi.org/10.1007/s10856-010-4115-4.

[57] B.E.J. Denton, J. V Howarth, The osmotic mechanism of cuttlebone, J. Mar. Biol. Assoc. United Kingdom. 41 (1961) 351–363.

[58] K.M. Sherrard, Cuttlebone morphology limits habitat depth in eleven species of Sepia (Cephalopoda: Sepiidae), Biol. Bull. 198 (2000) 404–414, https://doi.org/10.2307/1542696.

[59] K. Farbod, M.R. Nejadnik, J.A. Jansen, S.C.G. Leeuwenburgh, Interactions between inorganic and organic phases in bone tissue as a source of inspiration for design of novel nanocomposites, Tissue Eng. Part B Rev. 20 (2014) 173–188, https://doi.org/10.1089/ten.teb.2013.0221.

[60] L.-C. Gerhardt, A.R. Boccaccini, Bioactive glass and glass-ceramic scaffolds for bone tissue engineering, Materials (Basel). 3 (2010) 3867–3910, https://doi.org/10.1016/B978-1-84569-768-6.50005-3.

[61] T. Kokubo, H. Takadama, How useful is SBF in predicting in vivo bone bioactivity? Biomaterials. 27 (2006) 2907–2915, https://doi.org/10.1016/j.biomaterials.2006. 01.017.

[62] M. Tanahashi, T. Matsuda, Surface functional group dependence on apatite formation on self- assembled monolayers in a simulated body fluid, J. Biomed. Mater. Res. 34 (1997) 305–315, https://doi.org/10.1002/(SICI)1097-4636(19970305)34:3<305::AID-JBM5>3.0.CO;2-O.

Chapter 3

Cuttlefish Bone-Derived Biphasic Calcium Phosphate Scaffolds Coated with Sol-Gel Derived Bioactive Glass

Cuttlefish Bone-Derived Biphasic Calcium Phosphate Scaffolds Coated with Sol-Gel Derived Bioactive Glass

Ana S. Neto, Daniela Brazete, José M.F. Ferreira

Department of Materials and Ceramic Engineering, CICECO, University of Aveiro, 3810-193 Aveiro, Portugal

Materials 12 (2019) 2711

doi: 10.3390/ma12172711

Abstract

The combination of calcium phosphates with bioactive glasses (BG) has received an increased interest in the field of bone tissue engineering. In the present work, biphasic calcium phosphates (BCP) obtained by hydrothermal transformation of cuttlefish bone (CB) were coated with a Sr-, Mg- and Zn-doped sol-gel derived BG. The scaffolds were characterized by X-ray diffraction, Fourier transform infrared spectroscopy and scanning electron microscopy. The initial CB structure was maintained after hydrothermal transformation (HT) and the scaffold functionalization did not jeopardize the internal structure. The results of the in-vitro bioactivity after immersing the BG coated scaffolds in simulated body fluid (SBF) for 15 days showed the formation of apatite on the surface of the scaffolds. Overall, the functionalized CB derived BCP scaffolds revealed promising properties, but further assessment of the in-vitro biological properties is needed before being considered for their use in bone tissue engineering applications.

Keywords: Cuttlefish bone; Biphasic calcium phosphate; Porous scaffolds; Sol-gel coatings; bioactivity; Tissue engineering

1. Introduction

Bone is one of the most transplanted tissues. Autologous bone grafts are still considered the gold standard procedure, but unfortunately, their availability is limited and they are intimately associated with donor site morbidity [1]. Thus, bone tissue engineering represents an important challenge to overcome the shortcomings of bone grafts, where porous scaffolds can be combined with cells and bioactive growth factors, providing a suitable environment for tissue development [2].

Bioceramic-based scaffolds have been successfully used for bone repair and replacement. Among the different bioceramics, calcium phosphate materials (CaP) like hydroxyapatite (HA) and β-tricalcium phosphate (β-TCP) are the most commonly used ones as they are chemically similar to the inorganic part of the bone. HA is stable under physiological conditions and has a slow resorption rate and β-TCP has a more soluble phase with a lower mechanical stability. The mixtures of HA and β-TCP phases create biphasic calcium phosphate (BCP) materials and enable the control of the bioactivity and the balance between resorption and the solubilisation rates [3]. Bioactive glasses (BGs) have been used as an alternative to CaP materials. They have the capacity to strongly bond to the living tissues, through the development of a bone-like HA layer on the surface [4,5]. Moreover, BGs release Si, P or Ca ions that act as chemical stimuli for the activation of osteoprogenitor cells and, consequently, enhance bone formation. The release of these ions is also known to stimulate neovascularisation and angiogenesis and, thereby, promote bone healing [6,7]. BGs were firstly synthesized by melt-quenching technique. Nevertheless, the sol-gel approach has been gaining more relevance in the last decades [8–10]. When compared to melt-quenching, the sol-gel derived BGs are prepared at significantly lower temperatures and they have a higher specific surface area, which, consequently, enhances their bioactive response [11]. Apart from this, the sol-gel derived BGs can be prepared with amounts of SiO_2 up to 90 wt.%, whilst SiO_2 contents higher than 60 wt. % are hardly achievable by melt-quenching [12]. The high number of Si–OH groups in sol-gel derived BG is beneficial for further functionalization [13]. Moreover, the composition of sol-gel derived BG can be more easily tailored to achieve the desired physicochemical and biological properties. In this regard, the incorporation of metal ions in the silicate network have been widely investigated [14–18]. The incorporation of strontium (Sr) into the BGs enhances bone formation as it promotes osteoblast differentiation and simultaneously inhibits osteoclast differentiation. In addition, *in-vivo*

studies demonstrated that the Sr–doped BGs strongly bond to the bone through the apatite layer [19,20]. The incorporation of magnesium (Mg) into BGs improves the dissolution behaviour as it promotes the disruption of the silica network [21]. Furthermore, Mg–doped BGs promote osteoblast proliferation and differentiation [22]. On the other hand, the introduction of zinc (Zn) into BGs favours osteoblast proliferation and differentiation [16]. Additionally, Zn demonstrated to exert anti-inflammatory effects [23].

The combination of CaP with bioactive glasses (BG) has received an increased interest in the bone tissue engineering field, since it develops a synergetic effect improving the properties of the bone graft materials [24,25]. It was demonstrated that the incorporation of BG into a CaP material enhances the mechanical strength through the densification of the material. In addition, the bioactivity of CaP is lower when compared to those of BGs. Thereby, a combination of these types of materials creates bone grafts with enhanced biological responses [26].

The success of a bone tissue engineering approach is highly dependent on the performance of the scaffolds. Marine skeletons, like coral and cuttlefish bone (CB), have been proposed as bone graft materials as they are mainly calcium carbonate and, thereby, can be hydrothermally converted into CaP materials [27]. The internal CB lamellae matrix has an ideal microstructure with pore sizes and interconnectivity that favors bone development [28,29]. This work aims at developing BG-coated BCP scaffolds, taking advantages of their intrinsic porous structure and enhanced bioactivity. BCP scaffolds obtained through the hydrothermal transformation (HT) of CB were coated with a Sr-, Mg- and Zn-doped sol-gel derived BG (60% SiO_2 – 34% CaO – 2% SrO – 2% MgO – 2% ZnO – 2% P_2O_5 (mol %)), and the bioactivities of the uncoated and BG-coated scaffolds were tested in-vitro in simulated body fluid. The selected BG composition attempts to obtain homogeneous and amorphous materials with a good balance between degradability and bioactivity, while exploring the various biological benefits derived from the incorporation of doping ions in the coating layer.

2. Materials and methods

2.1. Preparation of BCP scaffolds

The BCP scaffolds were obtained through hydrothermal transformation (HT) of the hard aragonite porous structure of cuttlefish (*Sepia officinalis*). Firstly, the exact amount

of $CaCO_3$ present in the CB sample was determined by differential thermal and gravimetric thermal analyses (DTA/TG, Labsys Setaram TG-DTA/DSC, Caluire, France, heating rate 10 ºC min^{-1}). According to the obtained result, the CB was cut into small pieces and it was added to the required volume of the phosphorous precursor solution, di-ammonium hydrogen phosphate [$(NH_4)_2HPO_4$, Panreac AppliChem, Barcelona, Spain]. Subsequently, the as-prepared mixtures were sealed in poly(tetrafluorethylene) lined stainless steel autoclave. The reaction took place at 200 ºC for 24 h in the oven. The as-obtained scaffolds were subjected to a heat treatment at 700 ºC for 1 h and using a heating rate of 0.5 ºC min^{-1} to burn the organic material followed by a sintering at 1200 ºC using a heating rate of 2 ºC min^{-1} and a dwelling time of 2 h.

2.2. Preparation of Sol-gel derived BG and Coating of the BCP Scaffolds

In this study, a sol-gel derived BG with the composition of 60% SiO_2 – 34% CaO – 2% SrO – 2% MgO – 2% ZnO – 2% P_2O_5 (mol %) was used. To prepare the BG, tetra-ethyl-ortho-silicate (TEOS, $C_8H_{20}O_4Si$, Sigma–Aldrich, Darmstadt, Germany) and triethyl phosphate (TEP, $C_6H_{15}O_4P$, Sigma–Aldrich, Darmstadt, Germany) were mixed in 10 mL of water. The pH was adjusted to values between 1 and 2, using nitric acid (HNO_3, Panreac AppliChem, Barcelona, Spain) and mixed for 1 h. Calcium nitrate tetrahydrate [$Ca(NO_3)_2 \cdot 4H_2O$, Panreac AppliChem, Barcelona, Spain] was used as the precursor of calcium. Furthermore, strontium nitrate, $Sr(NO_3)_2$, Magnesium nitrate hexahydrate, $Mg(NO_3)_2 \cdot 6\ H_2O$, and zinc nitrate hexahydrate, $Zn(NO_3)_2 \cdot 6\ H_2O$, all from Sigma-Aldrich, Germany, were used as the precursors of strontium, magnesium and zinc. These nitrate salts were dissolved in 10 mL of water and, subsequently, added to the first solution and kept under magnetic agitation for 1 h to obtain a homogenous solution. The as-obtained solution was used for coating the BCP scaffolds. For this purpose, the scaffolds were immersed in the BG solution and placed in the vacuum chamber under a pressure of 0.4 bar for 20 min. Subsequently, the impregnated scaffolds were placed in an oven at 100 ºC for 24 h. The scaffolds were sintered at 700 ºC for 2 h and with a heating rate of 0.3 ºC min^{-1}.

2.3. Sample Characterization

2.3.1. X-Ray Diffraction

X-ray diffraction (XRD) was used to identify the crystalline phases of the BCP scaffolds derived from CB as well as to confirm the glass state of the synthesized sol-gel derived BG. The data were collected in 2θ range between 10º and 100º with a 2θ–step size of 0.0260º per second in a high resolution X-ray diffractometer (PANalytical X'Pert PRO, Almelo, Netherlands) with Cu Kα radiation (λ = 1.5406 Å) produced at 40 mA and 45 kV. The relative percentages of the crystalline phases were estimated by using the HighScorePlus, a spectra-fitting software.

2.3.2. Fourier Transform Infrared Spectroscopy

The sol-gel derived BG, as well as the uncoated and coated scaffolds, were examined by the attenuated total reflection Fourier transform infrared spectroscopy (FTIR-ATR). The data were collected over the spectral range of 400 – 4000 cm^{-1} with a total of 256 scans and a spectral resolution of 4 cm^{-1} in a FTIR Bruker Tensor 27 equipped with a Golden Gate Single Reflection Diamond ATR.

2.3.3. Dilatometry

The sintered uncoated scaffolds and the dried BG were grinded and powdered. From the obtained powder, cylindrical rods were prepared with a diameter of 4.50 mm and a length of approximately 10 mm and were used for dilatometry measurements (Bahr Termo Analyse DIL 801 L, Hüllhorst, Germany; heating rate of 5 ºC min^{-1}). The thermal expansion coefficient was obtained according to Equation (1),

$$\boldsymbol{\alpha} = \frac{\mathbf{1}}{\boldsymbol{L_0}}\left(\frac{\boldsymbol{\Delta L}}{\boldsymbol{\Delta T}}\right) \quad (1)$$

Here, α is the thermal expansion coefficient, L_0 is the initial sample length, ΔL is the change in length and ΔT is the change in temperature.

2.3.4. Microstructure

Micro computed tomography (μ-CT, Bruker, Billerica, MA, USA) was used to observe the interconnectivity of the raw CB microstructure. It used an exposure time of 800 ms, energy of 50 kV and intensity of 200 μA. The NRecon software was used for the reconstruction of cross-section images. The microstructure of the samples was also

observed by scanning electron microscopy (SEM, Hitachi SU-70, Hitachi High-Technologies Europe, GmbH, Krefeld, Germany) using an acceleration voltage of 15 kV. The samples were coated with carbon. The energy dispersive spectroscopy (EDS) was used to examine the presence of the doping elements in the samples.

2.3.5. Mechanical Properties

The uncoated and coated cubic shape scaffolds with approximately 3 mm sides were subjected to a uniaxial compressive load by using a universal testing machine (AG-IS10kN, Shimadzu, Kyoto, Japan). The samples were subjected to a maximum load of 200 N with a constant crosshead speed of 0.5 mm min^{-1} in ambient conditions. The compressive load was applied perpendicularly to the lamella of BCP scaffolds derived from CB, using 5 samples in each testing condition.

2.4. *In-Vitro* Bioactivity Test

The uncoated and coated scaffolds were immersed in simulated body fluid (SBF) solution with an ionic concentration similar to those of human blood plasma to evaluate the in-vitro scaffold's bioactivity. For this purpose, for a period of 14 days, the samples were immersed in an orbital shaker at 37 ºC. The SBF solution was prepared according to the international standard ISO 23317 but using a unified standard area of 0.5 cm^2 mL^{-1} proposed elsewhere [30]. After the immersion period, the samples were removed from the SBF solution, rinsed with distilled water and then left to dry in a silica desiccator. Once dried, the morphology of the scaffolds was analysed by SEM to observe the bioactive layer deposited onto their surfaces.

2.5. Statistical Analysis

The experiments were performed in triplicated and the values have been expressed as the mean ± standard deviation (SD). The statistical analysis was performed using a Student's t-test. $P < 0.05$ was considered statistically significant.

3. Results

3.1. Chemical and Structural Characterization

Figure 1 displays the XRD patterns of the sol-gel derived BG, as well as the ones regarding the scaffolds before and after coating with BG by immersion in the solution, followed by heat treatment at 700 ºC for 2 h. The sol-gel derived BG exhibited essentially an amorphous character. On the other hand, the scaffolds before and after the impregnation with BG, followed by heat treatment at 700 ºC for 2 h, exhibited similar patterns, with HA (# 04-015-7245) and β-TCP (# 04-006-9376) being the identified crystalline phases. As estimated by HighScorePlus software, the relative percentages of the crystalline phases presented in the scaffolds were 63.9% HA and 36.1% β-TCP before the BG coating and 64.6% HA and 35.4% β-TCP after the BG coating.

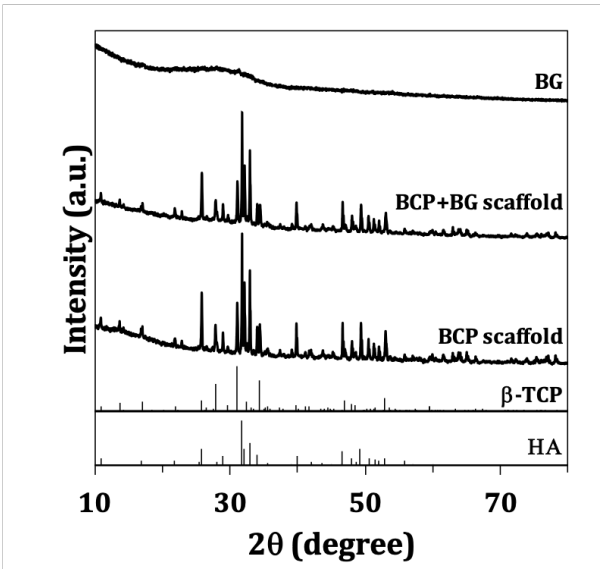

Figure 1. Sol-gel derived BG, BCP scaffolds and BG-coated scaffolds. The standard diffraction patterns of β-TCP and HA standards, ICDD PDF 04-006-9376 and 04-015-7245, respectively, are also present for comparison purposes.

The FTIR spectra of the sol-gel derived BG and the BCP scaffolds before and after the coating with BG are shown in Figure 2. The FTIR spectra of sol-gel derived BG exhibit a characteristic broad band for the asymmetric stretching for Si–O–Si from 900 cm^{-1} and 1300 cm^{-1} and centered at 1080 cm^{-1}. The peak at 800 cm^{-1} is also assigned to the stretching mode of Si–O–Si [31]. Moreover, the FTIR spectra of the uncoated and coated scaffolds are identical and exhibit the characteristic vibrational modes of $–PO_4$ and –OH groups. The band present at 470 cm^{-1} denotes the ν2 mode of O–P–O bending, while

the ν4 mode of O–P–O bending is present at 550 cm^{-1} and 600 cm^{-1}. The band at 960 cm^{-1} is associated with ν1 P–O stretching mode. The bands located at 1000 and 1088 cm^{-1} are due to the ν3 mode. The bands at 940 and 960 cm^{-1} denote the ν1 non-degenerate P–O symmetry stretching mode. The vibrational mode of –OH group appear at 630 cm^{-1} with low intensity and the stretching mode should appear at 3575 cm^{-1} [32].

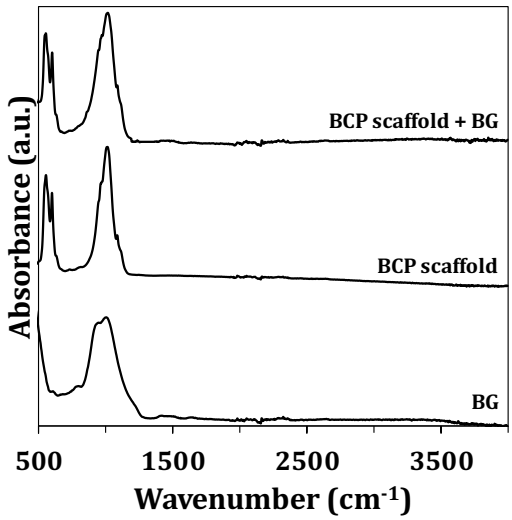

Figure 2. FTIR spectra of sol-gel derived BG, BCP scaffolds and BG-coated scaffolds.

3.2. Microstructure

The unique layered and interconnected porosity of CB was observed by μ-CT (Figure 3a). The porous architecture of scaffolds after HT and sintering processing steps, and also after BG coating and calcination, was analysed by SEM. From the images displayed in Figure 3b, one can observe that the internal structure of CB was preserved after HT and sintering.

Moreover, the sintering step promoted the development of grains. The BCP scaffolds were successfully coated with BG and as confirmed by EDS (Figure 3c), revealed the presence of the doping elements. The amounts of strontium, magnesium and zinc were 1.77, 2.07 and 1.11 mol%. The measured values for Sr, and Mg are comparable to the planned contents (2 mol%), while for Zn only ~55% of the planned amount has been effectively incorporated. Moreover, coating with the sol-gel derived BG did not obstruct the pores. The surface coating presents some cracks, which can be attributed to the high shrinkage extents that are typically observed for sol-gel derived BG during the dry and calcination steps. The coefficient of thermal expansion of the BG coating material was 2.27×10^{-6} $ºC^{-1}$, while that measured for the BCP scaffold derived from CB was 8.15 ×

10^{-6} $^{o}C^{-1}$ (i.e., about 3.6 times higher). However, the cracks observed in the sol-gel coatings are much less attributable to this difference in the coefficients of thermal expansion, but more to the extent of shrinkage undergone by the coating especially under the drying step.

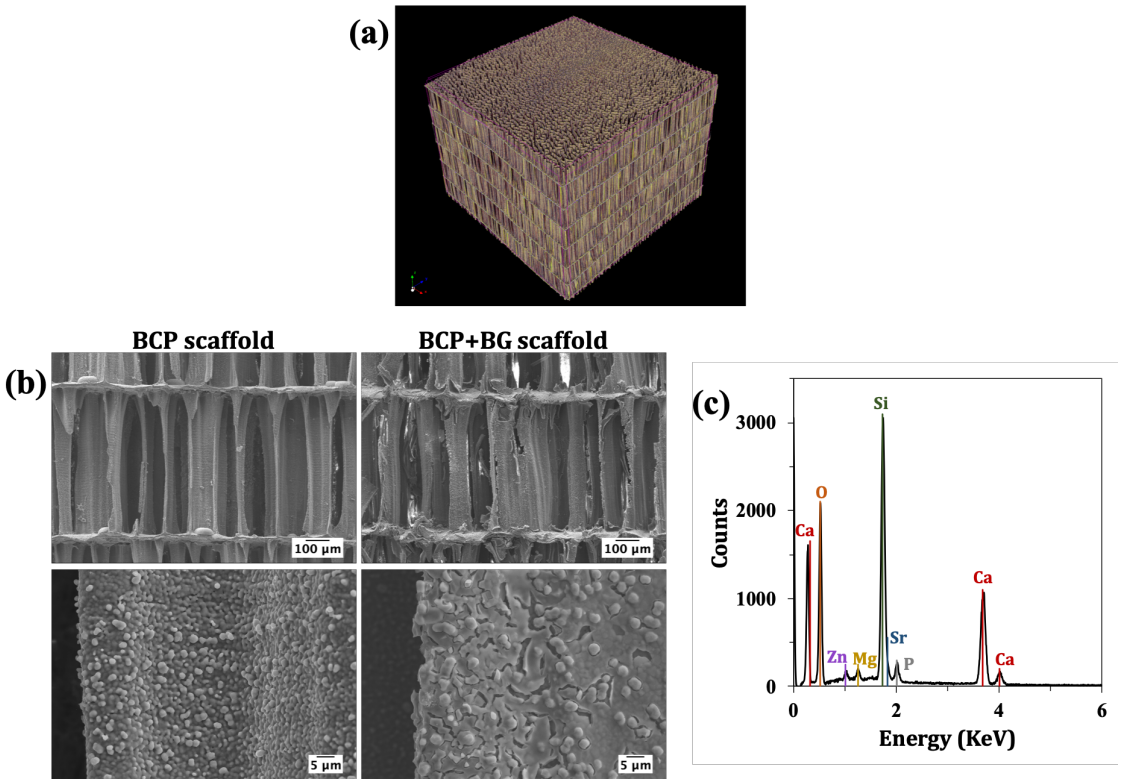

Figure 3. Microstructural and chemical features of the scaffolds: **(a)** µ-CT image showing the microstructure of raw CB highlighting its interconnected porosity; **(b)** SEM micrographs of uncoated and coated BCP scaffolds; **(c)** EDS analysis of the sol-gel derived BG coating.

3.3. Mechanical Properties

The characteristic stress-strain curves are displayed in Figure 4a. It can be seen that the uncoated scaffolds undergo a gradual collapse layer-by-layer, while in the coated ones, this behaviour is less well demarked. The average compressive strengths of the uncoated and coated scaffolds were calculated from the maxima compressive strength values measured during deformation. The results plotted in Figure 4b show that the average compressive strength of BCP scaffolds derived from CB was 0.26 ± 0.02 MPa, while a higher value of 0.36 ± 0.04 MPa was registered for BG-coated scaffolds. This means that the BG coating significantly improves the mechanical performance of the BCP scaffolds. Moreover, it was registered by the Young's moduli of 0.34 ± 0.04 and 0.53 ± 0.04 MPa for the uncoated and coated scaffolds, respectively.

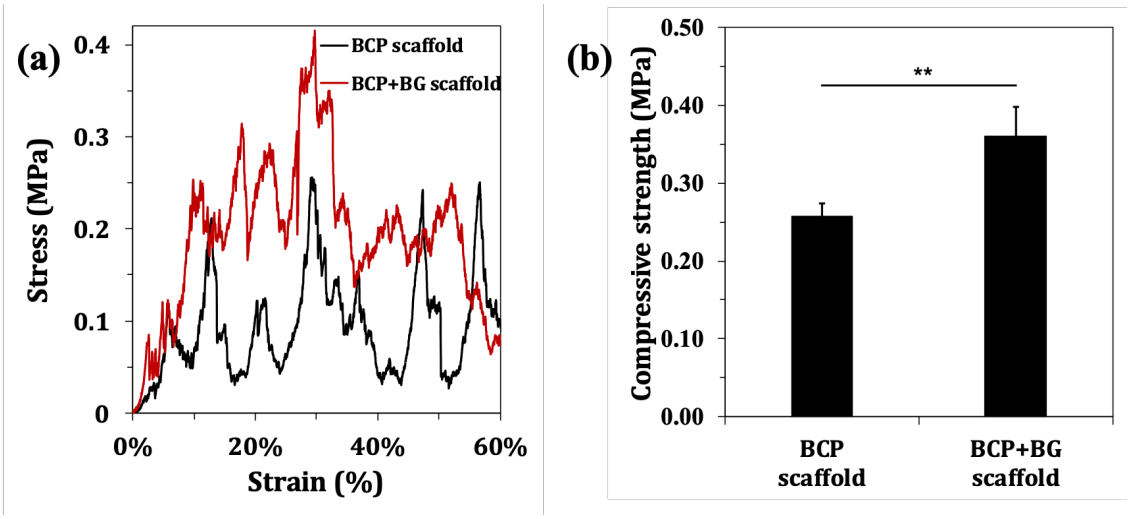

Figure 4. Compressive strength of uncoated and BG-coated BCP scaffolds: **(a)** representative stress-strain curve; **(b)** maximum compressive strength during the deformation period. The results are represented as mean ± SD (**P < 0.01).

3.4. *In vitro* Bioactivity Tests

The material capacity to bond the natural bone upon implantation is normally evaluated by immersion in SBF solution, which is recognized to be an interesting first approach to predicting the bioactivity of a material [30]. Figure 5 shows the SEM micrographs of the scaffolds after 14 days of immersion in SBF solution. After this immersion period, the roughness of the coated scaffolds significantly increased in comparison to the that of uncoated samples. The EDS analysis revealed that the precipitate mainly consists of Ca, P and O. Therefore, the BG coating also improves the *in-vitro* bioactivity of the scaffolds. These results can be explained considering that the calcium phosphate materials like hydroxyapatite are more chemically stable under pH conditions similar to those existing in the physiological fluid in comparison to BG [3]. This, combined with the ability to form a bone-like HA layer confer to bioactive glasses their capacity to strongly bond to the living tissues [4,5].

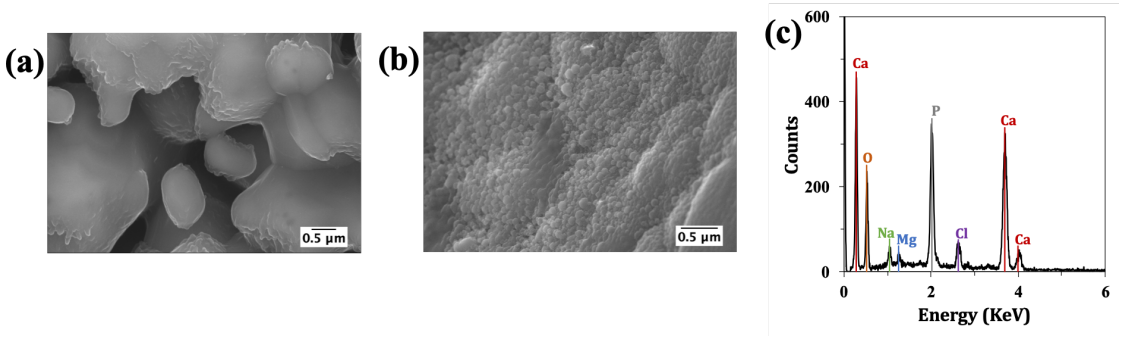

Figure 5. Microstructural and chemical features of the scaffolds after 14 days of immersion in simulated body fluid (SBF) solution: **(a)** SEM micrograph of uncoated BCP scaffolds; **(b)** SEM micrograph of BG-coated BCP; **(c)** EDS analysis of the precipitate.

4. Discussion

A Sr-, Mg- and Zn-doped sol-gel derived BG was prepared and used to coat BCP scaffolds derived from CB. The amorphous nature of the sol-gel derived BG was demonstrated by XRD (Figure 1) and also confirmed by the FTIR pattern (Figure 2), showing the characteristic Si–O bands. The absence of any calcium carbonate phase in the scaffolds after the HT transformation and the only presence of the XRD patterns characteristic of HA and β-TCP peaks, prove that the original aragonite was for the first time successfully and completely transformed into BCP scaffolds. The transformation of CB was previously studied by Sarin el al. [33], nevertheless a significant amount of CaO was present in the final product when the aim was to preserve the CB internal structure. However, the free CaO tends to react with body fluid to form $Ca(OH)_2$, therefore creating a cytotoxic alkaline environment after the implantation in vivo. Moreover, and in agreement with XRD, the FTIR spectrum of BCP scaffold demonstrated the presence of $–PO_4$ and –OH groups. Nonetheless, –OH groups are mainly nonexistent due to their absence in the β-TCP phase and the partial de-hydroxylation of HA upon sintering at 1200 °C. The XRD patterns of uncoated and coated scaffolds were identical, indicating that the surface coating remains amorphous and is fine enough to hide the BCP nature of the substrate. With respect to the FTIR spectra, the characteristic Si–O band located between 900 cm^{-1} and 1300 cm^{-1} appeared overlapped with $–PO_4$ bands, making it difficult to distinguish between the differences of the uncoated and coated scaffolds.

The µ-CT image of CB (Figure 3a) demonstrated the unique structural features of CB, which are known to be beneficial for bone development [28]. The unique

microstructure was preserved after the HT and sintering steps (Figure 3b). Moreover, it is important to highlight that after the BG coating, the interconnected porous structure was not compromised (Figure 3b). Through EDS analysis (Figure 3c), it was possible to observe that the doping elements Sr and Mg were present in the coating layer in amounts that were close to the planned ones. The incorporation extent of Zn was only ~55%. This lower efficiency of zinc for entering in the glass silicate network as the doping element may be related to its less marked network-modifying role in comparison to the alkaline earth elements. It was found recently that Zn^{2+} tends to adopt a mixed tetrahedral and octahedral coordination in the glassy network and copolymerizes with [SiO4] tetrahedra [34]. On average, a Zn^{2+} was coordinated with ~4.9 non-bridging oxygens (NBOs), a lower value in comparison to the alkaline earth elements (~5.9 NBOs for Ca^{2+}, and 5.1 NBOs for Mg^{2+}). The lower coordination number of Zn^{2+} suggests that it is probably closer to an intermediate role, reflecting its higher field strength with respect to alkaline earth ions.

Apart from this, the BG coating layer exhibited some cracks because of the sol-gel drying and sintering processes. Despite the observed difference between the thermal expansion coefficients of BCP scaffolds (8.15×10^{-6} ºC^{-1}) and BG coating (2.27×10^{-6} ºC^{-1}), the cracks observed in the SEM images of the coated scaffolds cannot be attributed to this difference. In fact, a coating with a lower coefficient of thermal expansion can undergo smaller dimensional changes upon cooling from the heat treatment temperature (700 °C) to room temperature in comparison to those experienced by the substrate. Therefore, these cracks are only due to the considerable shrinkage undergone by the sol-gel coating during the subsequent heat treatment schedules, especially upon the drying step.

Despite the fine thickness of the BG coating, the mechanical properties of the scaffolds improved in a significant way as seen in Figure 4. However, the compressive strength of the coated scaffolds (0.36 ± 0.04 MPa) are within the lower range of the compressive strength of trabecular bone that varies between 0.1 MPa and 16 MPa [35]. This result could be associated with the 92% porosity of the scaffolds. However, this does not seem to be a problem, as the scaffolds are thought of essentially as bone graft fillers. Therefore, they are not subjected to significant load bearing conditions, ven through the mechanical properties could be further improved by applying successive thinner sol-gel derived BG coatings.

The scaffolds exhibited a good in-vitro bioactivity, reflected by the increases in surface roughness after the immersion period of 14 days in the SBF, as can be observed in Figure 5. The less remarkable surface changes that occurred for the uncoated scaffolds can be attributed to their higher chemical stability under pH values, similar to that of physiological fluid [3]. Conversely, bioactive glasses have the ability to release other ionic species that may contribute to oversaturate the SBF solution, inducing the surface dissolution-precipitation reactions [4,5]. Besides these advantages, the various ionic species released from the BG-coating may activate the osteoprogenitor cells and stimulate the biological processes (neovascularisation and angiogenesis) necessary for promoting bone healing [6,7].

More extensive and remarkable surface changes are likely to occur during longer times of immersion in the SBF. The scaffolds are promising for being further in-vitro investigated in cell cultures. These investigations are still underway and will be reported in the near future.

Overall, the surface functionalization of the BCP scaffolds with a sol-gel derived BG enabled the materials to be obtained with higher bioactivity and compressive strength, and with the ability to release ionic species (Sr^{2+}, Mg^{2+} and Zn^{2+}) that are known to be beneficial for bone development.

5. Conclusions

In the present study, porous BCP scaffolds derived from aragonite CB and with the complete absence of any calcium carbonate phase were, for the first time, successfully prepared by HT transformation. This is a novel and very important achievement, since any untransformed calcium carbonate is likely to decompose during the subsequent sintering step, leading to the formation of free CaO. The free CaO, in turn, tends to react with body fluid to form $Ca(OH)_2$, therefore creating a cytotoxic alkaline environment after the implantation in vivo. The BCP scaffolds consisting of 63.9% HA and 36.1% β-TCP BCP were coated with a Sr-, Mg- and Zn-doped sol-gel derived BG, which enhanced their bioactivity in the SBF and compressive strength, enabling the accomplishment of the aimed targets. The BG coating was completely amorphous and the incorporation levels of doping alkaline earth ions (Sr^{2+}, Mg^{2+}) did not differ much from the planned ones, while the incorporation level of Zn^{2+} was noticeably lower (only ~55% relative to the planned one). The unique porous microstructure of raw CB was neither damaged

during the HT and sintering steps, nor compromised after the BG coating. The micro-cracked appearance of the sol-gel derived BG coating is solely due to the shrinkages undergone during the drying and sintering processes.

In summary, the porous BCP scaffolds surface functionalized with the sol-gel derived BG coating seem very promising for being further investigated as bone graft materials and constructs for bone tissue engineering.

Author Contributions: All the authors have contributed to this research article. J.M.F.F. conceived and designed the main structure of the article and, together with D.B. did the specific literature survey and analysis about sol-gel derived bioactive glasses. D.B. also did the first exploratory experiments on the sol-gel synthesis and characterization of bioactive glasses. A.S.N. is a PhD student doing research on synthetic bone graft substitutes based on calcium phosphates and on the use of CB for biomedical applications. Her PhD work programme, conceived and designed by J.M.F.F., aims at developing porous scaffolds by the hydrothermal transformation of CB into biphasic calcium phosphates while preserving its unique porous structure. A.S.N. was in charge of performing most of the literature survey and analysis, and of elaborating the first draft of the parts more closely related to her PhD work programme, as well of integrating the spare contributes received from the other authors into a single document. The supervisor conducted the final check of and provided refinements to the entire document.

Acknowledgments: This work was developed within the scope of the project CICECO-Aveiro Institute of Materials, FCT Ref. UID/CTM/50011/2019, financed by national funds through the FCT/MCTES." Ana S. Neto acknowledges to AdvaMTech, the PhD Program on Advanced Materials and Processing for the PhD grant, PD/BD/114132/2015, founded by the Portuguese Foundation for Science and Technology (FCT). The authors are very thankful to Dias de Sousa - Instrumentação Analítica e Científica, S.A., Setúbal, Portugal, for doing the μ-CT analysis raw CB.

References

1. Sen, M.K.; Miclau, T. Autologous iliac crest bone graft: should it still be the gold standard for treating nonunions? *Injury* **2007**, *38*, S75–S80, doi:10.1016/j.injury.2007.02.012.
2. O'Brien, F.J. Biomaterials & scaffolds for tissue engineering. *Mater. Today* **2011**, *14*, 88–95, doi:10.1016/S1369-7021(11)70058-X.
3. Bouler, J.M.; Pilet, P.; Gauthier, O.; Verron, E. Biphasic calcium phosphate ceramics for bone reconstruction: A review of biological response. *Acta Biomater.* **2017**, *53*, 1–12, doi:10.1016/j.actbio.2017.01.076.

4. Cao, W.; Hench, L.L. Bioactive Materials. *Ceram. Int.* **1996**, *22*, 493–507, doi:10.1016/0272-8842(95)00126-3.

5. Hench, L.L.; Splinter, R.J.; Allen, W.C.; Greenlee, T.K. Bonding mechanisms at the interface of ceramic prosthetic materials. *J. Biomed. Mater. Res.* **1971**, *5*, 117–141, doi:10.1002/jbm.820050611.

6. Jones, J.R. Reprint of: Review of bioactive glass: From Hench to hybrids. *Acta Biomater.* **2015**, *23*, S53–S82, doi:10.1016/j.actbio.2015.07.019.

7. Hoppe, A.; Güldal, N.S.; Boccaccini, A.R. A review of the biological response to ionic dissolution products from bioactive glasses and glass-ceramics. *Biomaterials* **2011**, *32*, 2757–2774, doi:10.1016/j.biomaterials.2011.01.004.

8. Fiume, E.; Barberi, J.; Verné, E.; Baino, F. Bioactive glasses: From parent 45S5 Composition to Scaffold-Assisted Tissue-Healing Therapies. *J. Funct. Biomater.* **2018**, *9*, 24, doi:10.3390/jfb9010024.

9. Baino, F.; Fiume, E.; Miola, M.; Verné, E. Bioactive sol-gel glasses: Processing, properties, and applications. *Int. J. Appl. Ceram. Technol.* **2018**, *15*, 841–860, doi:10.1111/ijac.12873.

10. Kaur, G.; Pickrell, G.; Sriranganathan, N.; Kumar, V.; Homa, D. Review and the state of the art: Sol-gel and melt quenched bioactive glasses for tissue engineering. *J. Biomed. Mater. Res. Part B Appl. Biomater.* **2016**, *104B*, 1248–1275, doi:10.1002/jbm.b.33443.

11. Zhong, J.; Greenspan, D.C. Processing and properties of sol-gel bioactive glasses. *J. Biomed. Mater. Res.* **2000**, *53*, 694–701, doi:10.1002/1097-4636(2000)53:6<694::AID-JBM12>3.0.CO;2-6.

12. Li, R.; Clark, A.E.; Hench, L.L. An Investigation of Bioactive Glass Powders by Sol-Gel Processing. *J. Appl. Biomater.* **1991**, *2*, 231–239, doi:10.16953/deusbed.74839.

13. Treccani, L.; Yvonne Klein, T.; Meder, F.; Pardun, K.; Rezwan, K. Functionalized ceramics for biomedical, biotechnological and environmental applications. *Acta Biomater.* **2013**, *9*, 7115–7150, doi:10.1016/j.actbio.2013.03.036.

14. Lázaro, G.S.; Santos, S.C.; Resende, C.X.; Dos Santos, E.A. Individual and combined effects of the elements Zn, Mg and Sr on the surface reactivity of a

SiO2·CaO·Na2O·P2O5bioglass system. *J. Non. Cryst. Solids* **2014**, *386*, 19–28, doi:10.1016/j.jnoncrysol.2013.11.038.

15. Wang, X.; Li, X.; Ito, A.; Sogo, Y. Synthesis and characterization of hierarchically macroporous and mesoporous CaO-MO-SiO 2-P 2O 5 (M = Mg, Zn, Sr) bioactive glass scaffolds. *Acta Biomater.* **2011**, *7*, 3638–3644, doi:10.1016/j.actbio.2011.06.029.

16. Saino, E.; Grandi, S.; Quartarone, E.; Maliardi, V.; Galli, D.; Bloise, N.; Fassina, L.; De Angelis, M.G.C.; Mustarelli, P.; Imbriani, M.; Visai, L. In vitro calcified matrix deposition by human osteoblasts onto a zinc-containing bioactive glass. *Eur. Cells Mater.* **2011**, *21*, 59–72, doi:10.22203/eCM.v021a05.

17. Imani Fooladi, A.A.; Hosseini, H.M.; Hafezi, F.; Hosseinnejad, F.; Nourani, M.R. Sol-gel-derived bioactive glass containing SiO 2 -MgO-CaO-P 2 O 5 as an antibacterial scaffold. *J. Biomed. Mater. Res. Part A* **2013**, *101A*, 1582–1587, doi:10.1002/jbm.a.34464.

18. Omar, S.; Repp, F.; Desimone, P.M.; Weinkamer, R.; Wagermaier, W.; Ceré, S.; Ballarre, J. Sol-gel hybrid coatings with strontium-doped 45S5 glass particles for enhancing the performance of stainless steel implants: Electrochemical, bioactive and in vivo response. *J. Non. Cryst. Solids* **2015**, *425*, 1–10, doi:10.1016/j.jnoncrysol.2015.05.024.

19. Lao, J.; Jallot, E.; Nedelec, J.-M. Strontium-Delivering Glasses with Enhanced Bioactivity: A New Biomaterial for Antiosteoporotic Applications? *Chem. Mater.* **2008**, *20*, 4969–4973.

20. Gentleman, E.; Fredholm, Y.C.; Jell, G.; Lotfibakhshaiesh, N.; O'Donnell, M.D.; Hill, R.G.; Stevens, M.M. The effects of strontium-substituted bioactive glasses on osteoblasts and osteoclasts in vitro. *Biomaterials* **2010**, *31*, 3949–3956, doi:10.1016/j.biomaterials.2010.01.121.

21. Dietrich, E.; Oudadesse, H.; Lucas-Girot, A.; Mami, M. In vitro bioactivity of melt-derived glass 46S6 doped with magnesium. *J. Biomed. Mater. Res. - Part A* **2009**, *88*, 1087–1096, doi:10.1002/jbm.a.31901.

22. Varanasi, V.G.; Saiz, E.; Loomer, P.M.; Ancheta, B.; Uritani, N.; Ho, S.P.; Tomsia, A.P.; Marshall, S.J.; Marshall, G.W. Enhanced osteocalcin expression by osteoblast-

like cells (MC3T3-E1) exposed to bioactive coating glass (SiO2–CaO–P2O5–MgO–K2O–Na2O system) ions. *Acta Biomater.* **2009**, *5*, 3536–3547, doi:10.1016/j.actbio.2009.05.035.

23. Varmette, E.A.; Nowalk, J.R.; Flick, L.M.; Hall, M.M. Abrogation of the inflammatory response in LPS-stimulated RAW 264.7 murine macrophages by Zn- and Cu-doped bioactive sol-gel glasses. *J. Biomed. Mater. Res. - Part A* **2009**, *90*, 317–325, doi:10.1002/jbm.a.32098.

24. Karadjian, M.; Essers, C.; Tsitlakidis, S.; Reible, B.; Moghaddam, A.; Boccaccini, A.; Westhauser, F. Biological Properties of Calcium Phosphate Bioactive Glass Composite Bone Substitutes: Current Experimental Evidence. *Int. J. Mol. Sci.* **2019**, *20*, 305.

25. Bellucci, D.; Sola, A.; Cannillo, V. Hydroxyapatite and tricalcium phosphate composites with bioactive glass as second phase: State of the art and current applications. *J. Biomed. Mater. Res. - Part A* **2016**, *104A*, 1030–1056, doi:10.1002/jbm.a.35619.

26. Bellucci, D.; Sola, A.; Gazzarri, M.; Chiellini, F.; Cannillo, V. A new hydroxyapatite-based biocomposite for bone replacement. *Mater. Sci. Eng. C* **2012**, *33*, 1091–1101, doi:10.1016/j.msec.2012.11.038.

27. Neto, A.S.; Ferreira, J.M.F. Synthetic and marine-derived porous scaffolds for bone tissue engineering. *Mater. (Basel).* **2018**, *11*, doi:10.3390/ma11091702.

28. Rocha, J.H.G.; Lemos, A.F.; Agathopoulos, S.; Valério, P.; Kannan, S.; Oktar, F.N.; Ferreira, J.M.F. Scaffolds for bone restoration from cuttlefish. *Bone* **2005**, *37*, 850–857, doi:10.1016/j.bone.2005.06.018.

29. Li, X.; Zhao, Y.; Bing, Y.; Li, Y.; Gan, N.; Guo, Z.; Peng, Z. Biotemplated Syntheses of Macroporous Materials for Bone Tissue Engineering Scaffolds and Experiments in Vitro and Vivo Biotemplated Syntheses of Macroporous Materials for Bone Tissue Engineering Sca ff olds and Experiments in Vitro and Vivo. *Acs Appl. Mater. Interfaces* **2013**, *5*, 5557–5562, doi:10.1021/am400779e.

30. Popa, A.C.; Stan, G.E.; Husanu, M.A.; Mercioniu, I.; Santos, L.F.; Fernandes, H.R.; Ferreira, J.M.F. Bioglass implant-coating interactions in synthetic physiological

fluids with varying degrees of biomimicry. *Int. J. Nanomed.* **2017**, *12*, 683–707, doi:10.2147/IJN.S123236.

31. Serra, J.; González, P.; Liste, S.; Serra, C.; Chiussi, S.; León, B.; Pérez-Amor, M.; Ylanen, H.O.; Hupa, M. FTIR and XPS studies of bioactive silica based glasses. *J. Non. Cryst. Solids* **2003**, *332*, 20–27, doi:10.1016/j.jnoncrysol.2003.09.013.

32. Raynaud, S.; Champion, E.; Bernache-Assollant, D.; Thomas, P. Calcium phosphate apatites with variable Ca/P atomic ratio I. Synthesis, characterisation and thermal stability of powders. *Biomaterials* **2002**, *23*, 1065–1072, doi:10.1016/S0142-9612(01)00218-6.

33. Sarin, P.; Lee, S.J.; Apostolov, Z.D.; Kriven, W.M. Porous biphasic calcium phosphate scaffolds from cuttlefish bone. *J. Am. Ceram. Soc.* **2011**, *94*, 2362–2370, doi:10.1111/j.1551-2916.2011.04404.x.

34. Goel, A.; Kapoor, S.; Tilocca, A.; Rajagopal, R.R.; Ferreira, J.M.F. Structural role of zinc in biodegradation of alkali-free bioactive glasses. *J. Mater. Chem. B* **2013**, *1*, 3073–3082, doi:10.1039/c3tb20163e.

35. Gerhardt, L.-C.; Boccaccini, A.R. Bioactive glass and glass-ceramic scaffolds for bone tissue engineering. *Mater. (Basel).* **2010**, *3*, 3867–3910, doi:10.1016/B978-1-84569-768-6.50005-3.

Chapter 4

Biphasic calcium phosphate scaffolds derived from cuttlefish bone coated with different polymers or with a bioactive glass: an *in vitro* cell culture study

Biphasic calcium phosphate scaffolds derived from cuttlefish bone coated with different polymers or with a bioactive glass: an *in vitro* cell culture study

Ana S. Neto[a], Ana C. Fonseca[b], Ana S. Rodrigues[c], Inês Barros[c], Catarina Miranda[c], João Ramalho[c], Luís Almeida[c], Jorge F. J. Coelho[b], José M.F. Ferreira[a]

[a] Department of Materials and Ceramic Engineering / CICECO – Aveiro Institute of Materials, University of Aveiro, 3810-193 Aveiro, Portugal

[b] CEMMPRE, Department of Chemical Engineering, University of Coimbra, Rua Sílvio Lima-Pólo II, 3030-790 Coimbra, Portugal

[c] Center for Neuroscience and Cell Biology (CNC), University of Coimbra, Faculdade de Medicina, Rua Larga, Pólo I, 1andar, 3004-504 Coimbra, Portugal

Abstract

This study reports the use of biphasic calcium phosphate (BCP) scaffolds derived from cuttlefish bone (CB) for bone tissue engineering applications. The *in vitro* cell culture studies were performed with human mesenchymal stem cells under static conditions. The undoped and ion (Sr^{2+}, Mg^{2+} and/or Zn^{2+}) doped BCP scaffolds maintain their viability for 72 h, as observed by live/dead staining. The MTT results demonstrated that the presence of Sr^{2+}, Mg^{2+} and Zn^{2+} (BCP-6Sr2Mg2Zn) is beneficial for cell proliferation. Being the most promising composition, BCP-6Sr2Mg2Zn samples were coated with poly(ε-caprolactone) (PCL), poly(ester amide) (PEA) or poly(ester urea) (PEU). The preliminary MTT results showed a greater cell viability and proliferation for the PEU coated samples. In alterative to the partial replacement of calcium, the doping elements (Sr^{2+}, Mg^{2+} and Zn^{2+}) were introduced through a sol-gel derived bioactive glass (BG) coating on undoped BCP scaffolds. Nevertheless, the preliminary MTT results indicated some pH-induced toxicity of BG coated samples due to ion leaching.

Keywords: Cuttlefish bone, Biphasic calcium phosphate, Polymeric coatings, *in vitro* cell culture, biocompatibility

1. Introduction

An ideal scaffold for bone tissue engineering should be biocompatible and be able to support cell adhesion and proliferation without any negative effect for the host tissue. It should be biodegradable preferentially at a rate similar to that of bone formation and the originated by-products should be non-toxic. Moreover, the scaffolds should have an interconnected porous structure, enabling the diffusion of nutrients and oxygen and the removal of waste products. The mechanical properties should be similar to the host bone and resistant enough for the surgical handling [1]. Upon having a scaffold with properties suitable for a bone substitute, one important step is to conduct *in vitro* biocompatibility assessment. This study uses cell cultures or constituents and occurs outside of the living organisms. It enables the study of cell viability, morphology and differentiation. Moreover, the *in vitro* studies allow a good reproducibility, can be accomplished within shorter time periods, and involve less legal and ethical conflicts when compared with *in vivo* studies [2]. To develop *in vitro* studies, cell lineages or primary cultures isolated from human or animal tissue can be used. These cells display different features according to their source and, therefore, their choice relies on the goal of the study [3,4]. In addition, these studies can be done under static or dynamic conditions.

Cuttlefish bone (CB) with pore sizes varying between 200 and 600 μm and an interconnectivity of approximately 93 %. This structure is mainly composed of aragonite and by a hydrothermal transformation (HT) can be converted into calcium phosphate (CaP) scaffolds [5]. Due to its properties, CB has been studied as a promising bone graft material, including the *in vitro* biocompatibility assessments [6–11]. Both cell lineages [7–9,11] and primary cultures [6,10] were used in these studies. Regarding the cell lineages, they were obtained either from human osteosarcoma (Human MG-63) [7–9] or from mouse preosteoblastic cells (MC3T3-E1) [11]. Likewise, in the primary cultures, the cells were obtained from different sources. Kim et al. [10] isolated human mesenchymal stem cells (hMSCs) from alveolar bone marrow and Hongmin et al. [6] obtained MSCs from bone marrow of adult New Zealand White rabbits. Despite having been used different cell types for the *in vitro* biocompatibility assessments, all studies evaluated cell viability, adhesion, proliferation and differentiation. Hongmin et al. [6] compared the cell behaviour on CB and hydroxyapatite (HA) derived from CB scaffolds. It was possible to infer that in both scaffolds the cells exhibited a good adhesion and proliferation. Nevertheless, differentiation was significantly higher on HA scaffolds

derived from CB. When compared with pure HA granules, the ones obtained from CB demonstrated to have a higher capacity for cell adhesion, proliferation and differentiation [9]. Kim et al. [10] prepared a Si-substituted CB-derived HA scaffold and observed that the introduction of Si was beneficial for cell behaviour. Indeed, in the presence of the doping element there was an improvement of cell adhesion and proliferation. Moreover, the alkaline phosphatase (ALP) activity as well as expression of different osteoblast marker genes (runt-related transcription factor 2, collagen type I, osteocalcin and 18S) was significantly higher on Si-doped samples. In another approach, different authors studied the incorporation of poly(ε-caprolactone) (PCL) into HA scaffolds derived from CB to improve the mechanical properties. The presence of PCL revealed to be non-toxic and importantly improved cell adhesion, proliferation and differentiation [7,8,11].

The main aim of this work is to study the *in vitro* cell viability and proliferation of human mesenchymal stem cells (hMSCs) in contact with biphasic calcium phosphate (BCP) scaffolds derived from cuttlefish bone (CB) and doped with strontium (BCP-6Sr), strontium and magnesium (BCP-6Sr2Mg), strontium and zinc (BCP-6Sr2Zn) or strontium, magnesium and zinc (BCP-6Sr2Mg2Zn). The most promising composition was coated with PCL, poly(ester amide) (PEA) or poly(ester urea) (PEU) and the *in vitro* cell culture behaviour was compared with the undoped composition also coated with the different polymers. The efficacy of the coating of undoped biphasic calcium phosphate (BCP) scaffolds with a sol-gel derived bioactive glass (BG) was also investigated as an alternative route for the incorporation the doping elements.

2. Materials and methods

2.1 Preparation of BCP scaffolds derived from CB

CBs were carefully cut into small pieces with quadratic shape (~ 10 mm × 10 mm × 2 mm) and subsequently submitted to hydrothermal transformation (HT) into BCP scaffolds. Undoped (BCP) and doped compositions containing strontium (BCP-6Sr), strontium and magnesium (BCP-6Sr2Mg), strontium and zinc (BCP-6Sr2Zn) or strontium, magnesium and zinc (BCP-6Sr2Mg2Zn) were prepared. Di-ammonium hydrogen phosphate [$(NH_4)_2HPO_4$, Panreac AppliChem, Spain] was used as a starting chemical precursor for phosphorous. Strontium nitrate, $Sr(NO_3)_2$, magnesium nitrate hexahydrate, $Mg(NO_3)_2\ 6H_2O$ and zinc nitrate hexahydrate, $Zn(NO_3)_2\ 6H_2O$, from Sigma-Aldrich, Germany, were used as the starting precursors for strontium, magnesium and zinc. The different compositions were prepared based on the method previously

described [12]. Briefly, a solution containing the respective precursors was prepared and placed into a poly(tetrafluorethylene) (PTFE) stainless steel autoclave together with CB pieces, followed by a HT at 200 ºC for 24 h. Subsequently, the samples were washed and dried. The heat treatment occurred at 700 ºC using a heating rate of 0.5 ºC min^{-1} for 1 h, followed by sintering at 1200 ºC for 2 h at a heating rate of 2 ºC min^{-1}.

2.2 Coating the BCP scaffolds with a sol-gel derived bioactive glass

A sol-gel derived bioactive glass (BG) containing 60% SiO_2 – 34% CaO – 2% SrO – 2% MgO – 2% ZnO – 2% P_2O_5 (mol. %) was first prepared. Briefly, the precursors of glass network-formers, tetra-ethyl-ortho-silicate (TEOS, $C_8H_{20}O_4Si$, Sigma-Aldrich, Germany) and triethyl phosphate (TEP, $C_6H_{15}O_4P$, Sigma-Aldrich, Germany) were sequentially added to distilled water, acidified with nitric acid (HNO_3, Sigma-Aldrich, Germany). In parallel, another aqueous solution containing the precursors of glass network-modifiers Ca, Sr, Mg and Zn was also prepared using calcium nitrate tetrahydrate [$Ca(NO_3)_2$ $4H_2O$, Panreac AppliChem, Spain], strontium nitrate, $Sr(NO_3)_2$, magnesium nitrate hexahydrate, $Mg(NO_3)_2$ $6H_2O$, and zinc nitrate hexahydrate, $Zn(NO_3)_2$ $6H_2O$, purchased from Sigma-Aldrich, Germany. After becoming transparent, these solutions were kept under stirring for further 1 h. Then, the solution of the glass network-modifiers was gradually added to the solution of glass network-formers and homogenised under magnetic stirring for 1 h to obtain the homogeneous BG sol. The coating process of the BCP scaffolds with BG was carried out by immersing them in the as-obtained BG, using a vacuum-assisted impregnation method previously described [13]. The excess of sol within the pores was immediately removed by capillarity using absorbent paper. Afterwards, the samples were dried at 100 ºC for 24 h and sintered at 700 ºC using a heating rate of 0.3 ºC min^{-1} for 2 h.

2.3 Coating the BCP scaffolds with different polymers

The scaffolds were coated with a well-known commercial polymer, poly(ε-caprolactone) (PCL, CAPA™6800 Mn = 80.000 g mol^{-1}) from Perstorp Specialty Chemicals AB, Sweden. For comparison, the scaffolds were also coated with two polymers synthesized in the laboratory, PEA (Mn = 26 900 g mol^{-1}) and PEU (Mn = 63 000 g mol^{-1}). The polymers were dissolved in dichloromethane (Sigma-Aldrich, Germany) at a concentration of 5% (w/v). To improve the dissolution of PEU, the addition of 0.9% (v/v) dimethyl sulfoxide as co-solvent was required. The impregnation of the

scaffolds with the polymer solutions occurred under the same vacuum conditions used for applying the BG coatings. After removing the excess solutions by capillarity, the samples were dried in a vacuum oven to ensure total vaporization of the solvent.

2.4 Isolation and culture of human mesenchymal stem cells from umbilical cord matrix

Human umbilical cords from healthy donors after birth, with the consent of the parent(s), were kindly donated by Crioestaminal Saúde e Tecnologia, Biocant Park, Portugal. The umbilical cords were stored between 12 and 48 h before tissue processing in sterile 50 mL tubes at room temperature. The samples were cut into small pieces of approximately 5 cm. The obtained pieces were washed with sterile phosphate buffered solution (PBS) to remove the blood. The umbilical veins were also washed to eliminate blood and blood clots. Moreover, to avoid contamination from endothelial cells, the umbilical veins and arteries were removed. Afterwards, the samples were dried in tissue culture plates to promote adhesion of the fragment to the polystyrene surface, and once adhered hMSC proliferation medium [Alpha-MEM without ribonucleosides and deoxyribonucleosides (Gibco, cat. no. 22561) supplemented with 10% fetal bovine serum (FBS, HyClone™), 1% Penincillin/Streptomycin and 1% Amphotericin B (Gibco)] was added to the cell culture plate. The samples were cultured for 10 days at 37 ºC with 5% CO_2 and 95% humidity, until the migration of hMSCs from the umbilical cord matrix and the formation of defined colonies. Lastly the fragments from umbilical cord matrix were removed and the cells were passage.

2.5 *In vitro* biocompatibility assessments

The scaffolds were sterilized with UV light and pre-wetted in medium for 2 h prior their use in cell experiments. After sterilization the scaffolds were transferred to the culture plate and cells were seeded in a drop wise manner at a cell density of 1.5×10^5 cells/well. To promote cell adhesion, the samples were incubated for 30 min prior the addition of culture medium.

2.5.1 Cell viability and proliferation

The cells seeded in scaffolds were cultured for 24, 48 and 72 h. At the end of each period the cell viability was measured using Live/Dead® viability/cytotoxicity kit (ThermoFisher). The staining was done according to the manufacturer's protocol.

Subsequently, the stained samples were observed by an inverted fluorescence microscopy.

Cell proliferation was determined using MTT assay. After each time point, MTT reagent (Sigma-Aldrich, Germany), 3-[4,5-dimethylthiazole-2-yl]-2,5-diphenyltetrazolium bromide, was added to each well. After 1 h incubation, the formazan crystals were dissolved using an acidified isopropanol solution (0.04 N HCl in isopropanol) and subsequently the absorbance was measured at 570 nm.

2.5.2 Statistical analysis

In this work, the experiments were performed in triplicate using two replicas in each experiment. The results are expressed as mean ± standard deviation (SD) and one-way-analysis of variance (ANOVA) was used for the statistical study. The results were considered statistically different when the p value is lower than 0.05.

3. Results

3.1 Cell viability

The Live/Dead assay was used to study the cell viability on the undoped and doped BCP scaffolds. The nuclei of viable and dead cells were stained in blue and red, respectively. Figure 1a shows that the cells maintained their viability over three days of culture. Figure 1b demonstrates that after 24 h of culture, the cell density was higher in the BCP-6Sr2Mg2Zn samples. Moreover, for all the investigated scaffold compositions, there was an increase of cell density after 72 h of culture.

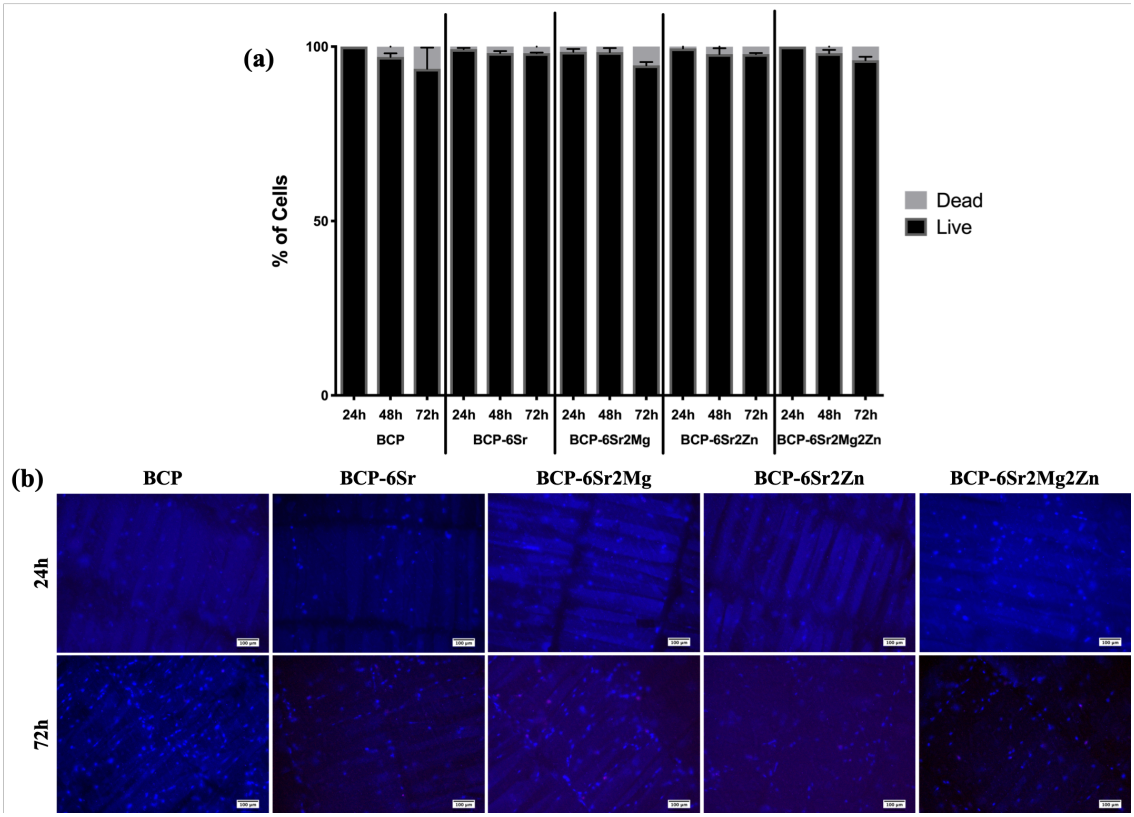

Figure 1. Live/Dead results (a) quantification of viable and dead cells. Data represents mean ± SD, n=3 (b) fluorescence images after 24 and 72 h of cell culture. The nuclei of healthy cells were stained with Hoechst 33342 (blue) and dead cells stained with propidium iodide (red).

3.2 Cell proliferation

3.2.1 Undoped and doped samples

Cell viability and proliferation were analysed by MTT assay and the obtained results for the undoped and doped scaffolds are shown in Figure 2. During the first 24 h, the growth rate was not significantly different among the different compositions tested. Regarding the BCP-6Sr2Mg2Zn samples, there was a significant improvement of cell metabolic activity over time. After 72 h, the cell proliferation in contact with BCP-6Sr2Mg2Zn samples was significantly higher than observed in the case of undoped BCP samples.

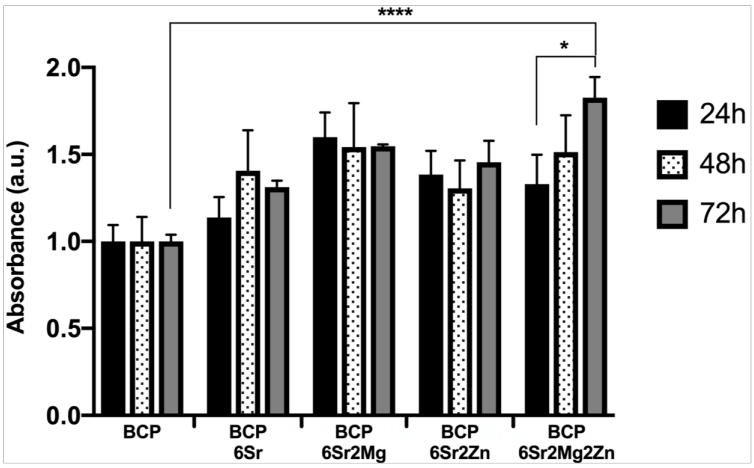

Figure 2. MTT results from undoped and doped scaffolds. Data represents mean ± SD, n=3. * $p < 0.05$ and **** $p < 0.0001$.

3.2.1 Coated samples

Based on the previous results, BCP-6Sr2Mg2Zn samples were coated with different polymers (PCL, PEA and PEU) and with a sol-gel derived BG. The aim was to investigate the influence of the coatings on cell behaviour. The results are presented in Figure 3. In general, there was a decrease of cell viability after 72 h, with the exception of PEA samples. The PCL and PEU coatings did not impair cell behaviour. Cell viability was indeed improved after PEU coating. On the other hand, BG coating compromised the cell viability and after 72 h, being observed an extensive cell death, probably due to excessive ionic leaching.

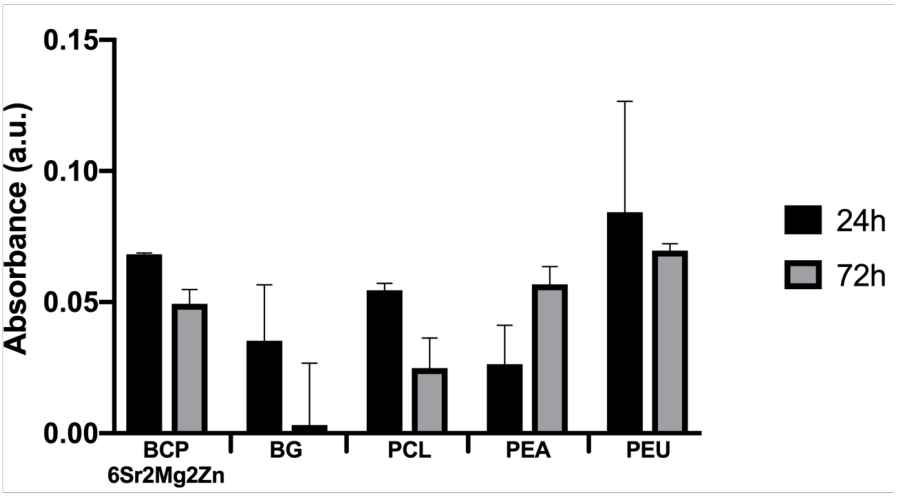

Figure 3. MTT results from the differently coated scaffolds. Data represents mean ± SD, n=1.

4. Discussion

Scaffolds derived from marine skeleton have been explored over the last years as a promising material for bone tissue engineering. In our pervious works [12,13] BCP scaffolds were obtained by HT of CB and strontium, magnesium and/or zinc ions were incorporated though partial calcium substitution or through sol-gel derived BG coating. The mechanical properties of HT samples were improved trough applying different polymeric coatings of PCL, PEA or PEU.

This work aims at assessing the *in vitro* performance of the scaffolds obtained in the previous works as potential bone grafts substitutes through cell viability and proliferation studies. This study was developed using hMSCs derived from the umbilical cord matrix. Despite being firstly isolated from the bone marrow [14], MSCs with similar characteristics can also be found in the fat tissue [15] and umbilical cord matrix [16]. These are undifferentiated cells with self-renewal capacity and can be differentiated into osteogenic, adipogenic and chondrogenic lineages [17].

Firstly, it was examined whether the doping elements introduced by partial calcium substitution would be beneficial for cell viability and proliferation. The live/dead staining results demonstrated that all the compositions have no noticeable cytotoxic effect on hMSCs. Moreover, it is important to highlight that the presence of the doping elements led to an increase in cell density. The live/dead staining results are consistent with MTT results, where the cell metabolic activity improves in the presence of strontium, magnesium and zinc. These results are in agreement with the literature where it is reported that these ions promote cell adhesion and proliferation [18–20], even though in the present work the concentrations of the doping elements [12] are lower than the ones reported in the literature.

Among the tested compositions, BCP-6Sr2Mg2Zn scaffolds have proven to be the most promising. Thus, BCP-6Sr2Mg2Zn scaffolds were coated with PCL, PEA or PEU and the impact of these coatings on cell behaviour was studied. Along with these samples, the feasibility of incorporating the doping elements through a sol-gel derived BG coating applied onto the surface of BCP scaffolds was also evaluated by performing similar *in vitro* cell behaviour studies. Unfortunately, it was only possible to do one replica. Therefore, it is difficult to drawn firm conclusions from the results obtained. A small decrease in cell proliferation was observed for PCL coated samples. Nevertheless, in previous works [7,11] it was reported that after PCL coating of HA scaffolds derived

from CB there was a significant improvement of cell proliferation. Fonseca et al [21] reported a good biocompatibility of PEA after seeding with fibroblasts, however in our work the scaffolds coated with PEA demonstrated to have lower biocompatibility in the first 24 h when compared with uncoated samples. The best result was achieved within PEU coated scaffolds, where there was an improvement of cell viability regarding the uncoated samples.

The coating of undoped BCP scaffolds with a sol-gel derived BG used to introduce the doping elements demonstrated to be cytotoxic, mainly after 72 h. The cellular toxicity can be explained by the shift of the medium pH to higher values, visually denoted from phenol red, the media pH indicator.

5. Conclusions

This *in vitro* cell culture study demonstrated that the undoped and doped BCP scaffolds obtained from HT of CB are nontoxic and provide an adequate support for cell adhesion and proliferation. We demonstrated that the presence of strontium, magnesium and zinc even in small quantities benefit cell proliferation. In addition, and despite being preliminary results, PCL and PEU coatings demonstrated to be nontoxic. Together, these results showed the potential use of the scaffolds derived from CB in bone tissue engineering. However, in order to have a more complete and conclusive *in vitro* study, more replicas of MTT assay and also differentiation studies should be performed for the different samples.

References

[1] M. Yamada, H. Egusa, Current bone substitutes for implant dentistry, J. Prosthodont. Res. 62 (2018) 152–161.

[2] C.A. De Souza Costa, J. Hebling, D.L.S. Scheffel, D.G.S. Soares, F.G. Basso, A.P.D. Ribeiro, Methods to evaluate and strategies to improve the biocompatibility of dental materials and operative techniques, Dent. Mater. 30 (2014) 769–784. doi:10.1016/j.dental.2014.04.010.

[3] V. Kartsogiannis, K.W. Ng, Cell lines and primary cell cultures in the study of bone cell biology, Mol. Cell. Endocrinol. 228 (2004) 79–102. doi:10.1016/j.mce.2003.06.002.

[4] G. Bouet, D. Marchat, M. Cruel, L. Malaval, L. Vico, In Vitro Three-Dimensional Bone Tissue Models: From Cells to Controlled and Dynamic Environment, Tissue

Eng. Part B Rev. 21 (2015) 133–156. doi:10.1089/ten.teb.2013.0682.

[5] J.H.G. Rocha, A.F. Lemos, S. Agathopoulos, S. Kannan, P. Valério, J.M.F. Ferreira, Hydrothermal growth of hydroxyapatite scaffolds from aragonitic cuttlefish bones, J. Biomed. Mater. Res. - Part A. 77 (2006) 160–168. doi:10.1002/jbm.a.30566.

[6] L. Hongmin, Z. Wei, Y. Xingrong, W. Jing, G. Wenxin, C. Jihong, X. Xin, C. Fulin, Osteoinductive nanohydroxyapatite bone substitute prepared via in situ hydrothermal transformation of cuttlefish bone, J. Biomed. Mater. Res. - Part B Appl. Biomater. 103B (2015) 816–824. doi:10.1002/jbm.b.33261.

[7] B.S. Kim, H.J. Kang, J. Lee, Improvement of the compressive strength of a cuttlefish bone-derived porous hydroxyapatite scaffold via polycaprolactone coating, J. Biomed. Mater. Res. - Part B. 101 (2013) 1302–1309. doi:10.1002/jbm.b.32943.

[8] B.S. Kim, S.S. Yang, J. Lee, A polycaprolactone/cuttlefish bone-derived hydroxyapatite composite porous scaffold for bone tissue engineering, J. Biomed. Mater. Res. - Part B. 102 (2014) 943–951. doi:10.1002/jbm.b.33075.

[9] B.S. Kim, H.J. Kang, S.S. Yang, J. Lee, Comparison of in vitro and in vivo bioactivity: Cuttlefish-bone-derived hydroxyapatite and synthetic hydroxyapatite granules as a bone graft substitute, Biomed. Mater. 9 (2014). doi:10.1088/1748-6041/9/2/025004.

[10] B.S. Kim, S.S. Yang, J.H. Yoon, J. Lee, Enhanced bone regeneration by silicon-substituted hydroxyapatite derived from cuttlefish bone, Clin. Oral Implants Res. 00 (2015) 1–8. doi:10.1111/clr.12613.

[11] D. Milovac, T.C. Gamboa-Martínez, M. Ivankovic, G. Gallego Ferrer, H. Ivankovic, PCL-coated hydroxyapatite scaffold derived from cuttlefish bone: In vitro cell culture studies, Mater. Sci. Eng. C. 42 (2014) 264–272. doi:10.1016/j.msec.2014.05.034.

[12] A.S. Neto, A.C. Fonseca, J.C.C. Abrantes, J.F.J. Coelho, J.M.F. Ferreira, Surface functionalization of cuttlefish bone-derived biphasic calcium phosphate scaffolds with polymeric coatings, Mater. Sci. Eng. C. 105 (2019) 110014. doi:10.1016/j.msec.2019.110014.

[13] A.S. Neto, D. Brazete, J.M.F. Ferreira, Cuttlefish Bone-Derived Biphasic Calcium Phosphate Scaffolds Coated with Sol-Gel Derived Bioactive Glass, Materials (Basel). 12 (2019) 2711. doi:10.3390/ma12172711.

[14] A. Friedenstein, R. Chailakhjan, K. Lalykina, The development of fibroblast colonies in monolayer cultures of guinea-pig bone marrow and spleen cells., Cell Tissue Kinet. 3 (1970) 393–403.

[15] M. Crisan, S. Yap, L. Casteilla, C.W. Chen, M. Corselli, T.S. Park, G. Andriolo, B. Sun, B. Zheng, L. Zhang, C. Norotte, P.N. Teng, J. Traas, R. Schugar, B.M. Deasy, S. Badylak, H.J. Buhring, J.P. Giacobino, L. Lazzari, J. Huard, B. Péault, A Perivascular Origin for Mesenchymal Stem Cells in Multiple Human Organs, Cell Stem Cell. 3 (2008) 301–313. doi:10.1016/j.stem.2008.07.003.

[16] D.L. Troyer, M.L. Weiss, Concise Review: Wharton's Jelly-Derived Cells Are a Primitive Stromal Cell Population, Stem Cells. 26 (2008) 591–599. doi:10.1634/stemcells.2007-0439.

[17] B. Delorme, S. Chateauvieux, P. Charbord, The concept of mesenchymal stem cells., Regen. Med. 1 (2006) 497–509. doi:10.2217/17460751.1.4.497.

[18] C.F. Marques, A. Lemos, S.I. Vieira, O.A.B. Da Cruz E Silva, A. Bettencourt, J.M.F. Ferreira, Antibiotic-loaded Sr-doped porous calcium phosphate granules as multifunctional bone grafts, Ceram. Int. 42 (2016) 2706–2716. doi:10.1016/j.ceramint.2015.11.001.

[19] S. Pina, S.I. Vieira, P. Rego, P.M.C. Torres, O.A.B. da Cruz e Silva, E.F. da Cruz e Silva, J.M.F. Ferreira, Biological responses of brushite-forming Zn-and ZnSr-substituted β-Tricalcium phosphate bone cements, Eur. Cells Mater. 20 (2010) 162–177. doi:10.22203/eCM.v020a14.

[20] B. Bracci, P. Torricelli, S. Panzavolta, E. Boanini, R. Giardino, A. Bigi, Effect of Mg2+, Sr2+, and Mn2+ on the chemico-physical and in vitro biological properties of calcium phosphate biomimetic coatings, J. Inorg. Biochem. 103 (2009) 1666–1674. doi:10.1016/j.jinorgbio.2009.09.009.

[21] A.C. Fonseca, J.F.J. Coelho, M.H. Gil, P.N. Simões, Poly(ester amide)s based on l-lactic acid oligomers and glycine: the role of the central unit of the l-lactic acid oligomers and their molecular weight in the poly(ester amide)s properties, Polym. Bull. 71 (2014) 3085–3109. doi:10.1007/s00289-014-1239-6.

Chapter 5

Rifampicin-loaded composite scaffold derived from cuttlefish bone for sustained drug delivery

Rifampicin-loaded composite scaffold derived from cuttlefish bone for sustained drug delivery

Ana S. Neto[a], Ana C. Fonseca[b], Beatriz [c], Carla Dias[c], Mariana Almeida[c], Paula Morais[c], Jorge F. J. Coelho[b], José M.F. Ferreira[a]

[a] Department of Materials and Ceramic Engineering / CICECO – Aveiro Institute of Materials, University of Aveiro, 3810-193 Aveiro, Portugal

[b] CEMMPRE, Department of Chemical Engineering, University of Coimbra, Rua Sílvio Lima-Pólo II, 3030-790 Coimbra, Portugal

[c] CEMMPRE, Department of Life Sciences, University of Coimbra, 3001-401 Coimbra, Portugal

Abstract

This study investigated the capacity of using scaffolds derived from cuttlefish bone (CB) as drug delivery systems and thereby avoiding bacterial infections. Biphasic calcium phosphate (BCP) scaffolds were obtained by hydrothermal transformation (HT) of CB. Rifampicin (RFP) was dissolved in poly(ε-caprolactone) (PCL), poly(ester amide) (PEA) or poly(ester urea) (PEU) polymeric solutions, which were posteriorly used to coat BCP scaffolds. The amounts of RFP incorporated in the scaffolds coated with PCL, PEA and PEU, were 0.55 ± 0.04, 0.48 ± 0.01 and 0.45 ± 0.02 wt.%, respectively. The drug release profiles in phosphate-buffered saline (PBS) solution over 6 days were similar among all the different samples, being characterized by a burst release in the first 8 h followed by a sustained release. The Korsmeyer-Peppas model revealed that the RFP release was controlled by non-Fickian diffusion for all the different polymeric coatings. Despite this similarity, the type of polymer used for the coating influence the rate of RFP release. A faster release was observed for samples coated with PCL, in which 67.33 ± 1.48 % of RFP was released in the first 8 h while in PEA and PEU coated samples there were burst releases of 42.88 ± 1.31 % and 47.23 ± 0.31 %, respectively. The antibacterial activity was evaluated against *Escherichia coli* (Gram-negative) and *Staphylococcus aureus* (Gram-positive) using RFP unloaded and loaded samples. The coated scaffolds revealed to be very effective in the reduction of bacterial growth for both strains, being particularly effective in the reduction of *S. aureus* growth.

Keywords: Cuttlefish bone, Biphasic calcium phosphate, Polymeric coatings, Rifampicin, Drug delivery system

1. Introduction

Bacterial infections are one of the major problems associated with implantation of medical devices and they could lead to an increase in patient morbidity and mortality [1]. In orthopaedic procedures, bacterial infections can be observed with the same level of complexity in the implantation of conventional devices and in tissue engineering approaches by using scaffolds [2]. After implantation one of the most important step is the inhibition of bacterial adhesion. Thus, in order to have a successful implantation, the integration of the material into the surrounding tissue must occur prior to an irreversible bacterial adhesion. The irreversible adhesion of microorganisms produces a biofilm that protects the bacteria from phagocytosis and antibiotics [3,4]. These bacterial infections might be avoided using scaffolds that allow an early local antibiotic delivery. The effectiveness of a delivery system is highly dependent on the controlled release profile of the drug. Since there is a high risk of infection immediately after implantation, the delivery system should promote an initial burst release of the antibiotic. This initial burst release should be followed by a sustained release to avoid a latent infection [3].

Calcium phosphates (CaP) are the most used biomaterials in the field of bone tissue engineering due to their similarity to the mineral component of bone and excellent bioactivity. Nowadays, biphasic calcium phosphate (BCP) represents the gold standard of CaP biomaterials [5]. BCP commonly combines a stable hydroxyapatite (HA) phase and a more soluble one, β-tricalcium phosphate (β-TCP) and, thereby, enabling a better control over the bioactivity and biodegradability of the scaffold. By this way, the stability of the material is guaranteed during bone ingrowth [6]. Despite all the potential of CaP materials, they have some drawbacks, mainly their brittleness and low strength. These disadvantages can be mitigated by applying a polymeric coating, which improves the robustness of the material [7]. For medical devices, synthetic polymers, featured by better reproducible synthesis and capacity to easily tune their physicochemical properties, are more advantageous than the natural ones [8]. The synergetic combinations between CaP and polymers have also been explored for drug delivery purposes in bone tissue engineering [9–11]. Despite the capacity of CaP scaffolds to incorporate pharmaceutical drugs through surface adsorption [12,13], they have a low efficiency as a sustained release systems. Moreover, the relatively high temperatures required for the development of CaP scaffolds with high skeletal density and suitable mechanical properties decrease the remaining porous surface area available for adsorption, making them potentially

unsuitable for the incorporation and release of pharmaceutical drugs [14]. These drawbacks can be overcome through the incorporation of the required pharmaceutical drug in a polymeric coating [14]. The drug release from a polymeric coating is characterized by an initial burst release followed by a sustained release [15]. Different factors influence the profile of drug release, namely, the coating degradation, the interaction with the polymer, and the diffusion of the drug. Moreover, the characteristics of the scaffolds like porosity, pore size and interconnectivity play crucial roles in the drug release profile [14].

Cuttlefish bone (CB) has a unique architecture with approximately 93% porosity [16]. The successful hydrothermal transformation (HT) of CB into BCP scaffolds was previously reported [17]. Due to the scaffold's brittleness and low strength, some previous studies reported the reinforcement of CB derived HA scaffolds with a polymeric coating [18–20]. In our previous work, poly(ε-caprolactone) (PCL), poly(ester amide) (PEA) or poly(ester urea) (PEU) coatings were used to improve the mechanical properties [17]. Nonetheless, in this work a further step was undertaken and the polymeric coatings were explored as vehicles to incorporate and release an antibiotic to avoid bacterial infection, thus obtaining multifunctional scaffolds. For this purpose, BCP scaffolds derived from CB were coated with PCL, PEA or PEU solutions, in which rifampicin (RFP), an antibiotic, was dissolved. RFP has a broad-spectrum against Gram-positive and-negative bacteria strains, which binds to the enzyme RNA-polymerase and blocks the bacterial DNA function [21]. Being one of the most potent and broader spectrum antibiotics, RFP has been explored as pharmaceutical drug to prevent the formation of a biofilm [22–24].

2. Materials and methods

2.1 Preparation of BCP scaffolds

CBs from cuttlefish, *Sepia officinalis*, were cut into cylinders with approximately 6 mm diameter and 3 mm height. Through differential and gravimetric thermal analysis (DTA/TG, Labsys Setaram TG-DTA/DSC, France, heating rate of 10 ºC min^{-1}) it was possible to infer the exact amount of $CaCO_3$ of CB. According to this result, the CB cylinders were subjected to a hydrothermal transformation (HT). Briefly, samples were sealed in a poly(tetrafluorethylene) (PTFE) lined stainless steel autoclave with the required volume of an aqueous solution of $(NH_4)_2HPO_4$ (Panreac AppliChem, Spain) for

24 h at 200 ºC. The obtained scaffolds were subjected to a heat treatment to eliminate the organic matter at 700 ºC for 1 h and using a heating rate of 0.5 ºC min^{-1}. Sintering took place at 1200 ºC with a heating rate of 2 ºC min^{-1} and a dwelling time of 2 h.

2.2 Preparation of polymeric coated scaffolds loaded with RFP

The sintered BCP scaffolds were coated with PCL (Perstorp Specialty Chemicals AB, Sweden, CAPA^{TM}6800 M_n = 80.000 g mol^{-1}), PEA (Mn = 26 900 g mol^{-1}) and PEU (Mn = 63 000 g mol^{-1}). The polymeric solutions were prepared at a concentration of 5 % (w/v); PCL was dissolved in dichloromethane (Sigma, Germany), while PEA and PEU were dissolved in chloroform (Fisher Scientific, United Kingdom). In order to improve the solubility of these last polymers, 2% (v/v) of *N, N'*-dimethylformamide (Sigma-Aldrich, Germany) was added to the chloroform solution. The coating of the scaffolds was achieved through a dip coating method using a vacuum equipment for 20 min and a pressure of 0.4 bar. Three different samples were obtained: BCP coated with PCL (BCP-PCL), BCP coated with PEA (BCP-PEA) and BCP coated with PEU (BCP-PEU). In order to obtain RFP loaded samples, RFP powder (Panreac AppliChem, Spain) was dissolved in the polymeric solution at a concentration of 1.5 mg.mL^{-1}. The scaffolds were coated with the RFP containing solution, using the procedure described above, yielding three different samples coated with PCL, PEA and PEU and further loaded with RFP: BCP-PCL-RFP, BCP-PEA-RFP and BCP-PEU-RFP, respectively.

The initial RFP content was calculated by immersing the scaffolds into a dimethyl sulfoxide (DMSO) solution enabling the drug dissolution. Subsequently, the RFP content was determined by UV-Vis spectrophotometry using a wavelength of 338 nm. A calibration curve (Figure S1) was constructed in an appropriate RFP concentration range in DMSO

2.3 Characterization of the obtained scaffolds

The scaffolds prior and after RFP loading were characterized by Fourier transform infrared (FTIR) spectroscopy, X-ray diffraction (XRD) and differential scanning calorimetry (DSC). FTIR spectra were obtained at room temperature using an Agilent Technologies Carey 630 spectrometer equipped with a Golden Gate Single Reflection Diamond ATR. Data were collected over a range from 650 to 4000 cm^{-1} using a spectral resolution of 4 cm^{-1} and 64 accumulations. XRD measurements were conducted in a High-Resolution X-ray diffractometer (PANalytical X´Pert Pro) with Cu Kα radiation (λ

= 1.5406 Å) using a step-scanning mode with 2θ angle varying from 10º to 100º and a step size of 0.0260º per second. DSC measurements were done in a Netzsch DSC-214 under a nitrogen atmosphere using an aluminium pan with approximately 5 mg of sample. It was used a heating rate of 10 ºC min^{-1} within a temperature range of –40 ºC to 500 ºC.

2.4 *In vitro* RFP release study

In order to study the RFP release, the scaffolds were placed in a glass tube containing 2 mL of PBS. The tubes were incubated at 37 ºC in a shaker and samples were collected at different time points: 10 min, 30 min, 1 h, 2 h, 6 h, 8 h, 24 h, 2 days, 3 days, 4 days, 5 days and 6 days and the medium was renewed at each time point. RFP concentration was determined by UV-Vis spectrophotometer using a wavelength of 332 nm. A calibration curve was constructed in an appropriate RFP concentration range in PBS (Figure S2). The measurements were performed in triplicate.

The kinetic release of RFP from the polymeric coated BCP scaffold was modelled using Korsmeyer-Peppas model (equation 1)

$$\frac{M_t}{M_\infty} = kt^n \left(\frac{M_t}{M_\infty} \leq 0.6\right) \quad (1)$$

where M_t and M_∞ are the amount of drug release at time t and infinity, respectively; k is the release constant and n is the release exponent and it is associated with the mechanism of release [25].

2.6 Antibacterial activity assay

The antibacterial assays of the RFP-loaded and unloaded scaffolds were performed against Gram-negative, *Escherichia coli* ATCC25922, and Gram-positive, *Staphylococcus aureus* ATCC25923. Bacterial strains were grown at 37 ºC for 24 h in Luria-Bertani (LB) medium. Afterwards, it was prepared a bacterial suspension in 10 mL of PBS solution with a turbidity adjusted to 0.5 according to McFarland standards (1.5×10^8 CFU mL^{-1}). The as-obtained suspension was diluted 10-fold and subsequently 375 µL was mixed with 1125 µL of LB medium and added into the wells containing the different polymeric (PCL, PEA or PEU) coated BCP scaffolds with or without RFP. The well without any scaffold was used as a positive control. The samples were incubated with orbital shaker at 115 rpm and 37 ºC. The number of viable bacteria that persisted in the culture medium at 24, 48 and 72 h and in the scaffolds (only at 72 h) was analysed by

spread plate method. Briefly, 100 µL of the bacterial suspension was removed from the well and evenly spread on LB agar plates. With respect to the scaffolds that were in contact with the bacterial suspension, they were gently washed twice with PBS and the adherent bacteria were detached by ultrasonication for 10 min. The obtained bacteria suspension was also spread on LB agar plates. Lastly the LB dishes were incubated at 37 ºC overnight and it was obtained the number of colony-forming units (CFUs). The experiments were repeated in triplicate and using two replicates in each experiment.

3. Results

3.1 Characterization of the scaffolds

The chemical groups present in the BCP scaffolds uncoated, and after coating with PCL, PEA and PEU, and further RFP loaded were assessed by FTIR-ATR (Figure 1). The BCP scaffolds exhibit the characteristic $–PO_4$ groups. The band at 960 cm^{-1} is related to ν_1 $–PO_4$ stretching, and the stretching ν_3 $–PO_4$ mode displays intense bands at 1028 and 1082 cm^{-1}. The characteristic –OH band at 3575 cm^{-1} is not observed in the FTIR-ATR spectrum. This could be a consequence of the HA partial de-hydroxylation at 1200 ºC and of its absence in β-TCP phase. The polymer coated scaffolds exhibit a superposition of the BCP spectrum with the characteristic spectra of the polymers. In the PCL coated scaffolds, it is possible to observe the characteristic bands of C=O stretching vibrations (ester linkage) at 1720 cm^{-1}, CH_2 stretching modes at 2946 and 2896 cm^{-1} and bending modes at 1362, 1399 and 1457 cm^{-1}. At 1239, 1041 and 1107 cm^{-1} are observed the bands associated with C–O–C stretching vibrations. The C–O and C–C stretching of amorphous and crystalline phases appear at 1166 and 1293 cm^{-1}, respectively. In a similar way, the scaffolds coated with PEA exhibited characteristic bands of stretching vibrations of N–H group (amide linkage) and C=O group (ester linkage) at 3300 and 1733 cm^{-1}, respectively. The bands at 2851 and 2924 cm^{-1} are ascribed to symmetric and asymmetric stretching vibrations of CH_2 group, respectively. Furthermore, the bands associated with amide I and amide II groups are observed at 1645 and 1540 cm^{-1}, respectively. Lastly, the PEU coated samples also exhibit the characteristic PEU bands. The band at 1560 cm^{-1} is associated with the bending of N–H group and stretching of C–N group of urea linkage. The band located at 3370 cm^{-1} corresponds to the stretching vibration of the N–

H group of urea linkage. The vibration of C=O of ester and urea are located at 1735 and 1636 cm^{-1}, respectively. RFP has its characteristic bands of C=O at 1559 cm^{-1}, furanone (C=O) at 1638 cm^{-1}, acetyl (C=O) at 1720 cm^{-1} and amide (N–CH_3) at 2890 cm^{-1} [26]. The addition of RFP did not alter the spectra of the samples. Indeed, the spectra were identical before and after the incorporation of RFP.

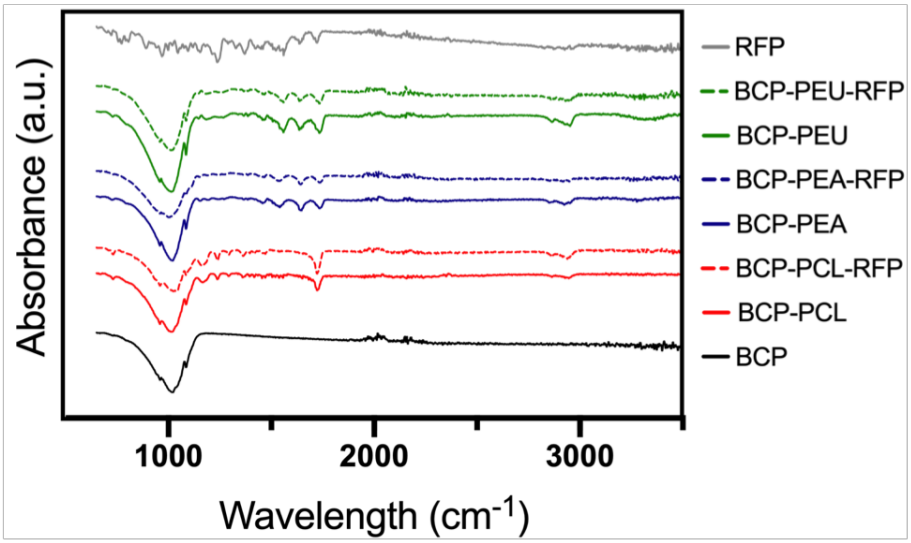

Figure 1. FTIR-ART of BCP scaffolds, uncoated and after coating with different polymers (BCP-PCL, BCP-PEA and BCP-PEU) and further loaded with RFP (BCP-PCL-RFP, BCP-PEA-RFP and BCP-PEU-RFP).

Despite not being detected through FTIR, the presence of RFP is clearly observed in Figure 2 where the samples with RFP change their colour from white to burnt orange.

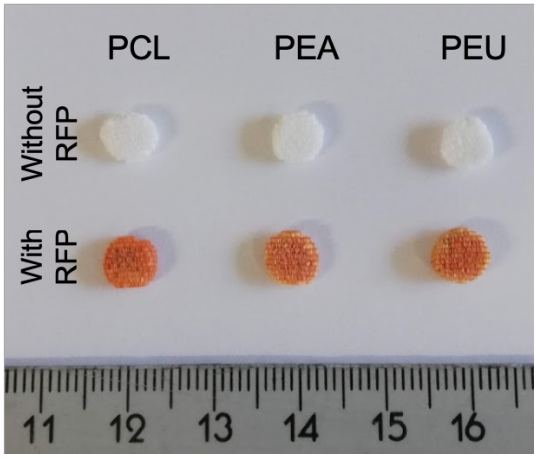

Figure 2. BCP scaffolds coated with different polymers (PCL, PEA and PEU - white), and further loaded with RFP (burnt orange).

3.2 *In vitro* RFP release study

The quantity of RFP present in the scaffolds was determined by dissolving those in 3 mL of DMSO and measuring its concentration using UV-Vis spectrophotometry at the 338 nm wavelength. The RFP contents in the PCL, PEA and PEU coated samples were 0.55 ± 0.04, 0.48 ± 0.01 and 0.45 ± 0.02 wt.%, respectively. The loading capacity of the PCL coated scaffolds was significantly higher when compared with the other two polymers.

The drug release profiles were determined over a period of 6 days and the results are displayed in Figure 3. The cumulative release profiles for the different compositions are similar, being characterized by two stages, an initial burst release (~ 8 h) followed by a sustained release. Despite this similarity, the fraction of RFP released from the scaffolds is dependent on the polymer used for the coating. Indeed, during the first 8 h the RFP release from BCP-PCL-RFP (67.33 ± 1.48 %) was significantly higher when compared with the BCP-PEA-RFP and BCP-PEU-RFP systems, which only released 42.88 ± 1.31 % and 47.23 ± 0.31 %, respectively. After 6 days, the total released RFP contents reached 85.33 ± 0.36 %, 80.11 ± 0.23 % and 61.73 ± 0.16 % for BCP-PCL-RFP, BCP-PEA-RFP and BCP-PEU-RFP, respectively.

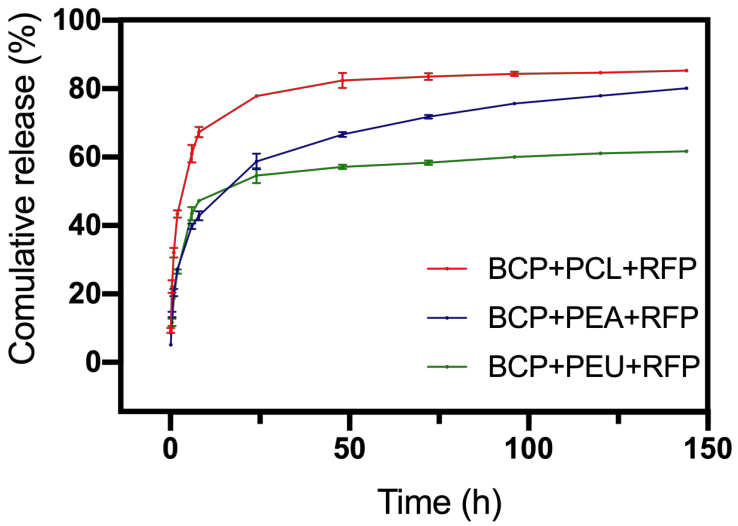

Figure 3. In vitro release profiles of RFP from the BCP scaffolds coated with PCL, PEA and PEU.

The RFP release was studied through the Korsmeyer-Peppas model described in Equation (1) and the results are presented in Table 1. From the obtained drug release curves, it is possible to infer that the values of release exponent (n) were between 0.46 and 1, which is reported as a non-Fickian diffusion for cylindrical samples. Moreover,

the calculated constant (*k*) values were 0.3058, 0.1660 and 0.1841 for BCP-PCL-RFP, BCP-PEA-RFP and BCP-PEU-RFP, respectively. The correlation coefficient was maintained above 0.93 for all the scaffolds compositions.

Table 1. Exponent (*n*), constant (*k*) and correlation coefficient (R^2) obtained from the Korsmeyer-Peppas model for the release of RFP from the BCP scaffolds coated with PCL, PEA and PEU.

Scaffold	*n*	*k*	R^2
BCP-PCL-RFP	0.6215	0.3058	0.9807
BCP-PEA-RFP	0.4639	0.1660	0.9372
BCP-PEU-RFP	0.4640	0.1841	0.9890

3.4 Antibacterial activity assay

The antibacterial activity of the different scaffolds against *E. coli* (Table 2a) and *S. aureus* (Table 2b) was assessed by the spread plate method.

Table 2a. Antibacterial activity of the different scaffolds against *E. coli*.

	E. coli			
Scaffold	24 h	48 h	72 h	Adherent
BCP-PCL	Countless			
BCP-PCL-RFP	4.25 ± 0.25	0.00 ± 0.00	0.00 ± 0.00	6.00 ± 6.00
BCP-PEA	Countless			
BCP-PEA-RFP	28.25 ± 5.25	0.83 ± 0.85	0.00 ± 0.00	3.83 ± 5.42
BCP-PEU	Countless			
BCP-PEU-RFP	Countless*	Countless	Countless	Countless

Countless – countless CFUs.
Countless* - countless CFUs but with a reduction in the cell number when compared with the positive control.

Table 2b. Antibacterial activity of the different scaffolds against *S. aureus*.

	S. aureus			
Scaffold	24 h	48 h	72 h	Adherent
BCP-PCL	Countless			
BCP-PCL-RFP	0.00 ± 0.00	0.17 ± 0.24	0.00 ± 0.00	0.00 ± 0.00
BCP-PEA	Countless			
BCP-PEA-RFP	0.00 ± 0.00	0.33 ± 0.47	0.00 ± 0.00	0.83 ± 1.18
BCP-PEU	Countless			
BCP-PEU-RFP	0.17 ± 0.24	0.00 ± 0.00	0.33 ± 0.47	10.00 ± 10.50

Countless – countless CFUs.

The polymer coated samples did not exhibit any antimicrobial activity. On the other hand, the samples loaded with RFP were effective in the reduction of bacterial growth. After 24 h of incubation with *E. coli*, the BCP-PCL-RFP samples demonstrated to have a higher reduction of bacterial growth when compared with the other two RFP loaded samples. It is important to underline that, after 72 h of incubation, the BCP-PCL-RFP and BCP-PEA-RFP scaffolds led to a 100% reduction in the number of *E. coli*. Moreover, in these compositions, few bacteria remained adhered to the scaffolds, demonstrating the inability to develop a biofilm. Concerning the incubation with *S. aureus*, the different RFP loaded scaffolds demonstrated to be effective in the reduction of bacterial growth, inhibiting the formation of a biofilm and the growth of *S. aureus* to approximately 100% after 24 h of incubation.

4. Discussion

A complete transformation of CB into a BCP scaffold was firstly reported in our previous work. The unique CB architecture was preserved after HT and sintering. In addition, the polymeric coating with PCL, PEA or PEU significantly improved the mechanical properties of the scaffolds without having any significant negative impact in scaffold porosity [17]. This means that the composite scaffolds smartly combine the highly porous inorganic BCP with the polymeric coatings, enhancing the overall properties and expanding the potential applications. Moreover, this synergetic effect can also be explored in the context of drug delivery. The main goal of this work was to develop a composite scaffold derived from CB that could function as a drug delivery system and, thereby, avoid the development of a biofilm at the implantation site.

The amount of RFP incorporated in the PCL coated samples, 0.55 ± 0.04 wt.%, was significantly higher in comparison those incorporated in the PEA and PEU coated samples, 0.48 ± 0.01 and 0.45 ± 0.02 wt.%, respectively. This discrepancy could be a consequence of the higher viscosity of the PCL polymeric solution in comparison with the viscosity of PEA and PEU solutions. This resulted in a thicker coating as shown in SEM images, corroborated by the slightly lower porosity values after the coating, as reported in our previous work [17]. Due to the low amounts of RFP incorporated, it was impossible to detect differences between the coated samples with and without RFP by FTIR-ATR (Figure 1). From XRD and DSC (results presented in Supporting information, Figure S3 and Figure S4) it was also not possible to detect the presence of RFP in the samples. Nonetheless, its incorporation into the coated scaffolds can easily be inferred by the modification of their colour from white to burnt orange (Figure 2). Moreover, the *in vitro* drug release studies (Figure 3) and the antimicrobial studies (Tables 2a and 2b) are further clear evidences of the presence of RFP in the coated samples.

Te *in vitro* drug release studies (Figure 3) demonstrated that the polymeric coatings enable obtaining suitable RFP release profiles. All the RFP loaded samples exhibited similar release profiles, characterized by an initial burst release within the first 8 h, followed by a sustained release of the drug. The relative amounts delivered during the burst release period were 67.33 ± 1.48 %, 42.88 ± 1.31 % and 47.23 ± 0.31 % for the samples coated with PCL, PEA and PEU, respectively. With the introduction of RFP in the scaffolds, the aim was to prevent the risk of infection in the initial stages upon implantation. Therefore, the observed initial burst brings an important advantage to eliminate possible bacteria contaminations during the medical procedure. [27]. Moreover, it is important to highlight that the RFP released during the burst is still within the therapeutic levels, since a cytotoxic effect is only observed at a concentration of 100 $\mu g.mL^{-1}$ [28]. This behaviour can be justified though different mechanisms, like pore diffusion, surface desorption and the absence of a diffusion barrier that regulates the diffusive process [29].

The drug release kinetic mechanisms were studied using Korsmeyer-Peppas model, which enables the analysis of release behaviour for systems with different geometries and mechanisms. It can be used to describe the drug release from thin films and cylindrical or spherical samples. In this work, cylindrical samples were used. The mechanisms of drug release can be divided into Fickian diffusion, non-Fickian transport and zero-order release when n is 0.45, 0.45–1 and 1, respectively [25]. For the different

coating compositions used in the present work, the *n* value ranged between 0.46 and 0.62, which is characteristic of a non-Fickian diffusion. This diffusion behaviour denotes a release concomitantly controlled by diffusion and by dissolution [30].

Furthermore, it is worth highlighting that the release profile is highly dependent on the type of polymer used in the coating. Indeed, a faster RFP release from the scaffolds coated with PCL, in comparison to the scaffolds coated with PEA or PEU, was observed. The three different polymers, PCL, PEA and PEU, have carboxyl groups that enable the formation of hydrogen bonds with RFP. In addition, these groups have an affinity with calcium present in BCP scaffolds. Apart from carboxyl groups, PEA and PEU have amide groups that can also establish hydrogen bonds with RFP, while exhibiting an affinity with phosphorous from BCP scaffolds. Thus, the PEA and PEU coatings are expected to create stronger interactions with both BCP scaffolds and RFP in comparison to the PCL ones. The lower affinity between PCL and BCP scaffolds results in weaker and non-continuous interfaces that offer a higher surface area available for contacting with the PBS solution and for drug desorption. This, combined with the thicker PCL coating, derived from the higher viscosity of its solution, concur for the significantly higher amount of RFP retained in the PCL coating. All these factors account and determine the drug release behaviour and consistently justify the higher amount of drug liberated during burst release from PCL coated samples within the first 8 h.

RFP is a wide-spectrum antibiotic for both Gram-positive and Gram-negative bacteria. Thus, in the present work, the antibacterial activity of the obtained scaffolds was studied against Gram-negative *E. coli* (Table 2a) and Gram-positive *S. aureus* (Table 2b). Although RFP loaded scaffolds exhibits a good antibacterial activity against both types of bacteria, the efficacy depends on the bacteria strain. Concerning the incubation with *E. coli,* a faster decrease in the number of viable bacteria was registered for the samples coated with PCL, in comparison to a more gradual reduction observed for the BCP-PEA-RFP scaffolds. These results are in good agreement with those of drug delivery (Figure 3) and can be attributed to the significantly higher burst release of RFP from the BCP-PCL-RFP scaffolds in comparison to the scaffolds coated with PEA and PEU. The BCP-PEA-RFP scaffolds demonstrated to have a more sustained release up to an almost complete depletion of the drug during the investigated period. On the other hand, the scaffolds exhibited a stronger antibacterial activity against *S. aureus.* Indeed, after 24 h of incubation, the reduction of bacterial growth achieved almost 100% for all the

compositions. The higher sensitivity of *S. aureus* to RFP is associated with the better permeability of RFP through Gram-positive cell walls than through Gram-negative [31].

5. Conclusions

In this study, we successfully developed a drug delivery system using composite scaffolds derived from CB. BCP scaffolds were obtained by a hydrothermal transformation of CB. The polymeric coatings with PCL, PEA or PEU previously used to improve the mechanical properties was explored in this work as a drug delivery system in which, a pharmaceutical drug, RFP, was incorporated into the polymeric coating. The drug release kinetic mechanism of the different compositions was similar and characterized by a burst release in the first 8 h followed by a sustained release and known as a non-Fickian diffusion. It is important to highlight that in the samples coated with PCL there is a higher first release of RFP which could be associated with the weaker interaction between the polymer and the drug and also between the polymer and the BCP scaffold. The antibacterial activity of the different scaffolds against *E. coli* and *S. aureus* demonstrated that the samples without the antibiotic did not exhibit an antimicrobial activity. The samples with RFP were in the majority effective in the reduction of bacterial growth. These scaffolds were more effective in the reduction of *S. aureus* growth.

Supporting Information

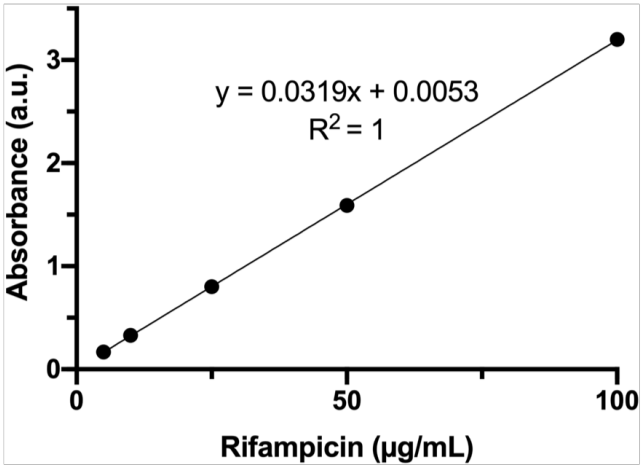

Figure S1. Calibration curve of RFP diluted in DMSO

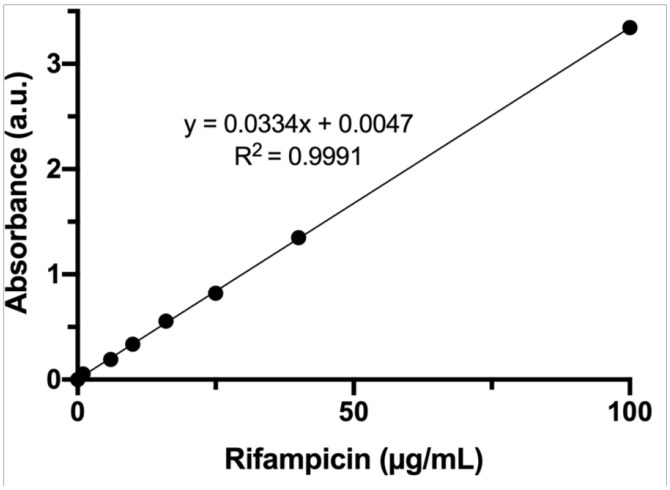

Figure S2. Calibration curve of RFP diluted in PBS

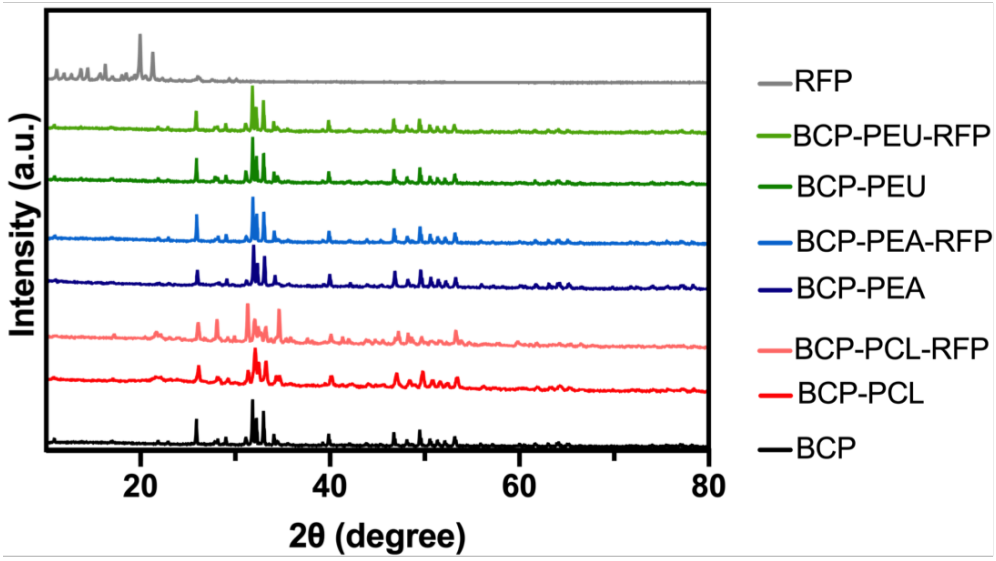

Figure S3. XRD of uncoated BCP scaffolds, coated with different polymers (BCP-PCL, BCP-PEA and BCP-PEU) and loaded with RFP (BCP-PCL-RFP, BCP-PEA-RFP and BCP-PEU-RFP).

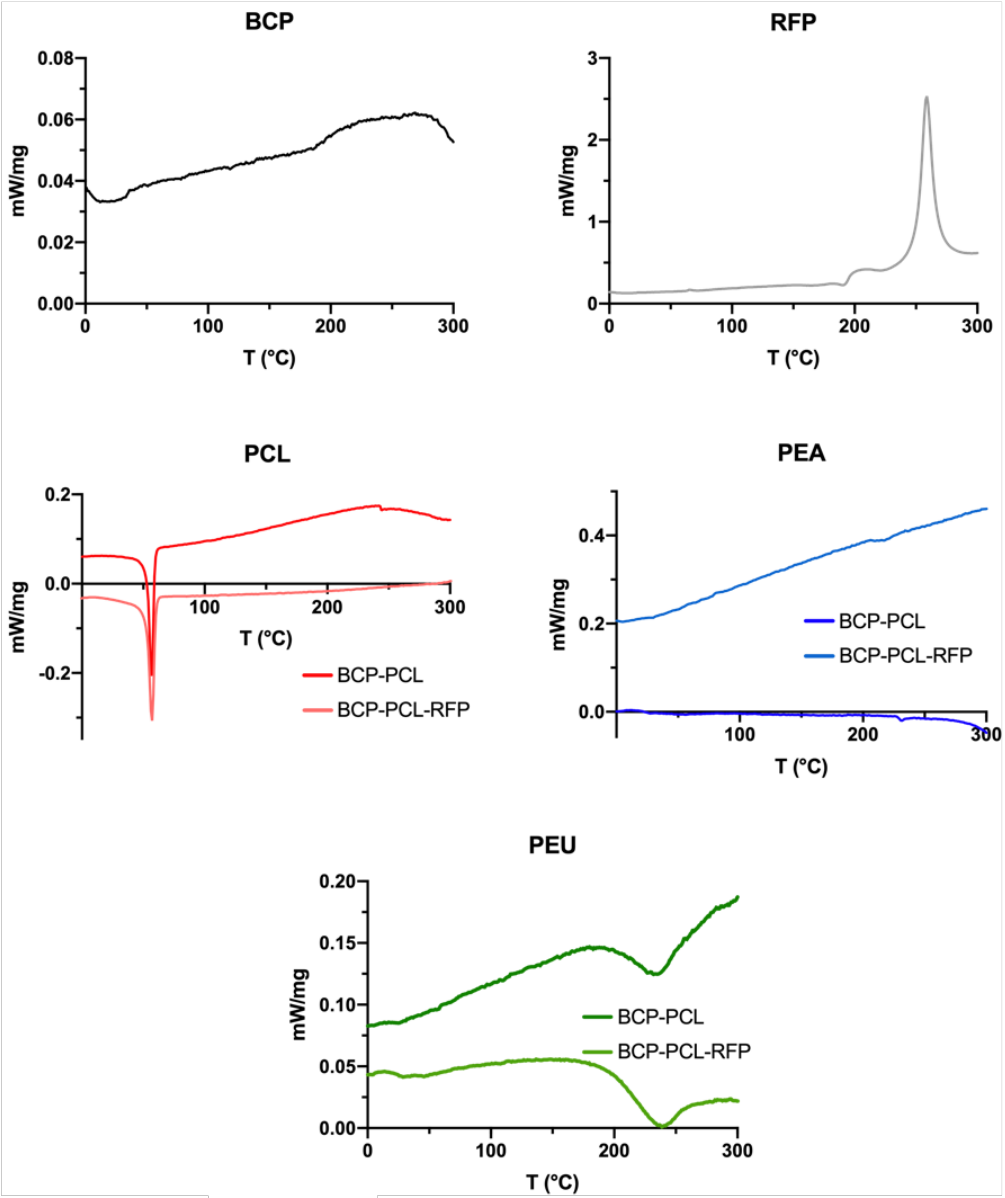

Figure S4. DCS of uncoated BCP scaffolds, coated with different polymers (BCP-PCL, BCP-PEA and BCP-PEU) and loaded with RFP (BCP-PCL-RFP, BCP-PEA-RFP and BCP-PEU-RFP).

References

[1] S.L. Percival, L. Suleman, C. Vuotto, G. Donelli, Healthcare-associated infections, medical devices and biofilms: risk, tolerance and control, J. Med. Microbiol. 64 (2015) 323–334. doi:10.1099/jmm.0.000032.

[2] V. Mouriño, A.R. Boccaccini, Bone tissue engineering therapeutics: controlled drug delivery in three-dimensional scaffolds, J. R. Soc. Interface. 7 (2010) 209–227. doi:10.1098/rsif.2009.0379.

[3] M. Zilberman, J.J. Elsner, Antibiotic-eluting medical devices for various applications, J. Control. Release. 130 (2008) 202–215. doi:10.1016/j.jconrel.2008.05.020.

[4] R.M. Donlan, Biofilms and Device-Associated Infections, Emerg. Infect. Dis. 7 (2001) 277–281.

[5] J.M. Bouler, P. Pilet, O. Gauthier, E. Verron, Biphasic calcium phosphate ceramics for bone reconstruction: A review of biological response, Acta Biomater. 53 (2017) 1–12. doi:10.1016/j.actbio.2017.01.076.

[6] S.E. Lobo, T.L. Arinzeh, Biphasic calcium phosphate ceramics for bone regeneration and tissue engineering applications, Materials (Basel). 3 (2010) 815–826. doi:10.3390/ma3020815.

[7] A. Motealleh, S. Eqtesadi, A. Pajares, P. Miranda, Enhancing the mechanical and in vitro performance of robocast bioglass scaffolds by polymeric coatings : Effect of polymer composition, J. Mech. Behav. Biomed. Mater. 84 (2018) 35–45. doi:10.1016/j.jmbbm.2018.04.022.

[8] M.S. Cortizo, M.S. Belluzo, Biodegradable Polymers for Bone Tissue Engineering, in: S.N. Goyanes, N.B. D'Accorso (Eds.), Ind. Appl. Renew. Biomass Prod. Past, Present Futur., 2017. doi:10.1007/978-3-319-61288-1.

[9] M. Araújo, R. Viveiros, A. Philippart, M. Miola, S. Doumett, G. Baldi, J. Perez, A.R. Boccaccini, A. Aguiar-Ricardo, E. Verné, Bioactivity, mechanical properties and drug delivery ability of bioactive glass-ceramic scaffolds coated with a natural-derived polymer, Mater. Sci. Eng. C. 77 (2017) 342–351. doi:10.1016/j.msec.2017.03.169.

[10] H.W. Kim, J.C. Knowles, H.E. Kim, Hydroxyapatite/poly(ε-caprolactone) composite coatings on hydroxyapatite porous bone scaffold for drug delivery, Biomaterials. 25 (2004) 1279–1287. doi:10.1016/j.biomaterials.2003.07.003.

[11] S. Bose, N. Sarkar, D. Banerjee, Effects of PCL, PEG and PLGA polymers on

curcumin release from calcium phosphate matrix for in vitro and in vivo bone regeneration, Mater. Today Chem. 8 (2018) 110–120. doi:10.1016/j.mtchem.2018.03.005.

[12] Z.N. Al-Sokanee, A.A.H. Toabi, M.J. Al-Assadi, E.A.S. Alassadi, The drug release study of ceftriaxone from porous hydroxyapatite scaffolds, AAPS PharmSciTech. 10 (2009) 772–779. doi:10.1208/s12249-009-9265-7.

[13] F. Chai, J.C. Hornez, N. Blanchemain, C. Neut, M. Descamps, H.F. Hildebrand, Antibacterial activation of hydroxyapatite (HA) with controlled porosity by different antibiotics, Biomol. Eng. 24 (2007) 510–514. doi:10.1016/j.bioeng.2007.08.001.

[14] S. Bose, S. Tarafder, Calcium phosphate ceramic systems in growth factor and drug delivery for bone tissue engineering: A review, Acta Biomater. 8 (2012) 1401–1421. doi:10.1016/j.actbio.2011.11.017.

[15] B. Kundu, C. Soundrapandian, S.K. Nandi, P. Mukherjee, N. Dandapat, S. Roy, B.K. Datta, T.K. Mandal, D. Basu, R.N. Bhattacharya, Development of new localized drug delivery system based on ceftriaxone-sulbactam composite drug impregnated porous hydroxyapatite: A systematic approach for in vitro and in vivo animal trial, Pharm. Res. 27 (2010) 1659–1676. doi:10.1007/s11095-010-0166-y.

[16] J.D. Birchall, N.L. Thomas, On the architecture and function of cuttlefish bone, J. Mater. Sci. 18 (1983) 2081–2086. doi:10.1007/BF00555001.

[17] A.S. Neto, A.C. Fonseca, J.C.C. Abrantes, J.F.J. Coelho, J.M.F. Ferreira, Surface functionalization of cuttlefish bone-derived biphasic calcium phosphate scaffolds with polymeric coatings, Mater. Sci. Eng. C. 105 (2019) 110014. doi:10.1016/j.msec.2019.110014.

[18] B.S. Kim, H.J. Kang, J. Lee, Improvement of the compressive strength of a cuttlefish bone-derived porous hydroxyapatite scaffold via polycaprolactone coating, J. Biomed. Mater. Res. - Part B. 101 (2013) 1302–1309. doi:10.1002/jbm.b.32943.

[19] D. Milovac, G. Gallego Ferrer, M. Ivankovic, H. Ivankovic, PCL-coated hydroxyapatite scaffold derived from cuttlefish bone: Morphology, mechanical properties and bioactivity, Mater. Sci. Eng. C. 34 (2014) 437–445. doi:10.1016/j.msec.2014.05.034.

[20] A. Rogina, M. Antunovic, D. Milovac, Biomimetic design of bone substitutes based on cuttlefish bone-derived hydroxyapatite and biodegradable polymers, J.

Biomed. Mater. Res. - Part B. 107B (2018) 197–204.

[21] E.A. Campbell, N. Korzheva, A. Mustaev, K. Murakami, S. Nair, A. Goldfarb, S.A. Darst, Structural mechanism for rifampicin inhibition of bacterial RNA polymerase, Cell. 104 (2001) 901–912. doi:10.1016/S0092-8674(01)00286-0.

[22] A.S. Kranthi Kiran, A. Kizhakeyil, R. Ramalingam, N.K. Verma, R. Lakshminarayanan, T.S.S. Kumar, M. Doble, S. Ramakrishna, Drug loaded electrospun polymer/ceramic composite nanofibrous coatings on titanium for implant related infections, Ceram. Int. 45 (2019) 18710–18720. doi:10.1016/j.ceramint.2019.06.097.

[23] J. Aragón, S. Feoli, S. Irusta, G. Mendoza, Composite scaffold obtained by electro-hydrodynamic technique for infection prevention and treatment in bone repair, Int. J. Pharm. 557 (2019) 162–169. doi:10.1016/j.ijpharm.2018.12.002.

[24] T.T. Ruckh, R.A. Oldinski, D.A. Carroll, K. Mikhova, J.D. Bryers, K.C. Popat, Antimicrobial effects of nanofiber poly(caprolactone) tissue scaffolds releasing rifampicin, J. Mater. Sci. Mater. Med. 23 (2012) 1411–1420. doi:10.1007/s10856-012-4609-3.

[25] P.L. Ritger, N.A. Peppas, A simple equation for description of solute release I. Fickian ans non-Fikian release from non-swellable devices in the form of slabs, spheres, cylinders or discs, J. Control. Release. 5 (1987) 23–36. doi:10.1016/S0168-3659(03)00195-0.

[26] R. Pati, R. Sahu, J. Panda, A. Sonawane, Encapsulation of zinc-rifampicin complex into transferrin-conjugated silver quantum-dots improves its antimycobacterial activity and stability and facilitates drug delivery into macrophages, Sci. Rep. 6 (2016) 24184. doi:10.1038/srep24184.

[27] V. Martin, I.A. Ribeiro, M.M. Alves, L. Gonçalves, R.A. Claudio, L. Grenho, M.H. Fernandes, P. Gomes, C.F. Santos, A.F. Bettencourt, Engineering a multifunctional 3D-printed PLA-collagen-minocycline-nanoHydroxyapatite scaffold with combined antimicrobial and osteogenic effects for bone regeneration, Mater. Sci. Eng. C. 101 (2019) 15–26. doi:10.1016/j.msec.2019.03.056.

[28] J. Yuan, B. Wang, C. Han, X. Lu, W. Sun, D. Wang, J. Lu, J. Zhao, C. Zhang, Y. Xie, In vitro comparison of three rifampicin loading methods in a reinforced porous β-tricalcium phosphate scaffold, J. Mater. Sci. Mater. Med. 26 (2015) 1–9. doi:10.1007/s10856-015-5437-z.

[29] X. Huang, C.S. Brazel, On the importance and mechanisms of burst release in

matrix-controlled drug delivery systems, J. Control. Release. 73 (2001) 121–136. doi:10.1016/S0168-3659(01)00248-6.

[30] S.K. Chandrasekaran, D.R. Paul, Dissolution-Controlled transport from dispersed matrixes, J. Pharm. Sci. 71 (1982) 1399–1402. doi:10.1002/jps.2600711222.

[31] W. Wherli, Rifampin: Mechanisms of Action and Resistance, Rev. Infect. Dis. 5 (1983) 407–411.

Chapter 6

Conclusions and future work

1. Conclusions

This thesis aimed at developing a bone graft substitutes for advanced therapies based on doped scaffolds derived from cuttlefish bone (CB) and, subsequently, combining the scaffolds with different polymeric coatings to improve the mechanical strength and allow the control releasing of drugs

Biphasic calcium phosphate (BCP) scaffolds were obtained from a hydrothermal transformation (HT) of CB. Due to the notorious benefits of introducing in the scaffolds trace amounts of ions present in bone composition, in the present work Sr^{2+}, Mg^{2+} and/or Zn^{2+} were successfully incorporated into the scaffolds either by partial replacement of calcium in the crystalline structure or by a sol-gel derived bioactive glass (BG) coating. The incorporation of Sr^{2+}, Mg^{2+} and Zn^{2+} by the partial replacement of calcium revealed to be beneficial for cell proliferation. The main drawbacks associated with these scaffolds, brittleness and low strength, were overcome by applying polymeric coatings. Four different polymers: poly(ε-caprolactone) (PCL), poly(DL-lactide) (PDLA), poly(ester amide) (PEA) and poly(ester urea) (PEU) were investigated as suitable coatings. These polymers significantly improved the mechanical properties of the scaffolds. Moreover, an improvement of cell proliferation was achieved with PEU coated scaffolds. This synergetic effect between ceramic scaffolds and polymeric coatings was explored to develop drug delivery systems. A pharmaceutical drug, rifampicin (RFP), was incorporated into the polymeric coating enabling a sustained drug release. These scaffolds demonstrated to have good antibacterial properties.

CB, a worldwide available material, possesses unique microstructural scaffold features that have already proven to be beneficial for bone development. The research studies carried out so far have been focused on the HT of CB into hydroxyapatite scaffolds preserving its internal structure. However, recognizing the important advantages of having BCP materials that combine both hydroxyapatite and β-tricalcium phosphate phases. This thesis reports for the first time the complete HT of CB into BCP scaffolds, which was confirmed by X-ray diffraction (XRD) and Rietveld refinement. The incorporation of doping elements, namely F^- and Si^{4+}, into the crystalline lattice of HA was already reported in the literature. In this work, the incorporation of Sr^{2+}, Mg^{2+} and/or Zn^{2+} into the BCP structure was accomplished in order to further enhance the regeneration potential of the CB-derived scaffolds. The presence of these ions in the crystalline

structure was confirmed through the shifts in the XRD patterns. Nevertheless, it was observed by inductively couple plasma (ICP) spectrometry a mismatch between the planned and the experimental obtained compositions. Despite obtaining lower concentrations than the planned ones, the *in vitro* cell culture study proved that beyond being nontoxic the presence of Sr^{2+}, Mg^{2+} and Zn^{2+} in the BCP-6Sr2Mg2Zn samples also promote the adhesion and proliferation of human mesenchymal stem cells.

As an alternative to calcium partial replacement in the crystalline lattices of BCP, these ions were also incorporated for the first time as a sol-gel derived BG coating applied onto the surface of the BCP scaffolds. In this vein, a BG with a composition of 60% SiO_2 – 34% CaO – 2% SrO – 2% MgO – 2% ZnO – 2% P_2O_5 was produced by the sol-gel route. Good similarity between the planned and experimental obtained compositions was confirmed by energy dispersive spectroscopy (EDS). In addition, with this coating it was possible to improve the compressive strength and the *in vitro* biomineralization activity tests in simulated body fluid. Nevertheless, despite these advantages, preliminary cell culture assessments indicated that the BG coating tended to increase the pH of cell culture medium and induce cytotoxicity.

Improvements in mechanical properties of CB-derived HA scaffolds with polymeric coatings of PCL, or a combination of PCL and polylactic acid (PLA), were already described in the literature. This thesis also studied the use of a polymeric coatings to improve the mechanical properties, maintaining the focus on synthetic polymers regarding their advantages over natural polymers. Nonetheless, besides using the commercially available PCL and PDLA polymers, two other polymers, PEA and PEU, were synthesized in the laboratory and applied as coatings. All the polymers tested contributed to significant improvements in the mechanical properties without jeopardize the initial CB microstructure. The best results were achieved with PEU coatings. The Preliminary *in vitro* cell culture results also indicated PEU coatings as being the most efficient in promoting cell proliferation.

The polymeric coating was explored for the first time as storage vehicle for a sustained drug delivery. RFP was incorporated into the PCL, PEA and PEU coatings applied onto the surface of scaffolds. All the BCP scaffolds coated with the different polymers exhibited similar behaviours with an initial burst release followed by a sustained release. However, a faster release was observed for the samples coated with PCL when compared with the samples coated with PEA or PEU. Moreover, all the scaffolds with RFP-loaded polymeric coatings demonstrated to have good antibacterial properties.

2. Future work

The development of suitable scaffolds for bone regeneration remains a big challenge. This thesis represents one more step towards the development of an ideal scaffold for bone tissue engineering. Nevertheless, in order to upgrade the scaffolds obtained through a HT of CB, further studies should be performed aiming at:

(1) Analysing the ion release profiles from scaffolds before and after applying the polymeric coatings, thereby, examining whether the polymeric coatings impair the ion release.

(2) Further improving the mechanical properties of the polymeric coated scaffolds by repeating the dipping process without compromising the porosity and impair the ion release from the BCP scaffold.

(3) Applying polymeric coatings onto the sol-gel derived bioactive glass coated scaffolds in order to further improve the mechanical properties.

(4) Complement the *in vitro* study with: (1) more replicas regarding the MTT study with BG and polymeric coated scaffolds in order to obtain conclusive results with statistical relevance; (2) scanning electron microscopy observation to study the morphology of the cells that adhere to the scaffolds; (3) the study of cell differentiation. Analyse how the different scaffold's composition influence cell differentiation; (4) the study of cell cytotoxicity in the scaffolds loaded with RFP.

(5) *In vivo* study to analyse the osteogenic properties of the implanted scaffold. This study will be useful to ascertain whether there is a formation of inflammatory tissue within the bone defect, the degree of reabsorption of the scaffold and the new bone formation rate.